

Summer 2022

Identifying Novel Pharmacogenetic Markers for Cancer Treatments: Exploiting Cancers Deficient in the Nucleotide Pool Sanitizing Hydrolases NUDT15 AND NUDT18

Jacob Chandler Massey

Follow this and additional works at: <https://scholarcommons.sc.edu/etd>



Part of the [Pharmacology Commons](#)

Recommended Citation

Massey, J. C.(2022). *Identifying Novel Pharmacogenetic Markers for Cancer Treatments: Exploiting Cancers Deficient in the Nucleotide Pool Sanitizing Hydrolases NUDT15 AND NUDT18*. (Doctoral dissertation). Retrieved from <https://scholarcommons.sc.edu/etd/6902>

This Open Access Dissertation is brought to you by Scholar Commons. It has been accepted for inclusion in Theses and Dissertations by an authorized administrator of Scholar Commons. For more information, please contact digres@mailbox.sc.edu.

IDENTIFYING NOVEL PHARMACOGENETIC MARKERS FOR CANCER TREATMENTS:
EXPLOITING CANCERS DEFICIENT IN THE NUCLEOTIDE POOL SANITIZING
HYDROLASES NUDT15 AND NUDT18

by

Jacob Chandler Massey

Bachelor of Science
University of Tennessee, Knoxville, 2015

Submitted in Partial Fulfillment of the Requirements

For the Degree of Doctor of Philosophy in

Pharmacology

College of Pharmacy

University of South Carolina

2022

Accepted by:

Michael Wyatt, Major Professor

Phillip Buckhaults, Committee Chair

Douglas Pittman, Committee Member

Michael Shtutman, Committee Member

Jason Stewart, Committee Member

Tracey L. Weldon, Vice Provost and Dean of the Graduate School

© Copyright by Jacob Chandler Massey, 2022
All Rights Reserved.

DEDICATION

To Nana: I love you, I miss you, and I sure wish you could've been here for this.

ACKNOWLEDGEMENTS

I would first like to thank my advisor, Dr. Mike Wyatt. I have truly enjoyed getting to work with you and learn from you over the past several years. Thank you for all the good times I've had in lab whether we were talking science, Ted Lasso, Monty Python, or anything else in between. I can't thank you enough for being such a great mentor, colleague, and friend.

To my committee members, Dr. Phil Buckhaults, Dr. Doug Pittman, Dr. Misha Shtutman, and Dr. Jason Stewart, I would like to thank all of you for your help and advice over the years as well. All of you at some point have had to deal with me showing up (completely unannounced) into your office asking for help with something and you all were always happy to help. Thank you all so, so much!

To all the past members of the Wyatt lab, especially Dr. Danda Chapagai and Dr. Chloé LeBegue-Polley, thank you for being great friends and lab mates. Danda, I could always rely on you to bounce ideas off of and be a friendly face every day in the lab. Chloé, I never, in a million years, thought that I would be as heavily involved with a project that had nothing to do with my PhD as I was with "HELin" and have as much fun as I did the entire way. Thank you both so, so much.

To my UofSC friends and family: The Hogans, Dr. Stephanie Ackerson, Logan Schuck, Dr. Olivia Spead, Dr. Erin Anderson, Dr. Megha Jhanji, Ashita Bhan, Manli Yang, Zach Mack, Dr. Carolyn Banister, Dr. Sajish Mathew, and Dr. Vitali Sikirzhyski, thank all of you for being so supportive, helpful, and such great friends over the years.

To my best friends: Michael Schilling, Brandon Hotsinpiller, and Dr. Cody Cook, thank all of you for your understanding when I would go radio silent for a couple of weeks at a time and still being so supportive when I would return. Undergrad and graduate school would've been a lot more difficult without you boys. I also must acknowledge your wonderful significant others: Jess, Whitney, and Rifeta, I'm so grateful that my friends have you three because you're all the best and the guys would be just the worst without you ladies...

To my family, thank all of you for being there every single step of the way. Mom and Dad, thank you for supporting me from day one and always being a phone call away with anything that I needed help with. I wouldn't be anywhere near the person I am today without you two. To Mitchell, I'd like to thank you and Taylin for all the support you guys have shown me and for always being genuinely curious about how my work has been going. To Sarah Stuart Partridge, thank you for being a great role model, a fantastic friend, and the closest thing I have ever had to a big sister. To Jan, Gramps, and the rest of the Melsom family and Connor, Ali, and Atlas (he'll be here by the time this is officially turned in!) Sanchez, thank all of you for being some of my biggest supporters and welcoming me into your family from basically the first day I met all of you. You all have been every bit as supportive as my own family and I can never thank you enough for it. I wouldn't be able to forgive myself if I didn't mention Winston here as well. Even though he has fallen asleep during every practice talk I have ever given at home, he has been by my side since he first became a Massey and has spent many long nights sitting with me at my home office being man's best friend. Thank you, buddy.

Finally! Last, certainly not least, and properly deserving of her own page in the Acknowledgements; I absolutely would not be writing this dissertation without the help of my future wife, Lindsay Paige. You have been my biggest supporter and #1 fan for almost 5 years now and I can't wait for us to keep cheering each other on for the rest of our lives. Thank you for everything you have done and for being my best friend. I love you!

ABSTRACT

The NUDIX hydrolases are a super family of enzymes with purported enzymatic activities of nucleotide hydrolases. The activity of the founding member, NUDT1 (also known as MTH1) is established to be a nucleotide hydrolase for d-8-oxoGTP, which is a mutagenic precursor if incorporated into DNA. Therefore, its activity serves to sanitize the nucleotide pool of mutagenic precursors. While known to be highly conserved among all organisms, the enzymatic and biological functions for nearly all the family members remain largely unexplored and unknown. Substrates of family members have been found to include canonical (deoxy)nucleotide triphosphates, oxidized (deoxy)nucleotide triphosphates, and non-nucleoside polyphosphates. Understanding the role of these enzymes would provide valuable information to aid in determining routes of cancer treatments when attempting to alter contents of the nucleotide pool. Of particular interest for this study are the members NUDT15 and NUDT18. NUDT15 has recently been identified as having a role in the metabolism of the active metabolites of 6-thioguanine (6-TG) and the anti-viral acyclovir (ACV), with both compounds showing greater therapeutic effect in NUDT15-deficient cells. NUDT15 also has an interesting link with the cell cycle regulating protein RB1, where a loss in copy number of RB1 also tends to create a loss in NUDT15 copy number as an apparent passenger deletion. Though this mechanism is not understood, both genes being within 500 kb of each other on Chromosome 13, and carcinogenic processes that drive loss of the important tumor suppressor protein RB1 also

causes loss of NUDT15. The role of NUDT18, on the other hand, remains largely unexplored with very little known of its enzymatic activities or biological functions. Here, using CRISPR generated NUDT15 and NUDT18 knock out cell lines, we attempted to identify novel substrates for NUDT15 and NUDT18 using previously published *in vitro* screenings as well as publicly available database mining.

We also characterize the Achilles heel of NUDT15 deficiency, namely cellular sensitivity to thiopurine drugs used as anticancer and immunosuppressive agents, and the antiviral agent acyclovir (ACV). We define the mechanism of action for 6-thioguanine (6-TG) and ACV treatments in NUDT15-deficient ovarian and prostate cancer cells. Using long-term treatment selectivity assays, we show with live-cell imaging that NUDT15-deficient ovarian cancer cells are more sensitive over time to 6-TG and ACV compared to NUDT15-proficient cells. Cell cycle analysis of NUDT15-deficient ovarian cancer cells shows a G2/M phase arrest following 6-TG treatment and a dramatic S-phase arrest after ACV treatment, consistent with their hypothesized mechanisms of action after incorporation into DNA. Also, using assays to assess DNA damage, we show that 6-TG and ACV treatments cause increased DNA damage in the NUDT15-deficient cells. Collectively, these results support using 6-TG or ACV as treatments in cancers found to be deficient in NUDT15. Because RB1 loss is a common carcinogenic event in a substantial subset of all cancers including prostate and NUDT15 is an apparent passenger loss in these, cancers, this represents a therapeutic window exploitable with extensively used, inexpensive therapeutics with highly defined dosing regimens and known, manageable side effects. In other words, this represents a true personalized medicine option for a subset of patients for which molecular genetic diagnosis is readily available.

TABLE OF CONTENTS

Dedication	iii
Acknowledgements	iv
Abstract	vii
List of Figures	xi
List of Abbreviations	xiii
Chapter 1: Introduction	1
1.1 Targeting the nucleotide pool and sanitation enzymes as a therapeutic option for cancer treatments	2
1.2 The purine antimetabolite family of thiopurines	4
1.3 The nucleoside analogue Acyclovir	7
1.4 The Nudix hydrolase family and their role as nucleotide pool sanitizing enzymes	8
1.5 NUDT15 deficiency as a marker in cancer treatments	10
1.6 Current knowledge about the role of NUDT18	13
1.7 Overall goal and achievements of the project	14
Chapter 2: Generation of NUDT15 and NUDT18 knockout ovarian carcinoma cells and identification of novel substrates	22
2.1 Introduction	23
2.2 Results	25
2.3 Discussion	30
Chapter 3: NUDT15 and its role in the metabolism of 6-thioguanine	41

3.1 Introduction.....	42
3.2 Results.....	43
3.3 Discussion.....	50
Chapter 4: NUDT15 and its role in the metabolism of ACV	63
4.1 Introduction.....	64
4.2 Results.....	65
4.3 Discussion.....	74
Chapter 5: General Conclusions	89
Chapter 6: Materials and Methods	99
References.....	108

LIST OF FIGURES

Figure 1.1 Comparison of the Structure of Thiopurines to Guanine	16
Figure 1.2 Metabolism of Thiopurines	17
Figure 1.3 Comparison of the Structure of Acyclovir and Ganciclovir to Guanine	18
Figure 1.4 Mechanism of Action of Acyclovir	19
Figure 1.5 Overlap of RB1 and NUDT15 copy number variation across multiple cancers in the cBioPortal Database	20
Figure 1.6 Copy Number Variation correlation between RB1 and NUDT15	21
Figure 2.1 Status of RB1, NUDT15, and NUDT18 across all cBioPortal cancer studies	33
Figure 2.2 Generation of CRISPR Knockouts in a Gene of Interest	35
Figure 2.3 Confirmation of NUDT15 CRISPR Knockout.....	36
Figure 2.4 Confirmation of NUDT18 CRISPR Knockout.....	37
Figure 2.5 NUDT18 KO cells show decreased growth rate compared to parental and NUDT15 KO cells	38
Figure 2.6 Treatment of NUDT15-deficient cells with potential novel substrates	39
Figure 2.7 Treatment of NUDT18 deficient cells with potential novel substrates	40
Figure 3.1 NUDT15 KO and KD cells show hypersensitivity to 6-thioguanine treatments.....	56
Figure 3.2 Selectivity assay shows a decrease in survival of GFP+ NUDT15 KO cells after continuous exposure to 6-TG	57
Figure 3.3 Triplex assay of NUDT15 KO cells treated with 6-TG	58

Figure 3.4 Cell-cycle profile of parental and NUDT15-deficient cells in response to 6-TG treatments.....	59
Figure 3.5 DNA Damage marker γ -H2AX induction after 6-TG treatments in NUDT15 KO cells.....	60
Figure 3.6 NUDT15 KO cells show increased chromosomal aberrations after 6-TG treatments	61
Figure 3.7 Comet assay measuring DNA damage in 6-TG treated parental and NUDT15 KO cells.....	62
Figure 4.1 NUDT15-deficient cells show increased sensitivity to acyclovir treatments	80
Figure 4.2 Selectivity assay shows a decrease in survival of GFP+ NUDT15 KO cells after continuous exposure to ACV	81
Figure 4.3 Triplex assay of NUDT15 KO cells treated with ACV.....	82
Figure 4.4 Cell-cycle profile of parental and NUDT15 KO Cells in response to ACV treatments	83
Figure 4.5 ACV treated NUDT15 KO cells are not actively synthesizing DNA in S phase	85
Figure 4.6 DNA Damage marker γ -H2AX is induced after ACV treatments	86
Figure 4.7 Comet assay measuring DNA damage in ACV treated parental and NUDT15 KO cells.....	87
Figure 5.1 Proposed model for 6-TG treatments in NUDT15-deficient cells.....	97
Figure 5.2 Proposed model for ACV treatments in NUDT15-deficient cells.....	98

LIST OF ABBREVIATIONS

6-MP	6-mercaptopurine
6-MMP	6-Methyl-mercaptopurine
6-TG	6-Thioguanine
6-TGMP	6-Thio-2'-deoxyguanosine-5'-monophosphate
6-TGTP	6-Thio-2'-deoxyguanosine-5'-Triphosphate
6-TGN	6-thioguanine nucleotides
8-oxo-dG	8-oxo-deoxyguanosine
ACV	Acyclovir
ANOVA	Analysis of the Variance
AZA	Azathioprine
CNV	Copy Number Variant
CRISPR.....	Clustered Regularly Interspaced Short Palindromic Repeats
DAPI	4', 6-diamino-2-phenylindole
dNTP	Deoxyribonucleoside Triphosphate
DMSO	Dimethyl Sulfoxide
DSBs	Double-Strand Breaks
EdU	5-Ethynyl-2'-deoxyuridine
GCV	Ganciclovir
GMPS.....	Guanosine monophosphate Synthase

gRNA	Guide RNA
HPRT	Hypoxanthine Phosphoribosyltransferase
HSV.....	Herpes Simplex Virus
HSV-TK.....	Herpes Simplex Virus Thymidine Kinase
HR.....	Homologous Recombination
IBD.....	Inflammatory Bowel Disease
IMPDH.....	Inosine monophosphate dehydrogenase
IR.....	Ionizing radiation
KD.....	Knockdown
KO.....	Knockout
MMR.....	Mismatch Repair
NHEJ.....	Non-Homologous End Joining
NT	Not Treated
NUDIX.....	Nucleoside Diphosphate-linked moiety X-type
PBS	Phosphate-Buffered Saline
PBST.....	Phosphate-Buffered Saline with Tween
PCR.....	Polymerase Chain Reaction
qPCR.....	quantitative Polymerase Chain Reaction
RNR	Ribonucleotide Reductase
ROS.....	Reactive Oxygen Species
RT-qPCR.....	quantitative Reverse Transcription Polymerase Chain Reaction
siRNA	Small Interfering RNA
SSBs.....	Single-Strand Breaks

ssDNA..... Single-Stranded DNA
TBST..... Tris Buffered Saline with Tween
TPMT..... Thiopurine Methyltransferase
UC..... Ulcerative Colitis
XO..... Xanthine Oxidase

CHAPTER 1
INTRODUCTION

1.1 Targeting the nucleotide pool and sanitation enzymes as a therapeutic option for cancer treatments

Recognized as one of the enabling characteristics of cancer, genomic instability is a feature in almost all cancer and can be the result of multiple mechanisms.¹ One of the causes of genomic instability, and often a target of cancer treatments, is the pool of nucleotides used for DNA and RNA synthesis.² The idea of targeting the nucleotide pool or the enzymes involved in DNA biosynthesis to treat cancer spans more than 70 years. One of the early cancer treatments targeting nucleotide pool alterations was methotrexate. Methotrexate, a folate antagonist, was first used in 1948 and showed significant remissions in acute lymphocytic leukemia patients.³ While the mechanism for methotrexate ultimately inhibits the biosynthesis of purine containing nucleotides, other classes of drugs, such as the thiopurines, act as antimetabolites that inhibit *de novo* purine biosynthesis or incorporate directly into DNA to cause cytotoxicity and apoptosis.⁴⁻⁶ Both the folate antagonist and thiopurine compounds continue to be used today as effective combination treatments and maintenance therapies for leukemias as well as effective anti-inflammatory and immunosuppressant compounds for autoimmune diseases such as Crohn's Disease and inflammatory bowel disease (IBD).^{7, 8}

A constant supply of deoxyribonucleoside triphosphates (dNTPs) in the nucleotide pool are required for sustained DNA synthesis during cancerous cell growth. This reliance on a steady supply of dNTPs selects for cancers that can bypass regulation of the *de novo* nucleotide synthesis pathway while simultaneously utilizing purine and pyrimidine salvage pathways.⁹⁻¹¹ Utilizing this knowledge, many anticancer drugs are antimetabolites that inhibit the enzymes involved in the metabolism of nucleotides. However, these

antimetabolites often interact with more than one enzyme in this process with an example being 5-fluorouracil (5-FU), a fluorinated pyrimidine base analog. 5-FU was determined to be an inhibitor for thymidylate synthase, but it also is metabolized into several fluorinated metabolites that ultimately become incorporated into DNA and RNA as 5-fluoro-dUTP, taking separate routes to cause cytotoxicity.¹²⁻¹⁶ While 5-FU also continues to be used today in the clinic for colorectal and breast cancers, its affinity for several enzymes supports the need to further study both the enzymes involved in the metabolism of synthesized antimetabolites and how these metabolites are broken down by sanitation enzymes in the cell.

Synthetic compounds have been used clinically to alter the nucleotide pool and adversely affect nucleotide synthesis in cancer treatments, however naturally occurring damage to nucleotides are a threat to genome integrity if modified nucleoside triphosphates that are blocking or mutagenic are incorporated into genomic DNA or RNA during replication or transcription, respectively. It is also imperative to understand the enzymes that are responsible for metabolizing these naturally occurring nucleotide pool contaminants. For example, deoxyguanosine can be quickly oxidized to 8-oxo-deoxyguanosine (8-oxo-dG) because of naturally occurring reactive oxygen species (ROS) from cellular respiration and ionizing radiation (IR).^{17, 18} The incorporation of an 8-oxo-dG residue from the nucleotide pool can ultimately lead to an AT→CG transversion mutagenesis event if the residue is not properly broken down prior to DNA synthesis. MutT is a member of a large family of hydrolases that is conserved among all species and is known as MTH1 and NUDT1 in humans.^{19, 20} MutT serves as the first line of defense in preventing the incorporation of the oxidized nucleotide by cleaving the pyrophosphate

from 8-oxo-dGTP.²¹ NUDT1 is the founding member of the 22 protein nucleoside diphosphate-linked moiety X-type (NUDIX) family that, as their name suggests, catalyze the hydrolysis of phosphorylated nucleosides.²² This family and the wide range of potential substrates in the nucleotide pool, both natural and synthetic, support further research into their roles in the cell and as viable targets to increase the efficacy of cancer treatments.

1.2 The purine antimetabolite family of thiopurines

As previously stated, the thiopurines have been used a successful treatment and maintenance therapy for leukemia and IBD for over 60 years.^{7, 8} The thiopurines are a guanine antimetabolite with a sulfur substituted at the 6-position in place of the usual oxygen atom (Figure 1.1). The family consists of three thiopurines that are still used in the clinic today: 6-mercaptopurine (6-MP), 6-thioguanine (6-TG), and azathioprine (AZA). Despite the long-term use of thiopurines, the metabolic process is still not fully understood, and patients still suffer cytotoxic effects from their use. Therefore, optimization of thiopurine treatments is still a necessity for its continued use.

While the therapeutic metabolite for all thiopurines ultimately ends up as 6-thioguanine nucleotides (6-TGN), the activation of each thiopurine is slightly different (Figure 1.2). AZA and 6-MP are both pre-drugs that require intracellular activation. AZA must first be at least partially enzymatically converted into 6-MP by glutathione S-transferase.²³ After conversion to 6-MP, there are three separate enzymatic pathways for the metabolites to follow: further activation into 6-thioinosine monophosphate (6-TIMP) by the purine salvage enzyme hypoxanthine phosphoribosyltransferase (HPRT), inactivation via methylation from thiopurine methyl transferase (TPMT), or eventual inactivation into 6-thiouric acid via xanthine oxidase (XO). The 6-MP/AZA metabolites,

when inactivated by XO, are excreted in the urine, however, inactivation via TPMT creates 6-methylmercaptopurine (6-MMP) which shows hepatotoxicity in maintenance therapy patients.²⁴ After activation by HPRT, 6-TIMP is further activated by inosine monophosphate dehydrogenase (IMPDH) into the therapeutically active 6-TGN metabolites. While 6-MP and AZA require several steps prior to becoming TGN nucleotides, 6-TG can directly be activated into 6-TGN via HPRT or inactivated via TPMT or XO in a process similar to AZA and 6-MP.²⁵⁻³² The nucleoside triphosphates 6-thio-GTP (6-TGTP) and 6-thio-dGTP, after reduction via ribonucleotide reductase (RNR), are the primary active metabolites. Recent evidence shows that both metabolites are hydrolyzed into the monophosphate form by NUDT15, where the metabolite can be further metabolized and inactivated.³³ Unpublished data from a collaborator at UofSC, Dr. Carolyn Banister, provided justification for exploring the function of NUDT18, a closely related family member to NUDT15, and whose function is poorly understood. A series of primary colon organoid normal and tumor pairs from individual patients were grown and screened for sensitivity to the approved oncology drug set. One colon cancer organoid was identified by its sensitivity to 6-mercaptopurine, and further characterization identified inactivating mutations in the *NUDT18* gene, and with corresponding wildtype *TPMT* and *NUDT15* genes. These observations support a need to further explore the roles of NUDT15 and NUDT18 in the metabolism of thiopurines and how they may lead to the exploitation of treatments based on pharmacogenetic vulnerabilities in tumors.

While DNA is the ultimate target of thiopurine treatments, the process of exerting DNA damage remains poorly understood. The 6-thio-dGTP metabolites are recognized as substrates for DNA polymerase and are incorporated in place of every 1:4,000-1:32,000

guanine bases.^{6, 34, 35} While the incorporation of 6-thio-dGTP is not toxic, methylation of the nucleotide during a second round of replication causes a 6-thio-dGTP:Thymine mispair that is recognized by mismatch repair (MMR) proteins. MMR is thought to remove the thymine nucleotide creating a lesion in the DNA that is replaced with another thymine mispairing.^{36, 37} This process creates an irreparable futile cycle that ultimately leads to the generation of DNA double strand breaks (DSBs) and cell death.³⁸ While the MMR mediated futile cycle causes DSBs and eventually cell death, cells can repair DSBs via homologous recombination (HR). HR is a repair mechanism that acts downstream of MMR after thiopurine treatments, leading to decreased sensitivity to thiopurines and increased survival.³⁹

While thiopurines are still an effective treatment today, issues pertaining to hepatotoxicity from the therapeutically inactive metabolite 6-MMP still arise and efforts to decrease risk or optimize treatments are currently underway. Methods to decrease hepatotoxicity involve screening for TPMT variants prior to starting a thiopurine treatment regime. TPMT screening has been in place for over 30 years with screening for NUDT15 potentially becoming a greater need. Some populations, in particular East Asian populations, have an increased rate of nonfunctioning NUDT15 allele variants that must be screened for prior to treatments.⁴⁰ The most likely course of action if an intolerant variant of either TPMT or NUDT15 is detected is to either prescribe 6-10% the normal dose or avoid thiopurines altogether.⁴¹ Another example for optimizing treatment involves using the XO inhibitor allopurinol to increase the amount of therapeutic 6-TGN in the serum and decrease concentrations of 6-MMP. This treatment allows lower doses of thiopurines to be used, due to the inhibition of XO as an inactivating enzyme, while still

maintaining a therapeutic concentration of 6-TGN without as high of a risk of an increase in the hepatotoxic 6-MMP metabolite.^{24, 42-45}

1.3 The nucleoside analogue Acyclovir

In 1977, Dr. Gertrude B. Elion published evidence of a newly synthesized guanine derivative with effective antiviral activity against herpes simplex virus (HSV) type 1. Originally known as acycloguanosine due to its acyclic side chain at position 9 on a natural guanosine metabolite, acyclovir (ACV) has continued to be prescribed today as an antiviral for a range of viruses including HSV, varicella-zoster virus, and cytomegalovirus.^{46, 47} The success of ACV as an antiviral has led to the production of several other nucleoside analogs for antiviral treatments including ganciclovir, which serves as a more potent treatment for cytomegalovirus (Figure 1.4).

The mechanism of action of ACV (Figure 1.5) is well understood and attributes its high selectivity for HSV infected cells. ACV achieves its antiviral effect after being metabolized into the active form acyclovir triphosphate. The initial step is the phosphorylation of the ACV side chain into ACV-monophosphate by the HSV thymidine kinase (HSV-TK) present in cells infected by the virus.^{47, 48} The ACV-monophosphate is then phosphorylated again by the cellular guanylate kinase before finally being phosphorylated to the triphosphate form by phosphoglycerate kinase, phosphoenolpyruvate carboxykinase, and pyruvate kinase.⁴⁹ The ACV-triphosphate then competes with the natural deoxyguanosine triphosphate to interact with the HSV DNA polymerase where it acts as both a substrate and an inhibitor for the substrate. The ACV-triphosphate is then incorporated into newly synthesizing DNA in place of the deoxyguanosine triphosphate. Due to the missing 3'-hydroxyl group needed for the

phosphodiester bond in the DNA backbone, elongation of DNA will halt, preventing any further replication.⁴⁷

The use of synthetic nucleotide analogs is a prevalent treatment for cancer and viruses. The idea of using an antiviral as a cancer treatment has precedence with several studies showing anti-proliferative and cytotoxic effects in cancer cells.⁵⁰ In fact, ACV has been shown to have antiproliferative effect in MCF7 human breast cancer cells and as an effective adjunct therapy to regulate Treg cells in glioblastoma patients.^{51, 52} Interestingly, recent studies support that NUDT15 may be involved in the metabolism of ACV and GCV and that the efficacy of either treatment is increased both as an anti-viral and an anti-cancer treatment.^{22, 53} While ACV becomes more efficient as an anti-cancer option in NUDT15-deficient cells, the mechanism remains to be determined.

1.4 The NUDIX hydrolase family and their role as nucleotide pool sanitizing enzymes

As previously mentioned, the NUDIX hydrolase family consists of 22 members ranging in name from NUDT1 to NUDT22.²² Due to the founding member NUDT1 previously being discovered and known as MutT, the family was originally known as the MutT family. MutT was originally identified in *E. coli* by Akiyama *et. al.* in 1989. Their findings show that, in the absence of the *mutT* gene in *E. coli*, there was an increase in AT→CG transversions at an increased rate of 100-10,000 times compared to wild type.^{21, 54} They found that MutT is directly involved in the degradation of the naturally occurring 8-oxo-dGTP as a result of spontaneous oxidation in the cell. Proteins found in humans and other mammalian cells with similar enzymatic activity and amino acid sequences were identified with human homolog becoming known as MTH1 (MutT Homolog-1).⁵⁵⁻⁶⁰ While MTH1 is the first line of defense in preventing the incorporation of 8-oxo-dGTP from

becoming incorporated in DNA, there are other glycosylases, OGG1/MutM and MYH/MutT, involved in the base excision repair DNA damage repair pathway that prevent the AT→CG transversion. The mechanism for preventing this transversion event is understood to be a conserved and well-studied method among various organisms.⁶¹

The NUDIX family were given their name due to the NUDIX box domain (GX₅EX₅[UA]xREx₂EExGU, where “U” is an aliphatic, hydrophobic residue and “x” is any amino acid) found in all family members. While there is some variation between members, the domain remains largely conserved and is the location of the phosphohydrolase activity.^{2, 62} The structural and amino acid sequence similarities between each of the family members does allow the possibilities of substrate and function redundancies. For example, three of the more similar members of the family are NUDT1, NUDT15, and NUDT18 with NUDT15 and NUDT18 being known as MTH2 and MTH3, respectively. In fact, a study by Carreras-Puigvert *et. al.* shows evidence that these three members share similar substrates *in vitro* with each enzyme having an activity against multiple substrates.⁶²

While there is mounting evidence that the NUDIX hydrolases are involved in the degradation of mutagenic bases, there is still much to learn about the physiological role of these enzymes. Of particular interest are NUDT15 and NUDT18. NUDT15, as previously described, has shown activity against the non-natural thiopurines and acyclovir, while NUDT18 has shown some evidence of activity against 8-oxo-GTP and 8-oxo-dGDP.⁶² However, *in vitro* studies show that NUDT15 has activity against canonical nucleotides including dCTP, dGTP, dTTP, and dUTP with little evidence of the purpose for the interaction with these substrates.⁶³ Regarding NUDT18, while some evidence has shown its ability to degrade 8-oxo-GTP, NUDT1 has far more activity showing that NUDT18 may

play a backup role in preventing the oxidized base from becoming incorporated into DNA.⁶⁴ Overall, while screening for NUDT15 prior to starting thiopurine treatments has increased in recent years, there has been little published pertaining to the physiological roles of NUDT15 and, especially, NUDT18.

1.5 NUDT15 deficiency as a marker in cancer treatments

The NUDIX family has a history of being targeted as a cancer treatment as evident from a 2014 Nature paper.⁶⁵ Cancer cells are known to have an increase in ROS, thus leading to an increase in oxidative damage to both DNA and the free bases in the nucleotide pool.⁶⁶ Therefore, the rationale was that inhibition of MTH1, the primary enzyme involved with 8-oxo-GTP degradation, leads to an increase in DNA damage and ultimately apoptosis in cancer cells. The initial findings were supportive of this hypothesis, demonstrating decreased cancer cell survival after treatment with an MTH1 inhibitor.⁶⁵ However, later studies using more potent inhibitors as well as CRISPR and siRNA provide evidence of an alternative, unknown mechanism for the original MTH1 inhibitor that was causing the lethality.^{67, 68} While targeting MTH1 did not have the desired effects, targeting NUDT15 for inhibition has shown potential as efficient and potent NUDT15 inhibitors are being developed.^{69, 70} These inhibitors allow for further analysis of potential novel NUDT15 substrates as well as increasing the efficacy of antiviral or other treatments in cells with NUDT15 inhibition.^{53, 69}

While work continues to create small molecules to inhibit NUDT15 and understand its role in cells, evidence is mounting that there may be clinically relevant allele variants of NUDT15 that need to be screened for prior to starting antimetabolite or nucleoside analog treatments, especially thiopurines. NUDT15 mutations or deficiencies

have no visible phenotype so screening for allele variants must be done prior to starting treatments. One major allele variant of interest, R139C, has been identified because of a missense mutation that causes a substitution of a cysteine in place of an arginine at the 139th amino acid residue. This substitution ultimately results in a thiopurine intolerance that has been seen in IBD and leukemia patients.^{40, 71-73} NUDT15 itself acts as a dimer, however the R139C variant was found to be missing a crucial ionic bond to maintain stability of the NUDT15 protein, thus causing the unstable protein to become rapidly degraded by the proteasome.³³ Therefore, this variant essentially creates a nonfunctioning NUDT15 protein that is no longer able to metabolize thiopurines. As of 2021, there have been 18 coding variants of NUDT15 alleles identified that have activity and stability ranging from “no change” to “no function” as well as some variants that have an unknown effect but are expected to create a non-functioning variant.^{74, 75} Using Genome Wide Association Studies (GWAS), a NUDT15 allele variant was identified in ~4.5% of all exome sequences in the study with East Asian (17.91%) and Latino/Admixed American (12.7%) having the highest frequencies of allele variations.⁷⁴ Due to almost 1 in 20 people having a NUDT15 variant allele, this data supports the need to screen all populations, especially those of East Asian or Latino descent, for NUDT15 variants prior to starting a thiopurine treatment. This also supports identifying other substrates of the NUDT15 enzyme to prevent any unintended toxicity, such as hepatotoxicity with thiopurines, in response to antimetabolite or nucleoside analog treatments.

While screening for NUDT15 variants is a necessity prior to starting thiopurine treatments, screening for variants is not as common of a biomarker for determining alternative cancer treatment options. Evidence found through publicly available databases

has provided evidence that NUDT15 copy number may be linked to changes in copy number of the cell cycle regulating protein RB1. In fact, data acquired from the cBio Cancer Genomics Portal (cBioPortal) supports that ~3% of the available samples in the database have an alteration in RB1 and, of those samples, 50% also have an alteration in NUDT15 copy number (Figure 1.5).^{76, 77} Further analysis also implies an almost direct correlation to copy number changes between samples with RB1 alterations (Figure 1.6A) and NUDT15 alterations (Figure 1.6B).^{76, 77} More strikingly, data acquired from The Cancer Genome Atlas (TCGA) Program shows that of the 140 prostate cancer samples with copy number variation (CNV) data, 133/140 (95%) have a loss in RB1 and 132/140 (94.29%) have an accompanying loss in NUDT15 CNV. These findings are likely due to the proximity of the NUDT15 and RB1 genes on the chromosome 13 as the genes are less than 300 kb apart. Due to RB1 being a cell cycle regulating protein thus being a tumor suppressor, its status is often screened for in a cancer diagnosis as means to proceed with therapy. Therefore, if NUDT15 is often a passenger loss when a loss in copy number of RB1 is detected, treatments that can take advantage of a NUDT15 deficiency may be able to be used in RB1-deficient cancers, if NUDT15 screening prior to treatments has not been performed.

Unpublished evidence from the United States Department of Veterans Affairs acquired by the University of South Carolina, College of Pharmacy, Clinical Pharmacy and Outcomes Sciences Department shows a potential example of a NUDT15 deficiency being utilized in a cancer prevention capacity. An 18-year study compiling data from men diagnosed with Crohn's Disease or UC has shown a significant 62% decrease in prostate cancer rates after treatment with 6-MP and the XO inhibitor allopurinol compared to those

with no treatment and 60% lower risk to the 6-MP treatment only. The men were being treated for UC or Crohn's Disease with the thiopurine therapy and gout with the allopurinol therapy. The study also notes that none of the men had a previous history of prostate cancer. While sequencing data from this study is not currently available, inferring from the data acquired from cBioPortal and TCGA pertaining to the prevalence of an RB1 and likely NUDT15 copy number loss in prostate cancer samples, this may be a real-world instance of NUDT15 loss leading to a potential biomarker for the course of cancer therapy.

1.6 Current knowledge about the role of NUDT18

While several studies pertaining to NUDT15 have been published in the last 5 years, information on NUDT18 has not been as bountiful. In fact, a PubMed search returns 5 studies containing NUDT18 in the title with the most recent being in 2018. Most available studies support that NUDT18 is also involved in the degradation of 8-oxoG and other oxidative damage to bases, though not in the primary role nor nearly as efficient as seen with NUDT1/MTH1.^{63, 78} However, NUDT18 may actually be involved with degrading the diphosphate of 8-oxoG instead of the triphosphate form.⁶⁴ Though the degradation of oxidized bases has been the accepted role of NUDT18, the data in the literature is not fully convincing and leaves a knowledge gap to be further explored.

As previously stated, NUDT1, NUDT15, and NUDT18 are genetically and structurally close related members of the NUDIX family. Evidence found by Carreras-Puigvert *et. al.* shows a cluster of substrate redundancy between these three enzymes with 8-oxoG variants and canonical nucleosides showing *in vitro* interactions with NUDT18 in particular.⁶² Though several of these substrates seem to have *in vitro* interactions with NUDT18, little is known about the *in vivo* interactions, providing a starting point to explore

natural and synthetic substrates for the NUDT18 enzyme. As previously mentioned, unpublished colon organoid data supports that 6-MP efficacy is increased in NUDT18 deficient samples with published data from Carreras-Puig *et. al.* showing a slight *in vitro* interaction with active thiopurine metabolites. This supports further exploration into the role of NUDT18 and whether this hydrolase could also be used as a biomarker for starting or selecting a course of cancer treatments.

1.7 Overall goal and achievements of the project

The over-arching goal of the project was to identify novel biomarkers in cancer that will aid in determining the course of treatments as a method to expand on personalized medicine. With this goal in mind, NUDT15 and NUDT18 were the two genes of interest for a multitude of reasons. Regarding NUDT15, the previously described link between concurrent RB1 copy number and NUDT15 copy number loss supports treating cancers with a loss of RB1 with treatments that are more effective in a NUDT15-deficient background. Two potential treatment options we expanded on were 6-thioguanine and acyclovir. For NUDT18, little is known on its function so we used previously published data to decide on potential substrates that NUDT18-deficient cells may show increased sensitivity towards.

The two primary aims of this project were to identify potential novel substrates for NUDT15 and NUDT18 and broaden our understanding of the mechanism behind the increased efficacy of 6-TG and ACV treatments in NUDT15-deficient cells. While we were not able to identify novel substrates for either NUDT15 or NUDT18, we were able to identify a potential change in growth in NUDT18-deficient cells that will need to be further explored and may have had a role into why we did not identify a novel substrate.

The treatments we used as potential substrates rely on DNA synthesis for the therapeutic effect but, due to the slower growth rate in NUDT18-deficient cells, toxicity may not have been detected during the exposure times. Regarding the increased sensitivity to 6-TG and ACV in NUDT15-deficient cells, all that was known prior to this study was NUDT15 metabolized, specifically hydrolyzed the triphosphate forms to the monophosphate forms, both drugs prior to incorporation into DNA with little published data on the mechanism of the sensitivity. Here we show more evidence of a striking increase in sensitivity in NUDT15-deficient cells with long-term treatments of both drugs using live-cell imaging as well as the underlying cell cycle-arrests and increases in DNA damage in response to the increased efficacy of both drugs.

The findings support the utilization of 6-TG or ACV as first-line treatments in cancers found to have a loss of NUDT15, thus aiding in the overall goal of expanding on personalized cancer treatments.

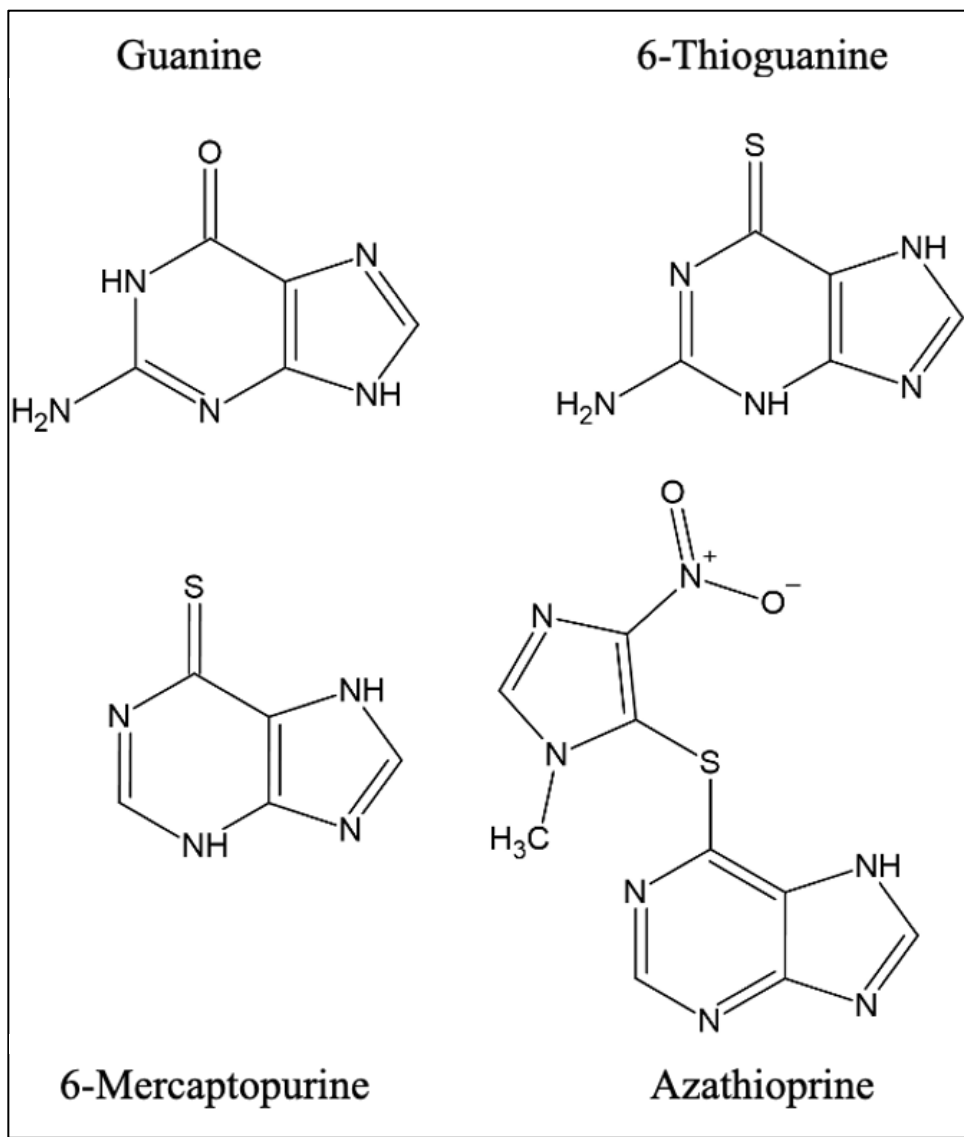


Figure 1.1 Comparison of the Structure of Thiopurines to Guanine. Structures of the canonical guanine and the antimetabolites making up the thiopurine family. From top left, clockwise: Guanine, 6-Thioguanine, Azathioprine, and 6-Mercaptopurine. Figure made using ACD/ChemSketch.

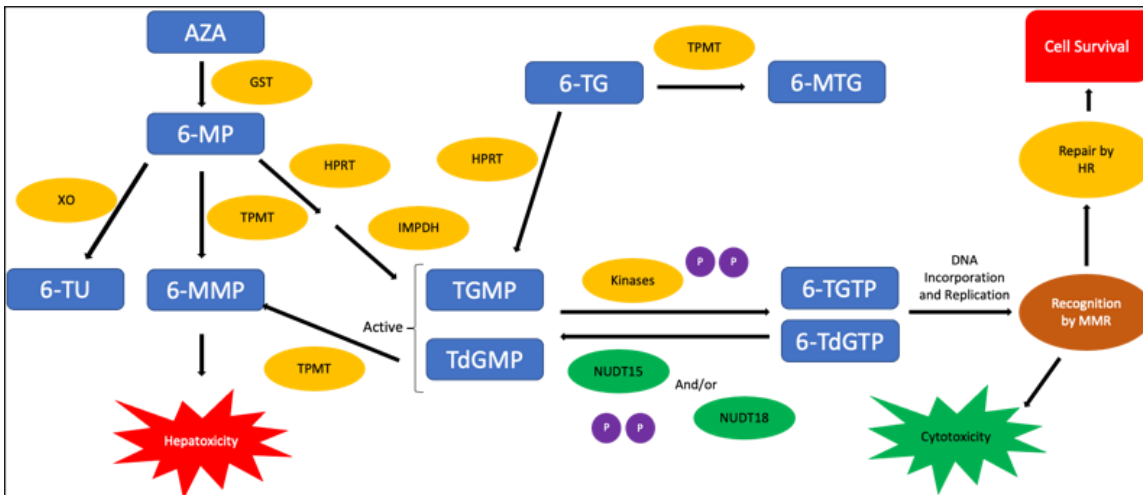


Figure 1.2 Metabolism of Thiopurines. The metabolic pathway of each thiopurine antimetabolite. Azathioprine (AZA) is prodrug first acted on by glutathione S-transferase (GST) to become 6-mercaptopurine (6-MP). 6-MP is either inactivated by XO or TPMT to 6-TU or 6-MMP, respectively, or activated by HPRT and IMPDH to the active metabolites. 6-Thioguanine (6-TG) is either inactivated by TPMT to 6-MTG or activated by HPRT into the active metabolite. The active metabolites are then phosphorylated by kinases in the cell to the triphosphate form where they are reduced to the deoxy triphosphate and incorporated into DNA. The active triphosphate metabolites may also be inactivated by the pyrophosphatase activity of NUDT15 and/or NUDT18 to the monophosphate form where the metabolite can be further inactivated to 6-MMP. After DNA incorporation and a round of replication, MMR recognizes the incorporated thiopurine and is unable to match a correct base pair. This causes a futile cycle and ultimately a DSB and toxicity in the target cells. The DSB, however, may be recognized by HR and repaired, providing a mechanism for cell survival. Figure modified from Moyer, 2021.

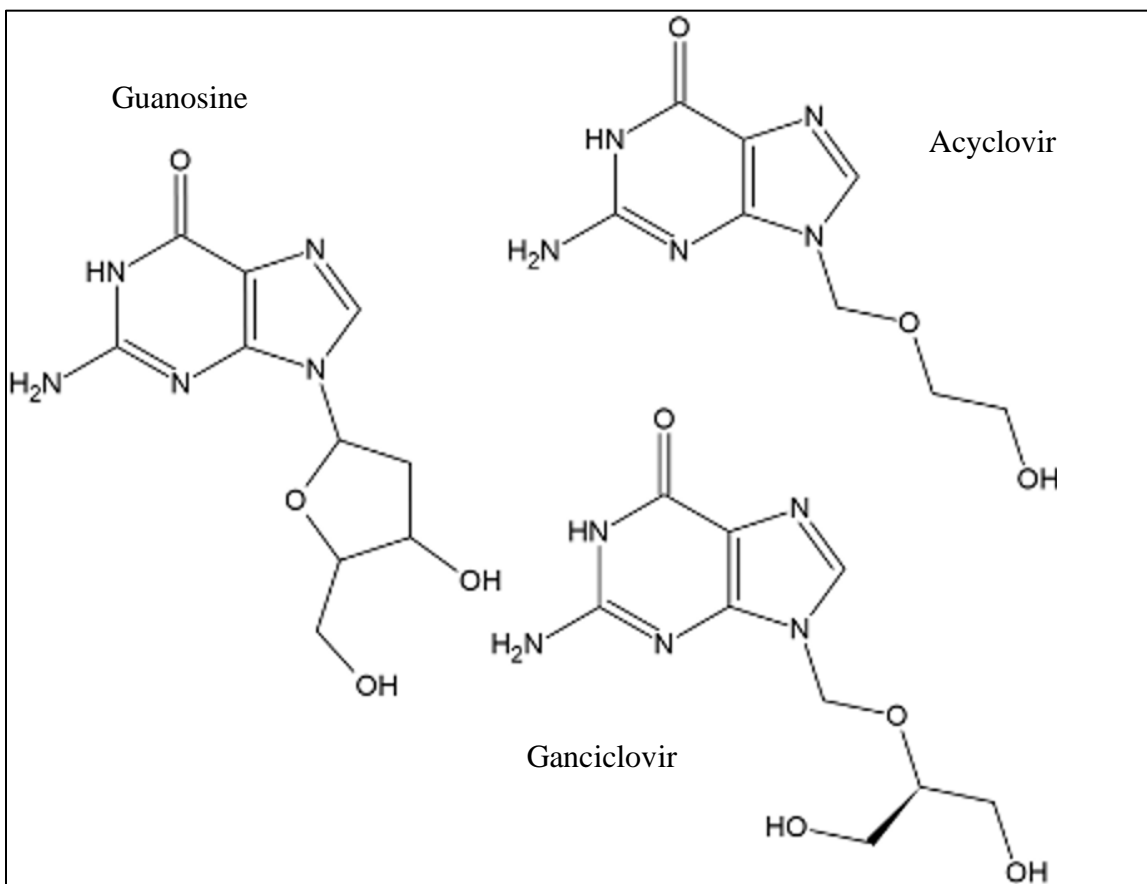


Figure 1.3 Comparison of the Structure of Acyclovir and Ganciclovir to Guanine. Structures of the canonical guanosine nucleoside and the anti-viral drugs acyclovir and ganciclovir. Starting at left, clockwise: Guanosine, Acyclovir, and Ganciclovir. Figure made using ACD/ChemSketch.

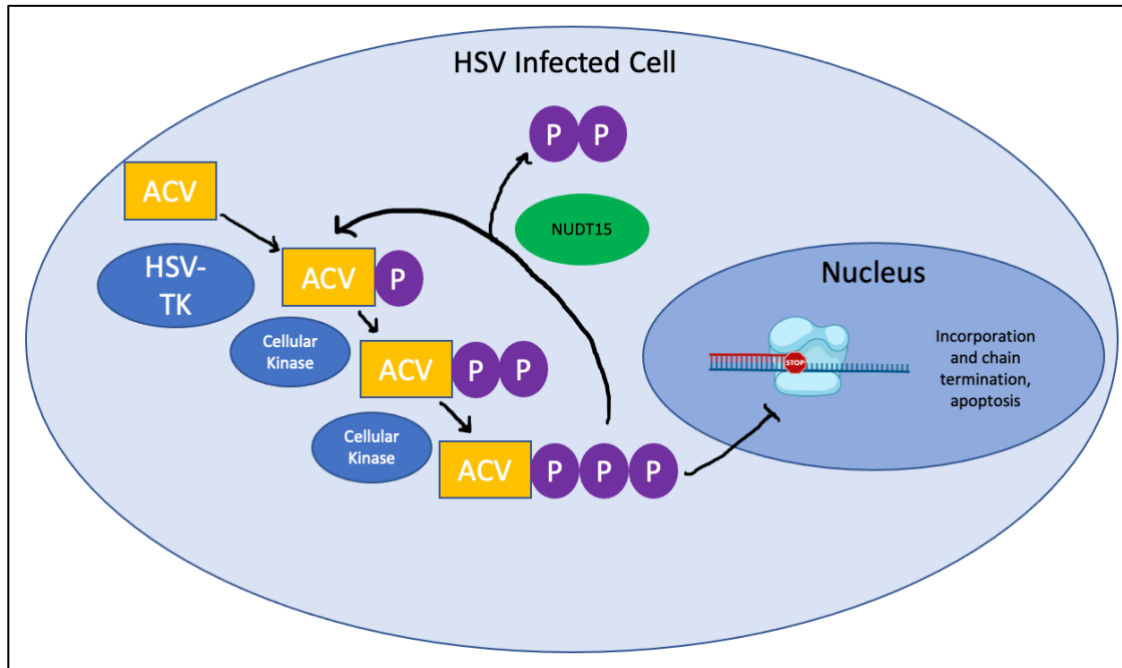


Figure 1.4 Mechanism of action of Acyclovir. The metabolic pathway of the guanosine derivative acyclovir (ACV). ACV is permeable across the cellular membrane where, in a Herpes Simplex Virus (HSV) infected cell, the metabolite is first phosphorylated by the HSV thymidine kinase. After phosphorylation into ACV-MP, cellular kinases will the further phosphorylate the metabolite until it reaches the active metabolite ACV-TP. ACV-TP is either incorporated into actively synthesizing host cell DNA or metabolized by NUDT15 into ACV-MP. If ACV-TP is incorporated into host cell DNA, this will lead to chain termination due to the missing hydroxyl group essential for DNA polymerase to continue chain growth. The stoppage in chain progression leads to apoptosis and ultimately the selective killing of HSV-infected cells. Figure partially created with BioRender.com.



Figure 1.5 Overlap of RB1 and NUDT15 copy number variation across multiple cancers in the cBioPortal Database. Data from cBioPortal shows an alteration of 7% and 1.8% of RB1 and NUDT15, respectively, in samples in the database, regardless of the cancer type in multiple studies. Of those samples, approximately 45% have an alteration in the copy number of RB1. In those samples with changes in RB1 copy number, approximately 50% also have a change in NUDT15 copy number. Figure acquired from cBioPortal.

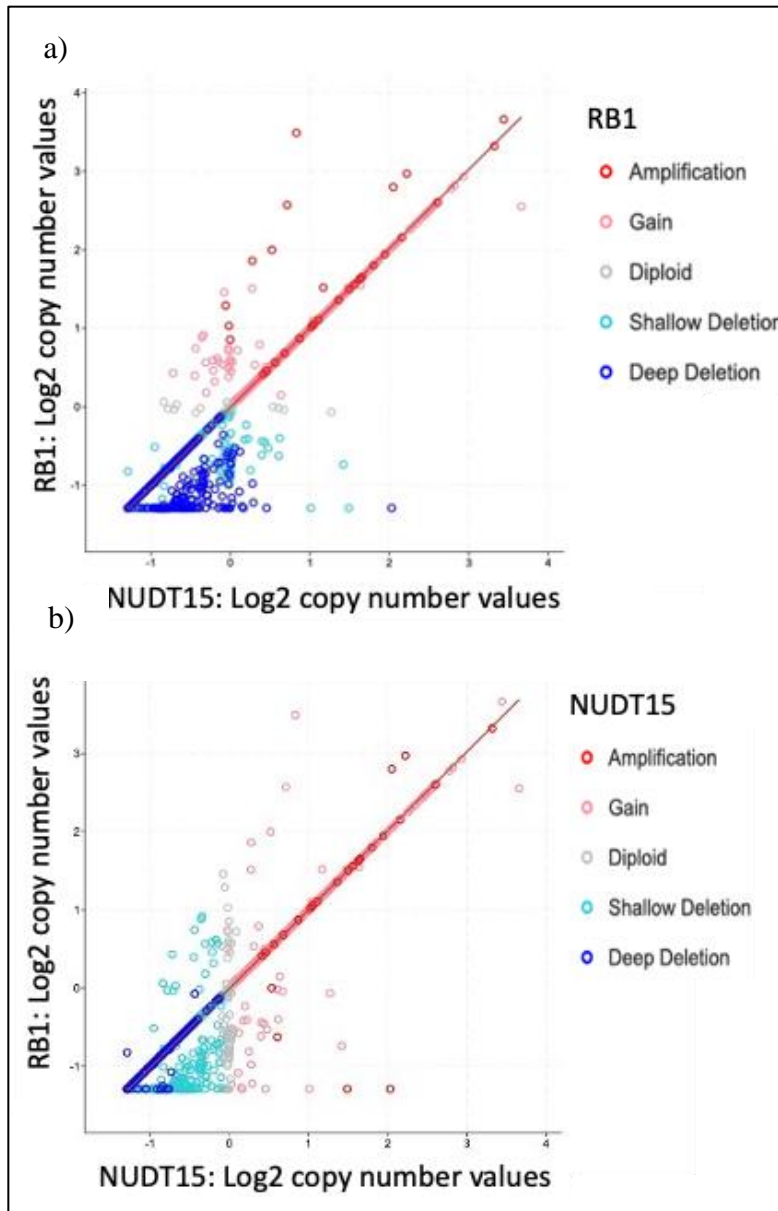


Figure 1.6 CNV correlation between RB1 and NUDT15. Evidence showing an almost direct correlation between the Log2 copy number of RB1 (y-axis) and NUDT15 (x-axis) across all studies and all cancers in the cBioPortal Database with CNV data of the two genes. A) Copy number status of RB1 with red being amplified and blue being a deep deletion of genetic information. B) Copy number status of NUDT15 with red being amplified and blue being a deep deletion of genetic information. Figures acquired and modified from cBioPortal.

CHAPTER 2

GENERATION OF NUDT15 AND NUDT18 KNOCKOUT OVARIAN CARCINOMA CELLS AND IDENTIFICATION OF NOVEL SUBSTRATES

2.1 Introduction

The nucleoside diphosphates linked to moiety-X (NUDIX) hydrolases are a super family of enzymes that are conserved across all species.^{19, 20} The founding member of the family, MutT, was first referenced in the 1950s but its function was not more fully understood until the 1990s where it later became known in humans as MutT Homolog 1, MTH1.²⁰ MTH1 remains the most well understood member of the NUDIX family of enzymes; however, the biological function of most other members of the NUDIX family remain poorly understood and others remain completely uncharacterized. After further research into other members of the family, evidence supports that the NUDIX family members have sequential and structural similarities with members NUDT15 and NUDT18 being the closest related to MTH1.⁶² NUDT15 has been identified more recently as being involved in thiopurine metabolism and pharmacogenetic variants of clinical relevance have been identified for screening prior to starting thiopurine treatments,^{33, 40} Yet, the biological function and other potential substrates of NUDT15 remain largely unknown. NUDT18 remains very poorly understood with little known about its biological function. Understanding the roles of NUDT15 and NUDT18 will better define their activities and impact on pharmacogenetics. Such knowledge could also advance personalized medicine by taking advantage of cancers with loss of function mutations in NUDT15 or NUDT18.

Data available through The Cancer Genome Atlas (TCGA) shows an interesting link between the cell cycle regulating protein RB1 and NUDT15. Both genes are located on Chromosome 13 less than 500 kb apart. Data from the TCGA shows that, out of 140 prostate cancer cases with copy number variant data available, 133 cases show a CNV loss in RB1. Of those 133 cases, 132 cases also have a loss in NUDT15 copy number showing

a common passenger loss likely because of the unknown mechanism that causes copy number loss of RB1. Analysis in the cBioPortal for Cancer Genomics database shows that this trend in simultaneous CNV loss for both RB1 and NUDT15 is common amongst multiple cancer types (Figure 2.1). For example, the only alteration to NUDT15 CNV is a loss of information in prostate and ovarian cancers with RB1 also commonly showing a loss in CNV. Since RB1 loss is commonly screened for prior to cancer treatments, detecting a loss in RB1 often correlates to a loss in NUDT15 which can then be exploited therapeutically through treatments, such as 6-TG, that would have increased efficacy in NUDT15-deficient cancers.

Database mining was performed to further explore how genetic defects in NUDT15 or NUDT18 might be exploited therapeutically. The Broad Institute's DepMap Portal was utilized to identify compounds to which cells deficient in either NUDT15 or NUDT18 may show increased sensitivity. One of the more interesting correlations found was that NUDT15-deficient cells may show an increased sensitivity to inhibitors of the protein kinase MEK. Additionally, using work published by Carreras-Puigvert *et. al*, several potential substrates were selected for which NUDT15 or NUDT18 showed *in vitro* activity, including the canonical nucleoside thymidine for NUDT15 and the thymidylate synthase inhibitor 5-fluorodeoxyuridine (5-FDU) for NUDT18. The potential for substrate redundancy between the NUDIX family encourages exploration whether different members show activity against the same substrates. Therefore, activity against 6-TG by NUDT18 and activity by NUDT15 against nucleotides oxidized by ionizing radiation will be assessed.

To address the need to further explore novel roles for NUDT15 and NUDT18 and identify either as a potential biomarker for determining a route for cancer therapy, CRISPR knockout cell lines in each gene were established with the aim to identify novel substrates based on previous studies and DepMap data analysis. This chapter reports the generation, characterization, and initial phenotypic testing of NUDT15 and NUDT18 knockouts in an ovarian cancer cell line.

2.2 Results

2.2A Generation and confirmation of NUDT15 and NUDT18 knockouts in OVCAR-8 Cells

To aid in determining the roles of NUDT15 and NUDT18 in cells, NUDT15 and NUDT18 knockouts (KOs) using CRISPR/Cas9 technology in the OVCAR-8 ovarian carcinoma cell line were established. CRISPR KOs were established using two lentiviral-delivered plasmids. The first plasmid encodes the Cas9 protein with an N-terminal FLAG tag and blasticidin resistance for selectivity. The second plasmid encoded two small guide RNA (sgRNA) sequences, a green fluorescent protein (GFP) marker, and puromycin resistance for selectivity. The two sgRNAs allow two Cas9-mediated DSBs to form, thus leading to the deletion of the genomic DNA material between the breaks. This deletion can then be detected by PCR as evident by the production of an approximately 500 bp product that is only possible if the deletion has occurred (Figure 2.2).

Using the above method, a NUDT15 KO cell line was created in the OVCAR-8 cells, herein referred to as “NUDT15 KO” or “NUDT15-deficient” cells. To confirm the KO, gDNA was amplified from the putative NUDT15-deficient cells and the WT parental cells stably expressing Cas9, herein referred to as the “parental” or “proficient” cells. As

previously described, PCR primers were designed to amplify the gDNA sequence surrounding the target sequence of the dual-sgRNA cut sites. An approximately 500 bp product was amplified in the NUDT15 KO cell line that was not detectable in the parental cell line supporting the generation of a NUDT15 KO (Figure 2.3A). Western blot analysis of the parental and putative NUDT15 KO cells further supports there was a successful KO of NUDT15 in the OVCAR-8 cells. The KO is evident by the robust NUDT15 expression in the parental cells compared to the absence of a band in the KO cell line (Figure 2.3B).

To develop NUDT18 KOs in the OVCAR-8 cells, clonal isolates were generated and the proposed ~500 bp product was amplified by PCR. Clones 969-4 and 969-9 were selected for further experimentation, herein referred to as “Clone 4” and “Clone 9”, respectively (Figure 2.4A). Clone 4 was selected due to the presence of the 500 bp product with larger bands suggested alternate repair of the DSBs at the gRNA cut sites. Clone 9 was selected because of the single product at 500 bp (Figure 2.4A). Three RT-qPCR primer pairs were designed to amplify a sequence not affected by the gRNA in “18 FR 1”, amplification of sgRNA site A in “18 FR 2”, and amplification of sgRNA site B in “18 FR 3” (Figure 2.4B). RT-qPCR shows that the mRNA for NUDT18 is almost non-existent in the putative NUDT18 KO cell lines, regardless of the location of the amplicon sequence, supporting two clones containing NUDT18 KOs. Using the $\Delta\Delta\text{CT}$ determined by normalizing NUDT18 mRNA to housekeeping gene GAPDH mRNA CT values, primer pair N18 FR1 detected 0.02% and 72.3% of NUDT18 mRNA compared to the parental cell line in Clones 4 and 9, respectively. Primer pair N18 FR2 detected 11.11% in Clone 4 and 0.1% in Clone 9 compared to the parental cells, while primer pair N18 FR3 had no detectable NUDT18 mRNA in either of the clones (Figure 2.4 C and D). Unlike NUDT15,

currently there is not a commercially available antibody to provide reliable NUDT18 protein expression analysis. Evidence of the predicted PCR product from the CRISPR dual-sgRNA system as well as the inability to detect NUDT18 mRNA supports the generation of two NUDT18 KO clones. Interestingly, a visible negative effect in cell growth was observed in the NUDT18 KO clones that was not seen in the NUDT15 KO cells compared to the parentals (Figure 2.5A). A growth curve shows that, after 6 days of growth, the parental and NUDT15 KO cells have almost identical growth and cell numbers of ~30,000 cells/mL (Figure 2.5A top row, Figure 2.5B blue and red) while both NUDT18 clones show smaller colonies and remain below 10,000 cells/mL (Figure 2.5A bottom row, Figure 2.5B purple and orange).

2.2B Search for novel substrates for NUDT15

With evidence supporting NUDT15 having an active role in thiopurine metabolism^{33, 63}, we first wanted to confirm the expected increase in sensitivity to 6-TG treatments in NUDT15-deficient OVCAR-8 cells. Due to the mechanism of action of thiopurines requiring two rounds of replication to exhibit cytotoxic effects, a colony forming assay was used to allow a longer treatment and recovery period to see changes in sensitivity to 6-TG. The NUDT15 KO cells show a significant increase in sensitivity starting at a 0.3 μ M dose of 6-TG with a less than 50% survival compared to the parental cells. Survival of the NUDT15 KO cells remain significantly lower at the higher doses (Figure 2.6A). This hypersensitivity to 6-TG was an expected phenotype in the NUDT15-deficient cells and served as a phenotypic confirmation of NUDT15 knocked out in the OVCAR-8 cells.

While NUDT15 is known to have activity against the 6-TG active metabolites 6-thio-GTP and 6-thio-dGTP, attempts were made to identify other novel substrates that the NUDT15-deficient cells may have changes in sensitivity to after treatment. NUDT15 KO cells were treated with the MEK inhibitor selumetinib after data mining in the Broad Institute DepMap identified a potential negative correlation between NUDT15 deficiency implying increased sensitivity to MEK inhibitors. Using a resazurin assay, there was no change in the sensitivity between the NUDT15 KO cells and the parental cells after 72 hours of treatment at a range of doses (Figure 2.6B). NUDT15 activity against ionizing radiation induced oxidative damage to the nucleotide pool through generation of ROS⁷⁹ was also assessed by a colony forming assay. However, there was no change in sensitivity to IR exposure in the NUDT15 KO cells compared to the parental cells after a recovery of 10 days (Figure 2.6C). Due to the increase in sensitivity to 6-TG in the NUDT15-deficient cells, cells were treated with another guanosine analog in ganciclovir to determine if a NUDT15 KO showed a change in sensitivity against a structurally similar compound. NUDT15 also showed activity *in vitro* against GTP⁶² so we predicted NUDT15 may have activity against GCV-triphosphate, a guanosine analog, prior to its incorporation into DNA. However, there was no change in sensitivity in the NUDT15 KO cells compared to the parental cells after a 72 hour exposure to GCV (Figure 2.6D).

2.2C Search for novel substrates for NUDT18

With little known about the natural function of NUDT18, attempts were made to identify novel substrates in the two NUDT18 KO clones. Substrates were identified based on published *in vitro* data⁶² and unpublished organoid culture data suggesting that NUDT18 deficiency causes sensitivity to 6-MP. Cells were treated with 6-TG to determine

if there was a redundancy in function between NUDT18 and NUDT15. Due to the structural similarity between NUDT15 and NUDT18, substrate redundancy or a similar function was possible between both enzymes that needed to be determined. Using a colony forming assay, there was no difference in sensitivity in either of the NUDT18 KO clones compared to the parental cells (Figure 2.7A).

Based on *in vitro* data published by Carreras-Puigvert *et al.*, NUDT18 showed low activity against both the canonical nucleoside thymidine and the antimetabolite 5-fluorodeoxyuridine (5-FDU).⁶² 5-FDU is the active metabolite of the thymidine kinase inhibiting drug 5-FU. A colony forming assay shows little difference in sensitivity in the NUDT18 KOs compared to the parental cells when treated with thymidine and 5-FDU (Figure 2.7B). High concentrations of thymidine are experimentally used to synchronize cells in G1/early S-phase but long term treatment will cause cell death.⁸⁰ We were curious as to whether a NUDT18 KO alters thymidine metabolism, thus leading to an increase in sensitivity to high doses of thymidine. However, after treating with high doses of thymidine in a colony forming assay, there was no change in sensitivity in the NUDT18 KO cells (Figure 2.7C).

Because of the published *in vitro* data,⁶² NUDT18 may have activity against the anti-viral ganciclovir (GCV) based on the structural similarity between GCV and guanosine. Evidence of NUDT18 showing activity against GDP *in vitro* supported our prediction that GCV-DP may be recognized by NUDT18 prior to the final phosphorylation into GCV-TP and DNA incorporation. After 72 hours of treatment with GCV, a resazurin assay showed there was no change in sensitivity between the NUDT18 KO cells and the parental cells (Figure 2.7D). NUDT18 KO cells were also treated with the anti-herpes drug

acyclovir (ACV). ACV is also a guanosine derivative and has a similar structure to GCV (Figure 1.3). After 72 hours treatment with ACV, no difference in sensitivity was seen in either of the NUDT18 KO cells compared to the parental cells.

2.3 Discussion

The NUDIX hydrolase family is a conserved group of enzymes involved in the sanitizing of the nucleotide pool and may be valuable enzymes to determine routes of cancer treatments. Using lentiviral delivered plasmids containing CRISPR-Cas9 and two sgRNA sequences, NUDT15 and NUDT18 were both knocked out in the ovarian carcinoma cell line OVCAR-8. Using PCR to amplify the 500 bp product signifying a deletion of genomic DNA in the *NUDT15* gene and a western blot to analyze levels of NUDT15 present, we confirmed that both the genetic material and the protein product were successfully knocked out in the NUDT15-deficient cell line (Figure 2.3). Regarding NUDT18, Clone 4 and Clone 9 were selected after PCR amplification of a 500 bp product supporting the deletion of genetic material at the *NUDT18* gene. Because of poor availability of an efficient NUDT18 antibody, RT-qPCR was used to determine the prevalence of NUDT18 mRNA in the putative knock out clones. RT-qPCR results support the mRNA coding for the NUDT18 protein is no longer stable or being produced at the location of the sgRNA target sites, thus supporting the NUDT18 protein no longer being produced (Figure 2.4).

After confirmation of NUDT15 and NUDT18 knockouts, an interesting difference in growth rates was easily detectable in the NUDT18 clones. Clones 4 and 9 show a drastic difference in growth rate compared to the parental and NUDT15 KO cells. This implies that NUDT18 may have an essential role in allowing normal cell proliferation that has not

been explored yet. Because of the putative role of the NUDIX hydrolases as nucleotide pool sanitizing enzymes, NUDT18 may be involved in the prevention of a naturally occurring nucleotide pool contaminant that slows cell growth rate. As the idea of substrate redundancy among family members makes experimentally determining individual roles for the NUDIX hydrolases difficult, NUDT18 may have a unique role that could be further explored through metabolomic studies.

While there is evidence of NUDT15 metabolizing the active forms of 6-TG and ACV,^{22, 33} the biological functions of NUDT15 and NUDT18 remain largely unknown. Based on *in vitro* data published by Carreras-Puigvert *et. al* and publicly available data from The Broad Institute DepMap portal, we chose nucleoside analogs that might be substrates for NUDT15 or NUDT18 and exposed NUDT15 and NUDT18 KO cells to these treatments that may show a change in sensitivity, thus a potential clue to their biological purposes. The NUDT15 KO cells show the expected hypersensitivity to 6-TG and to ACV (Chapters 3 and 4 respectively) but we were not able to detect a sensitivity change to other treatments (Figure 2.6). However, there is evidence of ganciclovir also showing increased efficacy in NUDT15-deficient cells,^{22, 53} but there is likely variation between cell models that may play a role in GCV efficacy that is not explored in this study.

Regarding NUDT18, a similar approach as in the NUDT15 KO cells to determine treatments was utilized. Very little is known on the function of NUDT18, so any data acquired is useful for directing future studies. To explore a potential substrate redundancy with NUDT15 and expand on unpublished patient-derived organoid data from a collaborator, cells were also treated with 6-TG to determine if there is a change in sensitivity in NUDT18-deficient cells. There was no observable change in sensitivity in

either of the NUDT18 KO clones. Again, this may be because of differences between the OVCAR-8 cell line and the organoids from the patient that have not been explored for this study. Using the *in vitro* data from Carreras-Puigvert *et. al*, NUDT18 showed activity against the thymidine synthase inhibitor 5-fluorodeoxyuridine and the canonical nucleoside thymidine. After treatments with both, there was no observable change in sensitivity in either of the NUDT18 clones compared to the NUDT18-proficient cell line. NUDT18 KO cells were also treated with the anti-viral drugs acyclovir and ganciclovir to determine if a similar change in sensitivity is observed as in the NUDT15 KO cells. After treatments, no change in sensitivity was observed with either drug, supporting there is no substrate redundancy with NUDT15 (Figure 2.7).

Overall, the findings presented in this chapter, while showing no clear novel substrates for either NUDT15 or NUDT18, may direct future studies to any of countless other modified nucleotides or other approved therapies that alter nucleotide pool contents. Future directions should also be focused on determining changes in the metabolites present in NUDT15 and NUDT18 KO cells to further narrow down biological functions of either enzyme. Because of the nature of the NUDIX hydrolases being involved in nucleotide pool sanitization, sequencing the genome of NUDT15 and NUDT18 KO cells may also increase mutations the natural substrates of either may have as cells are proliferating. Therefore, whole genome sequencing to look for mutational signatures may also provide a direction for determining the biological functions of NUDT15 and NUDT18.

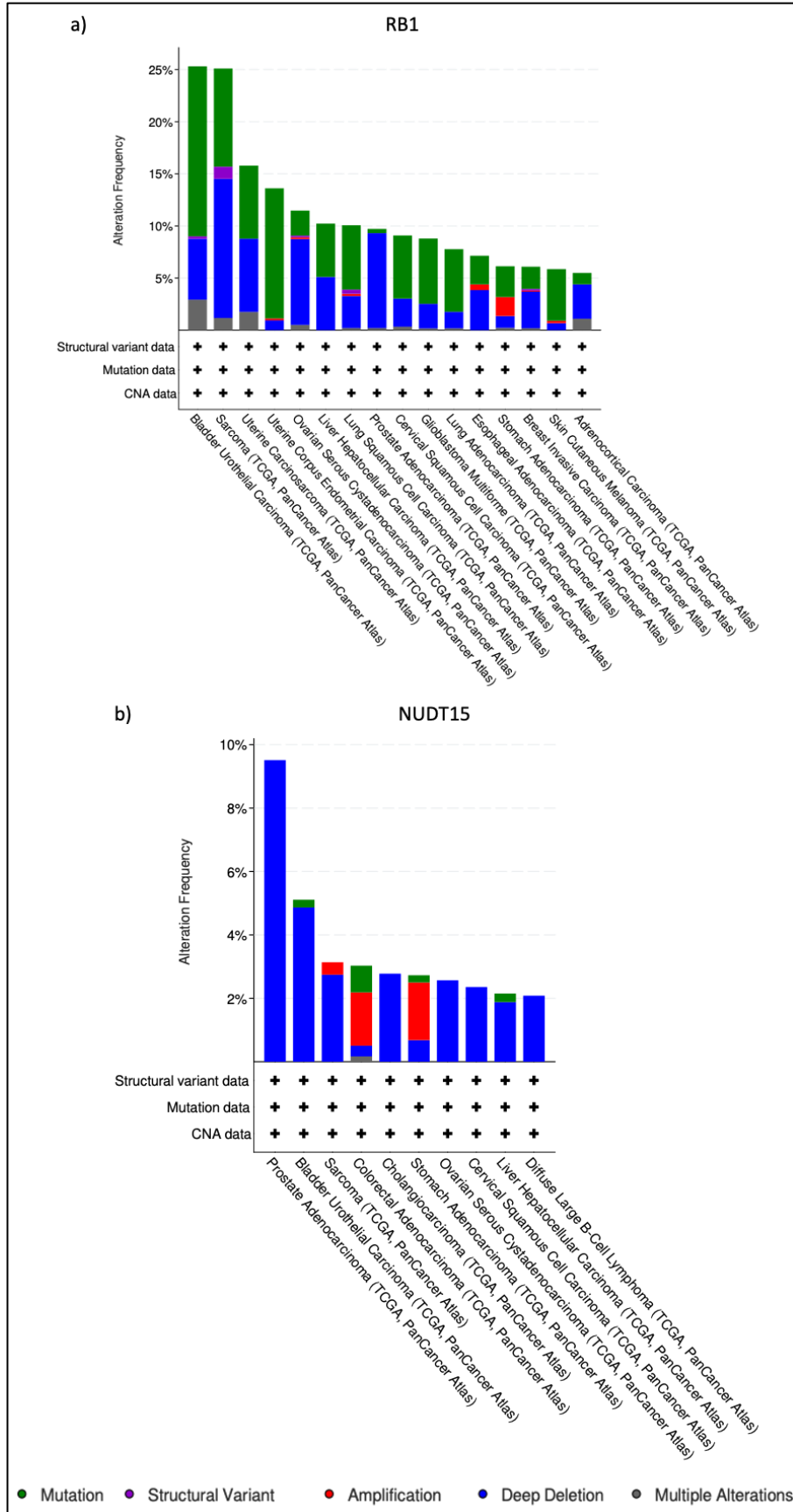


Figure 2.1 Status of RB1 and NUDT15 copy number across all cBioPortal Cancer studies (Previous Page). For both figures, the y-axis serves as the percentage of alteration frequency and the x-axis is the type of cancer with the study name in parenthesis. The color of each section of the bar graphs correspond to the legend below the figures. A) RB1 copy number status. B) NUDT15 copy number status. Figures collected from cBioPortal.

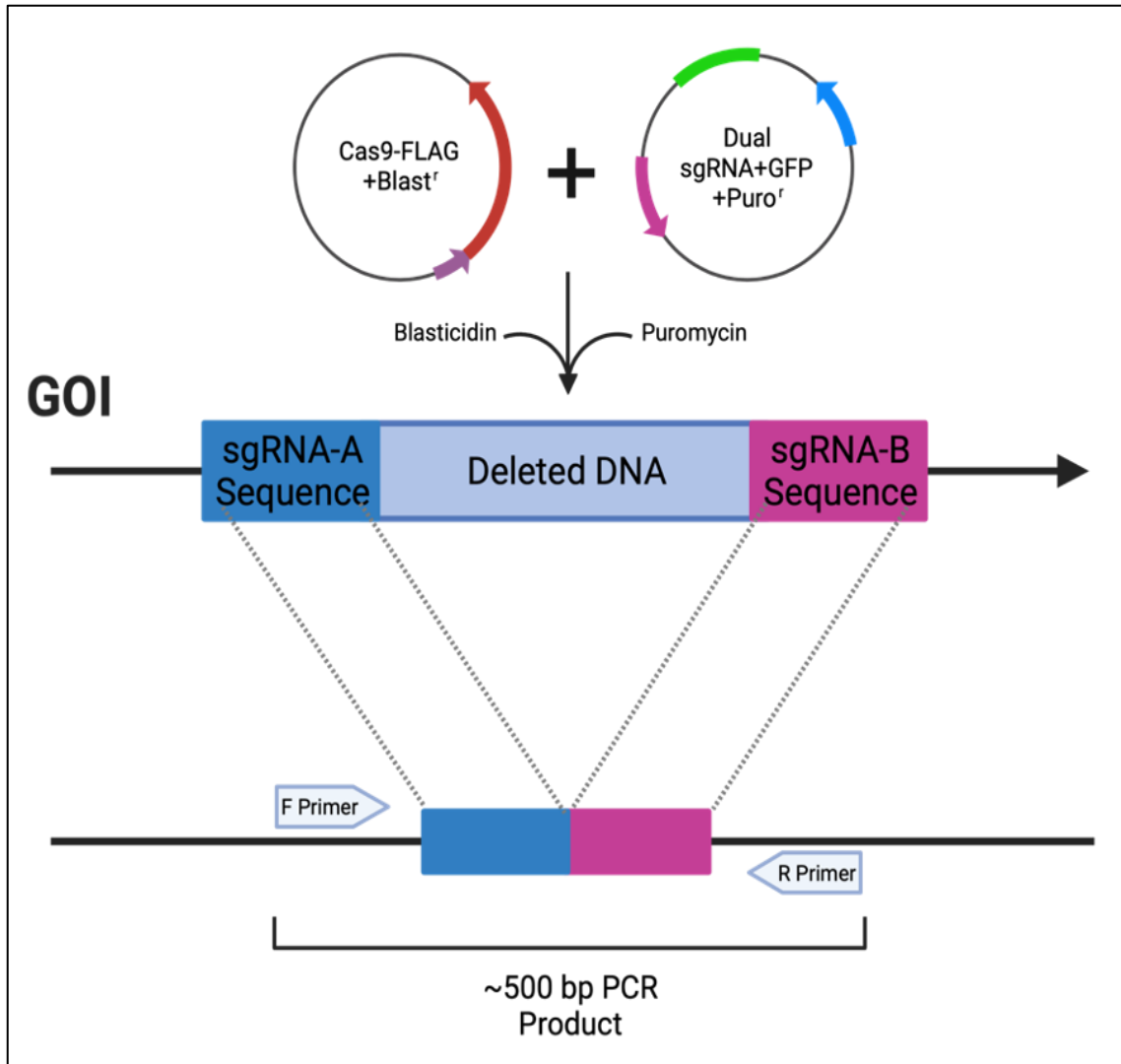


Figure 2.2 Generation of CRISPR KOs in a Gene of Interest (GOI) schematic. Plasmids containing FLAG-tagged Cas9 and dual sgRNAs for the gene of interest were stably transduced into OVCAR-8 cells using lentiviral vectors. The Cas9 vector was selected with 15 $\mu\text{g}/\text{mL}$ of blasticidin over 96 hours and the dual-sgRNA vectors were selected with 2 $\mu\text{g}/\text{mL}$ of puromycin over 72 hours. Cells after addition of the dual-sgRNA vector became stably GFP⁺. The dual sgRNA containing cells cause two DSBs at the location of the sgRNA sequence, causing a deletion of genetic information between the two sites. The new product, after deletion, could then be amplified via PCR to create an approximately 500 bp sequence as a confirmation of the deletion of DNA. Figure made using BioRender.

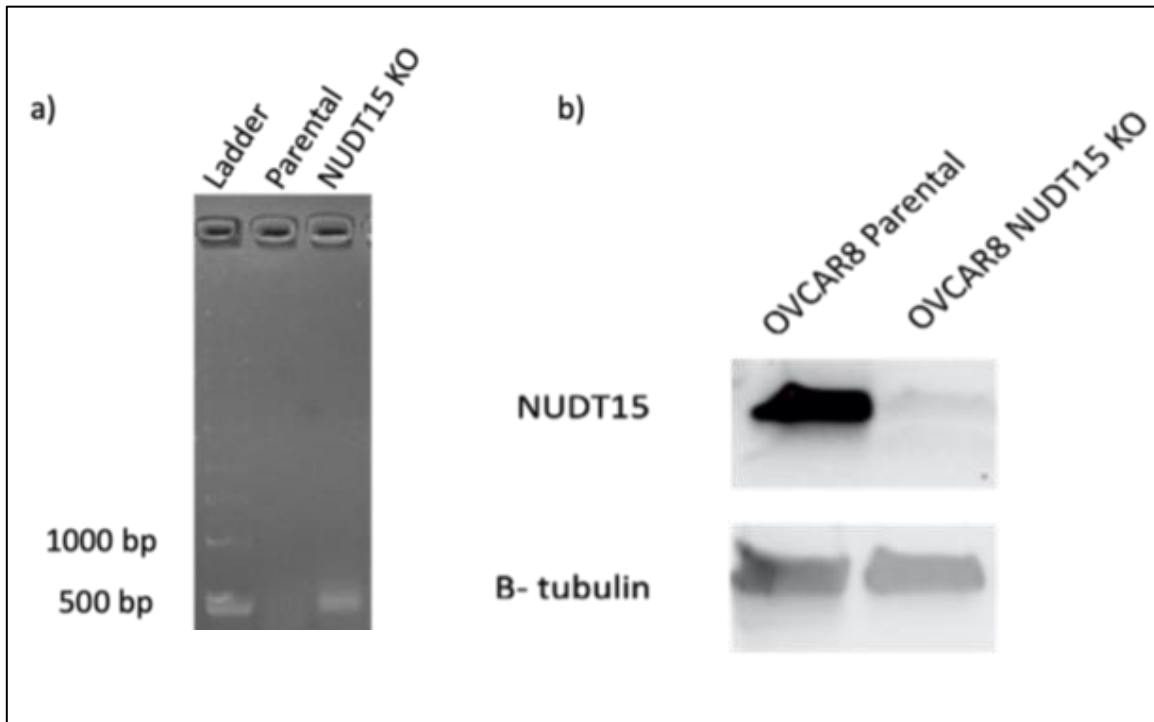


Figure 2.3 Confirmation of NUDT15 CRISPR Knockout. To confirm a knockout of NUDT15 in the OVCAR8 cells, gDNA and protein was isolated for PCR and western blot analysis. A) Primers were designed to flank the location of the dual-sgRNA target sequences with PCR amplification of an approximately 500 bp product supporting a KO of the genetic information coding for NUDT15. The left lane shows the 1 kb ladder. The middle lane shows parental OVCAR8 gDNA amplified with the primers and no discernable 500 bp product amplified. The right lane shows a 500 bp product formed in the NUDT15-deficient cell line, implicating a KO of genetic information at the dual-sgRNA target sequences. B) Western blot analysis supports a KO in the NUDT15-deficient cell line. The top left band shows robust NUDT15 expression in the proficient cell line while the right band shows a profound decrease in NUDT15.

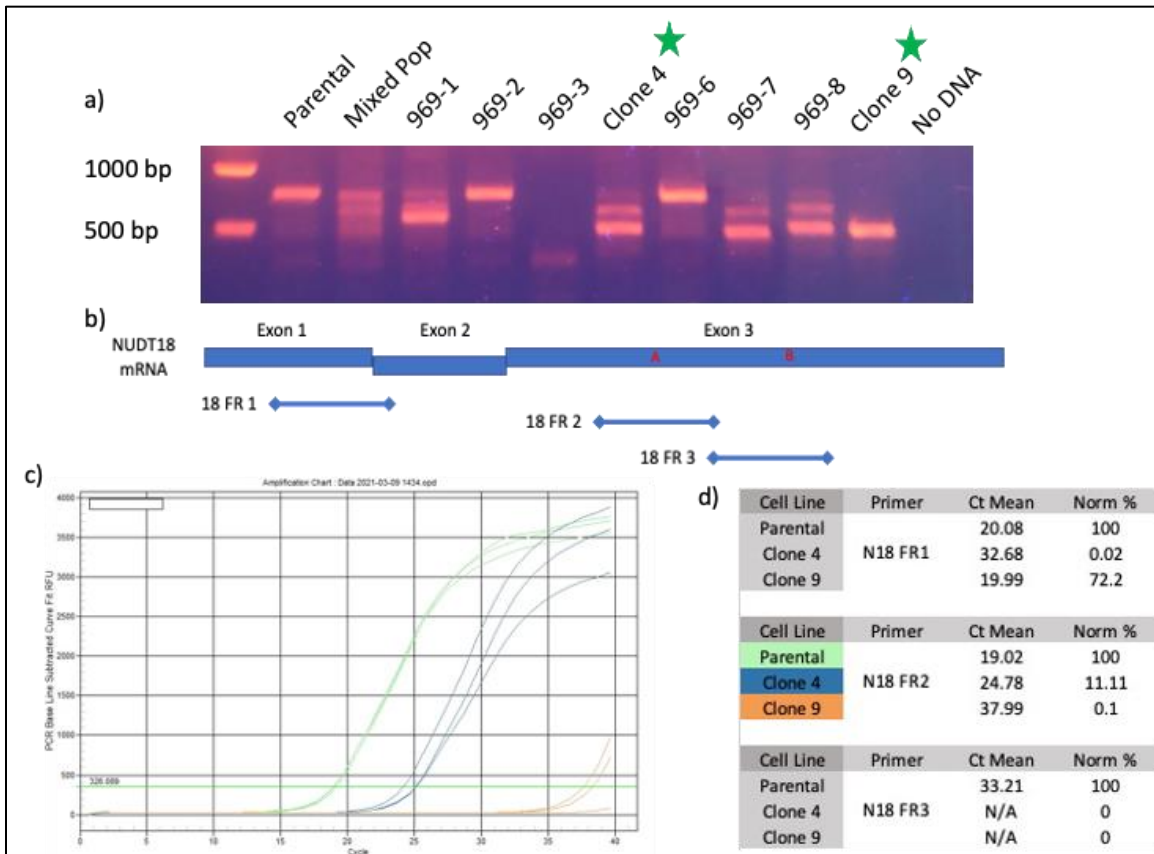


Figure 2.4 Confirmation of NUDT18 CRISPR Knockouts. To confirm a KO of NUDT18 in the OVCAR-8 cells, clonal isolates were established and the RNA of selected isolates were collected for RT-qPCR analysis. A) Clonal isolates were generated and the PCR amplification of an approximately 500 bp product supported that the dual gRNA vectors generated a KO. Clones 4 and 9 were selected for further analysis (green stars) due to the formation of a 500 bp product. B) A cartoon of the NUDT18 mRNA showing the locations of the two gRNA cut sites, labeled A and B, and the approximate location of each primer pair for qPCR. C) A representative image of the RT-qPCR amplification chart showing the differences in Ct values between the parental proficient cell line and the putative NUDT18 deficient cell lines using the N18 FR2 primer pair. D) Quantification and $\Delta\Delta\text{CT}$ normalization values of the presence of NUDT18 mRNA in the OVCAR-8 parental cells and the OVCAR-8 NUDT18 KO cells; $\Delta\Delta\text{CT}$ values determined by normalization to GAPDH mRNA.

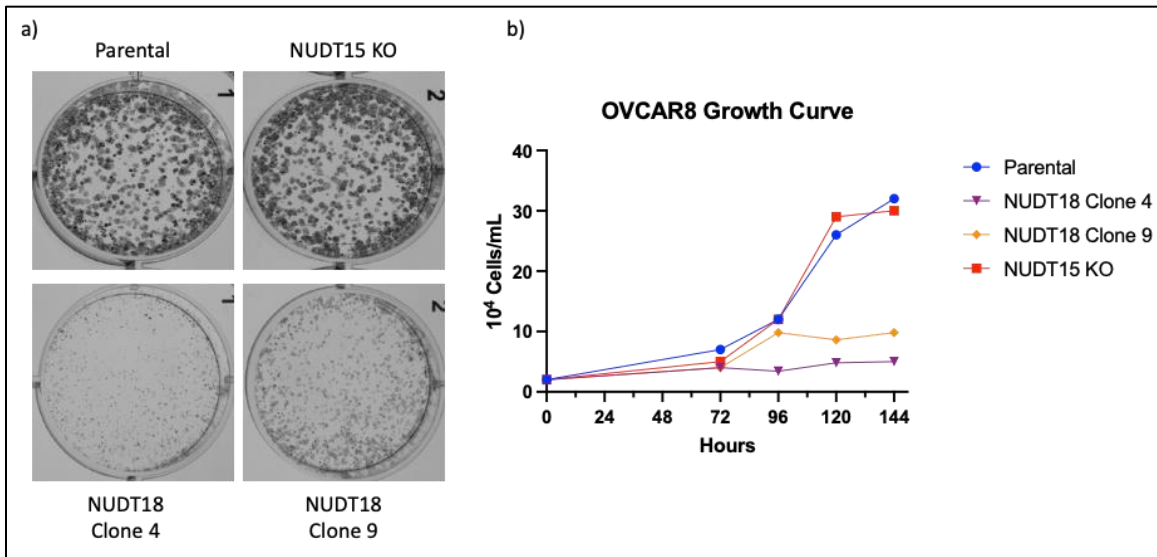


Figure 2.5 NUDT18 KO cells show decreased growth rate compared to parental and NUDT15 KO cells. Cells were seeded at a density of 2000 cells per well and were allowed to incubate for 72 hours prior to the first well being counted. Cells were then counted on a hemocytometer to determine the density of cells/mL at each indicated timepoint. A) Representative images of cells after 6 days of growth. B) Cell counts at each time point.

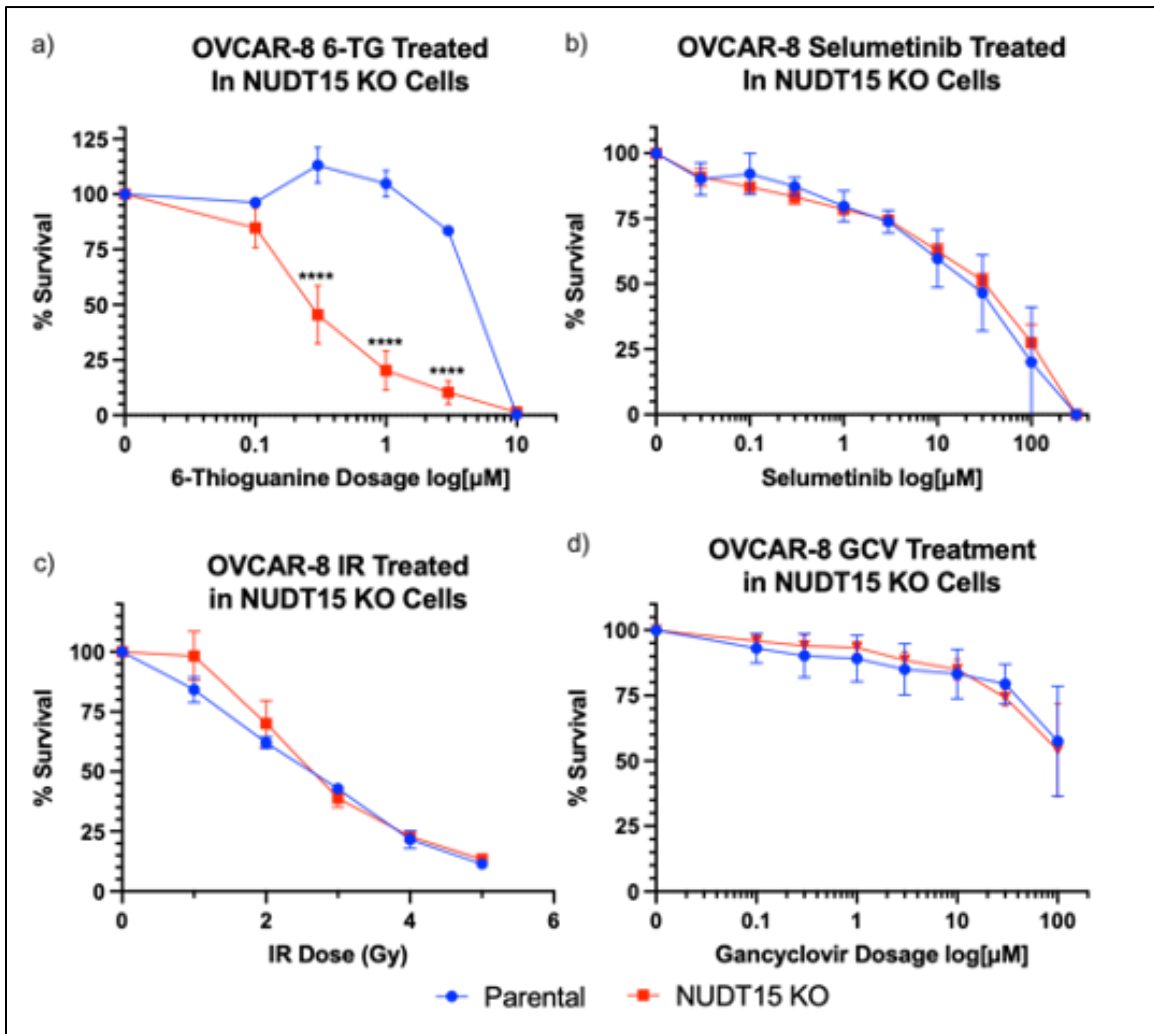


Figure 2.6 Treatment of NUDT15-deficient cells with potential novel substrates. Assays to provide kill curve data were utilized to determine potential novel NUDT15 substrates. A) NUDT15 KO cells show hypersensitivity to 6-thioguanine treatments after a 9-11 day recovery in a colony forming assay. B) NUDT15 KO cells treated with Selumetinib for 72 hours in a resazurin colorimetric assay. C) NUDT15 KO cells were treated with ionizing radiation and allowed to recovery for 9-11 days. D) NUDT15 KO cells were treated with gancyclovir for 72 hours in a resazurin colorimetric assay. **** p<0.0001

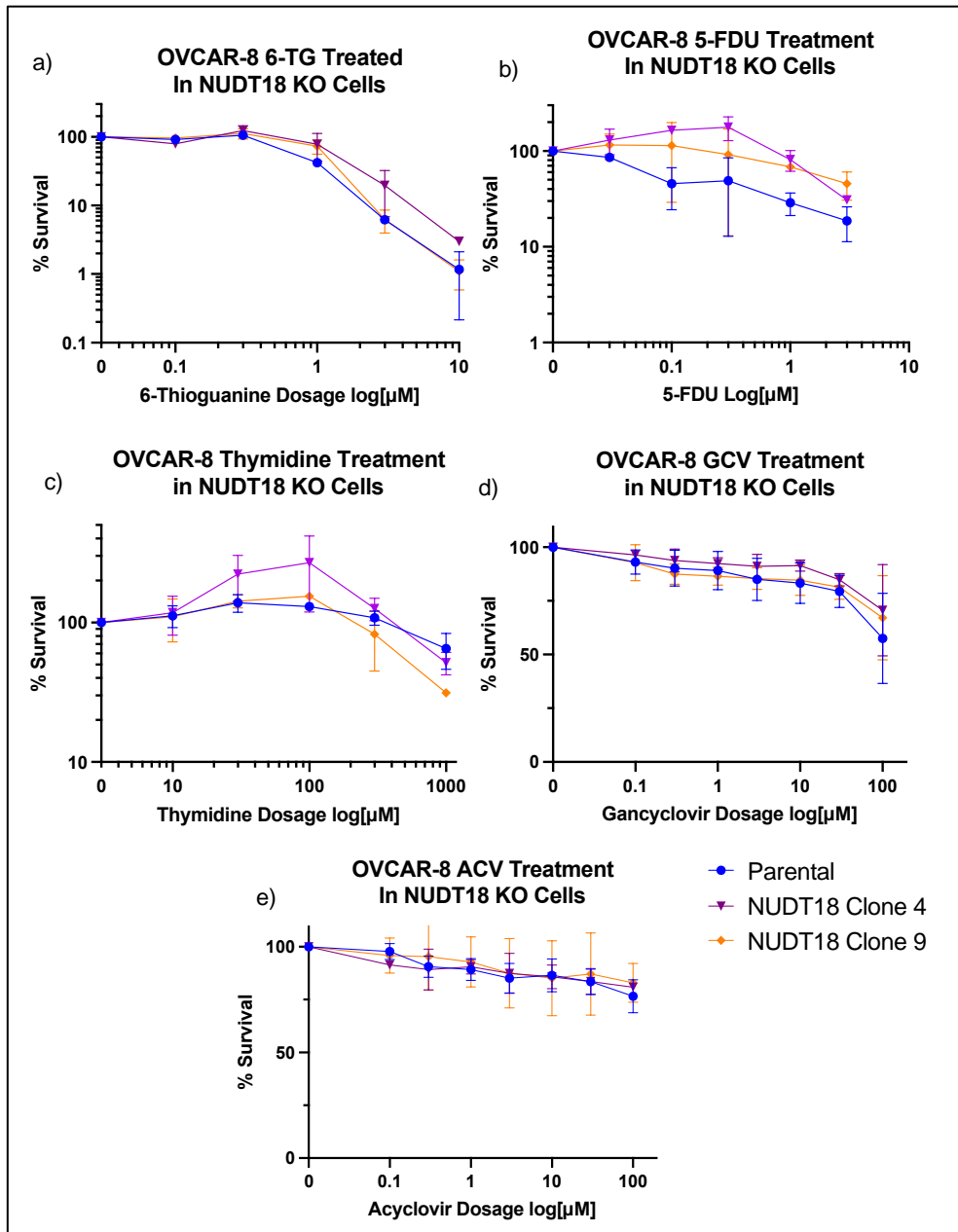


Figure 2.7 Treatment of NUDT18 deficient cells with potential novel substrates. Assays to provide kill curve data were utilized to determine potential novel NUDT18 substrates. A) NUDT18 KO cells were treated with increasing doses of 6-Thioguanine for 9-11 days in a colony forming assay. B) NUDT18 KO cells were treated with 5-Fluorodeoxyuridine for 9-11 days in a colony forming assay. C) NUDT18 KO cells were treated with Thymidine for 9-11 days in a colony forming assay. D) NUDT18 KO cells were treated with Ganciclovir for 72 hours in a resazurin-based colorimetric assay. E) NUDT18 KO cells treated with Acyclovir for 72 hours in a resazurin-based colorimetric assay.

CHAPTER 3

NUDT15 AND ITS ROLE IN THE METABOLISM OF 6-THIOGUANINE

3.1 Introduction

More than sixty years after being established as inexpensive and effective treatments against childhood leukemia as well as anti-inflammatory and immunosuppressant capabilities, the thiopurines class of compounds remain actively studied.^{8, 81, 82} The three members of the thiopurines include 6-thioguanine (6-TG), 6-mercaptopurine (6-MP), and azathioprine (AZA). Each drug eventually becomes metabolized to the active forms of 6-thio-GTP and 6-thio-deoxy-GTP prior to incorporation into DNA. Incorporation into DNA is not particularly toxic to the cells, however, through a somewhat poorly understood process, after a second round of replication, incorporated thiopurines will be detected by cellular mismatch repair (MMR) proteins.^{36, 37} This recognition will cause a lesion in the DNA that ultimately leads to a futile cycle as repair is attempted at irreparable sites, leading to cell death.³⁸ While the metabolism was thought to have long been understood, recently NUDT15 has been identified as being a critical component to the efficacy and cytotoxicity associated with thiopurine treatments by hydrolyzing the active 6-thio-GTP and 6-thio-dGTP metabolites prior to DNA incorporation.^{33, 40} Further exploring the role of NUDT15 in thiopurine metabolism would open the door to utilizing thiopurines as a treatment in a NUDT15 loss of function cancer cell line.

Understanding the role of NUDT15 also provides a potential route for personalized treatment in the clinic. Database mining shows a correlation between loss of the cell cycle regulating protein RB1 and a concurrent loss in copy number of NUDT15. Though the exact mechanism of RB1 loss is not understood, according to data available through cBioPortal, RB1 is altered in ~7% of samples in the database with ~45% of those samples

having a loss in RB1 copy number. Of the samples with a loss in RB1 copy number, almost 50% also have a loss in NUDT15 copy number, regardless of cancer type. RB1 copy number status is commonly screened for prior to starting cancer treatments using a highly sensitive PCR method,⁸³ therefore, a cancer patient with an RB1-deficient tumor may also have a passenger loss in NUDT15. This allows a potential targeted approach of utilizing treatments that would be more efficient in a cancer that has a confirmed loss in RB1 that likely also has a loss in NUDT15.

While NUDT15 was found to be actively involved in the metabolism of thiopurines, the mechanism of action of thiopurines in a NUDT15-deficient cell line has not been explored. Because of the common passenger loss of NUDT15 genetic information in cancers that also have a loss in RB1, NUDT15 also serves as a potential biomarker to determine a route for treatment. This chapter aims to determine the effects of thiopurine treatments in the NUDT15 CRISPR knockout OVCAR-8 ovarian carcinoma cell line to support capitalizing on a NUDT15 deficiency in cancer.

3.2 Results

3.2A NUDT15 KO OVCAR-8 cells show increased sensitivity to 6-TG

Published data shows that NUDT15 metabolizes the active 6-dThio-GTP metabolite into the inactive 6-dThio-GMP form and cells with NUDT15 deficiencies are significantly more sensitive to thiopurine treatments.³³ Using this known phenotype, NUDT15 KO cells were treated with 6-TG as a means to confirm this published finding in the OVCAR-8 cell line. The NUDT15 KO cells are significantly more sensitive to 6-TG treatments with less than 50% survival at a dose of 0.3 μM while the parental cells are unaffected at this dose. The NUDT15 KO cells have an LC_{50} of 0.28 μM , while the parental

cells have an LC_{50} of 4.32 μM , an over 15.4-fold difference. At a dose of 3 μM , the NUDT15 KO cells have approximately 10% survival while the parental cells have 90% survival (Figure 3.1A). This increased sensitivity to 6-TG is also seen in 22Rv1 prostate cancer cells with NUDT15 expression knocked down via NUDT15 siRNA. Though the lone significant ($p < 0.001$) difference is seen at 3 μM dose, a general trend of increased sensitivity is seen in the NUDT15-deficient cells compared to the Parental and Scrambled vector controls (Figure 3.1B).

To simulate chemotherapy treatment and provide additional evidence of increased sensitivity to 6-TG in NUDT15-deficient cells, long-term treatment selectivity assays were conducted using live-cell imaging. The NUDT15-deficient cells are GFP+ from the transfection of the sgRNA containing plasmid, providing a marker to track over the course of 6-TG treatments. Cells were treated with 6-TG over the course of 66 hours with images taken every 6 hours with time 0 being when the cells were first placed into the imager. Cells were treated with 0.1 μM and 0.3 μM of 6-TG to represent LC_{10} and LC_{50} doses in the NUDT15-deficient cells. Representative images show the expression of GFP+ cells remain at a similar presence as the GFP- negative cells after the first passage (Figure 3.2A, Top Row). Quantification of Passage 1 shows there was no significant difference between any of the treatment groups (Figure 3.2B Top Left). Quantification of Passage 2 again shows no significant difference in GFP+ cells between doses (Figure 3.2B, Top Middle). ⁸⁴Passage 3 show that at 0.1 μM and 0.3 μM doses, the GFP+ NUDT15-deficient cells are drastically reduced (Figure 3.2A, Middle Row) with quantification supporting there are significant (both $p < 0.01$) differences in the ratios of GFP+ cells in 6-TG treated cells compared to the NT (Figure 3.2B, Top Right). Passage 4 is not shown but quantification

of images again shows significant (both $p < 0.01$) differences between the 6-TG treated cells and the NT control cells (Figure 3.2B, Bottom Left). At Passage 5, the GFP⁺ cells are almost completely abolished after treatments with 6-TG (Figure 3.2A, Bottom Row) with quantifications supporting significant (both $p < 0.0001$) differences between the prevalence of GFP in the 6-TG treated cells versus the NT (not-treated) control cells (Figure 3.2B, Bottom Right). Note the phase image of Passage 5 cells treated with 0.3 μM of 6-TG shows a slight decrease in confluency versus the 0.1 μM of 6-TG appear confluent. This change in confluency implies that, while the NUDT15-deficient cells are far more sensitive than the proficient, the proficient cells may still decrease in viability after long-term exposure to that dose of 6-TG.

3.2B NUDT15-deficient cells show decreased viability after 6-TG treatments

To analyze the viability, cytotoxicity, and apoptosis in NUDT15 KO cells after 6-TG treatment, the ApoTox-Glo™ Triplex Assay was performed. NUDT15 KO cells (red bars) show significantly less viability after 6-TG treatments at 48, 72, and 96 hours after 0.1 μM , 0.3 μM , or 1 μM 6-TG treatments compared to NUDT15-proficient cells (blue bars) at the same doses and times (Figure 3.3A). While NUDT15 KO cells treated with 6-TG do not show as much of a fold change in viability compared to the NT NUDT15 KO cells at 48 hours, the 72 and 96 hour exposures show a decrease in viability compared to the NT control baseline (Figure 3.3A). 6-TG treatments cause no significant difference in cytotoxicity between the parental cells and NUDT15-deficient cells after 48 hours (Figure 3.3B, left). However, results show significantly increased cytotoxicity in the parental cells at the 0.3 μM dose for the 72 hour ($p < 0.05$) and at 0.1 μM and 0.3 μM doses for the 96 hour ($p < 0.0001$) treatments (Figure 3.3B middle, right). When measuring apoptosis, there

is little apoptosis induced at the 48 hour and 72 hour time points, except for a slight but significant ($p < 0.05$) increase in apoptosis at 0.1 μM of 6-TG after 48 hours in parental cells compared to NUDT15 KO cells. Apoptosis induction of ~2-fold was seen following 1 μM 6-TG treatment after 96 hours, though there was no significant difference between NUDT15-proficient or deficient cells (Figure 3.3C).

Taken together, NUDT15 KO cells show decreased cell viability after 6-TG exposure but do not show an increase in cytotoxicity or induced apoptosis. Previous evidence shows that cells treated with a higher dose of 6-TG will arrest in G_2 , whereas cells treated with lower doses continue through mitosis,⁸⁴ which may explain the decrease in viability with little change in cytotoxicity that is often seen in cells undergoing a cell cycle arrest.⁸⁵ While these cells have passed through mitosis, the cells may not experience apoptosis or have changes in membrane integrity but will undergo a mitotic catastrophe event that will eventually lead to cell death, potentially beyond the timing of this experiment. Note that prior studies in multiple systems have demonstrated that cell death caused by thiopurines is prolonged, taking 96 hours or more for death to occur.^{38, 39, 84, 86}

3.2C NUDT15 KO cells show a G_2/M arrest in response to 6-TG

Previous studies have shown that 6-TG induces a G_2/M phase arrest in cells mediated by MMR. A cell cycle arrest may also explain the decrease in NUDT15 KO cell viability without the increase in cytotoxicity or apoptosis after 6-TG treatments seen with the ApoTox-Glo™ assay (Figure 3.3). Here we aim to see if a deficiency in NUDT15 causes a G_2/M phase arrest in 6-TG treated cells. After a 24 hour exposure to 6-TG, no significant difference between the parental cells and the NUDT15 KO cells at any stage of the cell cycle nor any significant difference in sub G_1 cells at any dose or time point

examined was observed (data not shown). After 48 hours of 6-TG exposure, interestingly an ~87% increase in S-phase NUDT15 KO cells treated with 0.3 μ M 6-TG compared to untreated (NT) NUDT15 KO cells was observed; an accumulation in S-phase is not seen at the 1 μ M dose (Figure 3.4A, tan bars 4-6). The change in S phase cell distribution was also significantly ($p < 0.001$) different compared to the NUDT15-proficient cells at the same concentration, namely with ~70% fewer NUDT15-proficient cells in S phase compared to NUDT15-deficient cells (Figure 3.4A, tan bars 1-3). After 72 hours of 6-TG exposure, there is an ~88% increase in S-phase NUDT15 KO cells at the 0.3 μ M dose (Figure 3.4B, tan bars 4-5). The expected significant ($p < 0.0001$) increase in G₂/M phase cells at the 1 μ M dose in the NUDT15 KO cells compared to the NUDT15-proficient cells at the same dose after 72 hours exposure (Figure 3.4C, blue bars, lanes 4-6). The increase in G₂/M phase cells marks an ~95% increase when compared to the NT NUDT15 KO cells. This supports previous findings that cells with increased sensitivity to 6-TG progress through mitosis at lower doses of 6-TG, while higher doses of 6-TG cause a G₂ arrest.⁸⁴

3.2D NUDT15 KO cells show increased DNA damage after 6-TG treatments

Induction of DNA damage marker γ -H2AX was assessed by western blot after treatments with 6-TG in parental (blue bars) and NUDT15-deficient cells (red bars). Following treatments of 0.3 μ M and 1 μ M of 6-TG, increases in γ -H2AX are induced in the NUDT15 KO cells after 48 and 72 hours exposure to 6-TG (Figure 3.5A, lanes 7 and 8). Quantification of the bands show at 0.3 μ M, there is an almost 4-fold increase in γ -H2AX in the NUDT15 KO cells compared to the parental cells at both 48 and 72 hours of treatments (Figure 3.5B). A similar trend was seen in NUDT15 KO cells treated with 1 μ M 6-TG except with an ~3.5-fold increase at 48 hours and a slightly lower ~1.75-fold increase

at 72 hours compared to parental cells (Figure 3.5C). This data shows the induction of γ -H2AX in NUDT15-deficient cells after treatment with 6-TG that is measurable at 48 to 72 hours after exposure.

We next examined if 6-TG treatments caused chromosomal instability and aberrations in NUDT15-deficient cells. Examples of aberrations scored included gaps/breaks, chromosome radials, fusions/end joinings, and complex exchanges with examples shown in Figure 3.6A. NUDT15-proficient and deficient cells were treated with 0.3 μ M or 1 μ M of 6-TG for 6 hours before recovering for 18 hours and undergoing a 4 hour colcemid incubation to block cells during the second round of mitosis. The parental cells showed little change in chromosomal aberrations compared to the baseline of damage scored in the NT control (Figure 3.6B, bars 1-3). The NUDT15 KO cells show increases in all four forms of scored aberrations with \sim 5% and \sim 8% of all counted chromosomes containing an aberration in the 0.3 μ M and 1 μ M 6-TG treated cells, respectively (Figure 3.6B, lanes 4-6). More noticeable is a striking increase in radials at the 1 μ M dose in the NUDT15 KO cells signifying a more prevalent occurrence of a desperate means for cells to initiate repairs of damaged chromosome (Figure 3.6B, lane 6, red). NUDT15 KO cells also show a complex exchange-type aberration in \sim 1.6% and \sim 2.1% of all scored chromosomes in the 6-TG treated cells. The formation of complex exchange aberrations are poorly understood but are presumed to be failed attempts at faithful repair and a secondary end-joining process ligating broken fragments of chromatids or chromosomes. (Figure 3.6B, lanes 5-6, purple). Slight increases in both gaps/breaks (differences of \sim 1.6% and \sim 0.7%) and fusions (differences of \sim 1.0 % and \sim 1.3%) were detected in the NUDT15 KO 6-TG treated cells compared to the NUDT15-proficient parental cells (Figure 3.6B,

blue and green). However, the percentage of damaged chromosomes is much higher than the less than ~0.2% of damaged chromosomes in the NT NUDT15 KO cells. The chromosomal aberration data supports the prior observations that a deficiency in NUDT15 contributes to chromosomal instability after treatments with 6-TG.

To gain additional direct evidence of DNA damage, we also performed an alkaline comet assay with the percentage of DNA in the comet tail serving as an indicator for DNA strand damage in cells (Figure 3.7D). NUDT15-proficient (blue bars) and deficient (red bars) cells were treated with 6-TG at 0.3 μM or 1 μM doses for 24, 48, and 72 hours. We found that at 24 hours the NUDT15-proficient cells show significantly more damage at 0.3 μM ($p < 0.0001$) and 1 μM ($p < 0.0001$) than the NUDT15 KO cells, which remained at similar background damage (Figure 3.7A), which was unexpected, yet not quite so surprising because the fold induction at this time point is less than what was seen at the later time points. After 48 hours, there was no significant difference between the NUDT15-proficient or deficient cells at any dosage with the 6-TG treated cells in both lines showing increased damage, though the damage in the NUDT15-deficient line was greater comparing fold induction. The NUDT15-proficient cells showed a 0.7-fold and a 3-fold increase in percentage of tail DNA at 0.3 μM and 1 μM compared to NT while the deficient showed a 2.3-fold and a 4-fold increase compared to NT (Figure 3.7B). The increase in damage in the NUDT15-deficient cells treated with 1 μM of 6-TG was an almost 4-fold increase from the same dose after 24 hours of treatment (Figure 3.7A & B). Due to the mechanism of action of 6-TG, damage is expected to be caused by 6-TG treatments after the second round of DNA replication in cells, therefore increased damage in both cell lines at 48 hours is not necessarily a surprise. After 72 hours, there is a significant ($p < 0.0001$)

increase in NUDT15 KO cells treated with 1 μ M 6-TG with almost 4 times as much damage compared to the NT NUDT15 KO and more than 2 times the damage of the parental cells at the same dose (Figure 3.7C). Comparing fold changes, evidence of increased percentage of DNA in comet tails supports an increase of DNA damage in NUDT15-deficient cells after treatments with 6-TG.

3.3 Discussion

Even though thiopurines have been used in the clinic for over 50 years, we are continuing to learn of new uses and situations to utilize their efficacy as cancer treatments. One such scenario involves treatment of cancers with a loss of RB1 copy number. As stated, a loss of RB1 strongly correlates with a loss of NUDT15. While the mechanism of how these genes are simultaneously lost remains unknown, the loss of NUDT15 can provide a potential route of treatment in a patient with a screened RB1 loss. Knowing that NUDT15 is involved in thiopurine metabolism³³, and that NUDT15-deficient cells hypersensitive to 6-thioguanine treatments, the mechanism for how these cells respond to 6-TG needed to be explored to ultimately provide care in the clinic.

After generating NUDT15 CRISPR knockouts in OVCAR-8 ovarian carcinoma cells, the NUDT15-deficient cells were treated with 6-thioguanine in a colony forming assay to confirm the expected increase in sensitivity. NUDT15 KO cells first show a slight, though insignificant, increase in sensitivity in doses as low as 0.1 μ M of 6-TG. As dosage of 6-TG increases, NUDT15 KO cells begin to significantly show a decrease in survival while the proficient cells show little change in sensitivity up to a 3 μ M dose of 6-TG. This finding is also supported in 22Rv1 prostate cancer cells with siRNA targeting NUDT15 showing KD NUDT15 also creates increased sensitivity to 6-TG. (Figure 3.1) NUDT15

KO cells have an LC₅₀ of 0.28 μM, while the parental cells have an LC₅₀ of 4.32 μM, an over 15.4-fold difference, strongly reinforcing the sensitivity seen to 6-TG in a NUDT15-deficient background. This finding is also supported in 22Rv1 prostate cancer cells with siRNA targeting NUDT15 showing KD NUDT15 also creates increased sensitivity to 6-TG. While this lone figure strengthens the case for treating a patient with a NUDT15-deficient cancer with 6-TG, the mechanism for how these cells respond to the increase of 6-TG efficacy must be further expanded.

To more accurately portray a continued exposure to 6-TG similar to what is seen with chemotherapy treatment, we used live cell imaging to detect changes in cell viability of GFP+ NUDT15 KO cells over a period of time with continuous treatment with 6-TG (Figure 3.2). A gradual decrease in GFP+ cells was observed over the course of treatments implying that the NUDT15-deficient cells were at a selective disadvantage because of the 6-TG treatments. While the NUDT15-proficient cells show an increased survival at the end of the fifth passage with 6-TG, cells should be analyzed for any mutagenic changes that could occur after being treated with 6-TG over the course of therapy. Worth noting is that the 0.1 μM 6-TG treated cells show almost no GFP+ NUDT15-deficient cells with minimal change to the growth of the parental cells while there may be some cytotoxic effects to the parental cells at the 0.3 μM dose after prolonged treatment, causing a change in cell density at later time points. Therefore, the proper dosage would have to be determined clinically to see as much of a therapeutic effect in NUDT15-deficient cancer cells with as minimal of a cytotoxic effect in the proficient cell line.

While the colony forming assay and selectivity assays support strong evidence of NUDT15-deficient cells being much more sensitive to 6-TG treatments, little has been

done to show how cells are being damaged by 6-TG treatments in NUDT15-deficient cells. Using the ApoTox-Glo™ assay, the viability, cytotoxicity, and induced apoptosis after 6-TG treatments was evaluated (Figure 3.3). As expected, decreased viability in the NUDT15 KO cells was observed compared to the parental cells lines at all indicated doses and times, especially at the 72 and 96 hour time points where viability in the NUDT15-deficient cells drop below baseline levels in NT control cells. This trend follows expected results of 6-TG damaging effects being observable after at least two rounds of DNA replication,³⁶⁻³⁸ which the OVCAR-8 cells would have undergone after at least 72 hours. The cytotoxicity results, however, do show increases of cytotoxicity in the NUDT15-proficient cells that is not seen to the same extent in the NUDT15-deficient cells at each dosage and time points. The only time point where there is not an increase of cytotoxicity in both cell lines compared to the NT control cells baseline is the 1 μ M dose after 96 hours, which is likely because cells show a doubling in induced apoptosis. This trend of showing a decrease in viability but no increase in cytotoxicity is likely the result of an arrest in the cell cycle where cells are no longer proliferating but membrane integrity has not been compromised. There is precedence in cells sensitive to 6-TG to be able to continue through mitosis at lower concentrations of 6-TG and die later, perhaps longer than the timeframe of this experiment, because of mitotic catastrophe during the next cell division event, but cells will undergo a G₂ arrest at higher doses of 6-TG.^{38, 39, 84, 86} Therefore, an analysis of the cell cycle profile after 6-TG treatments is required determine whether a dose-dependent G₂ arrest is occurring.

Using flow cytometry, an arrest of cells in G₂/M phase cells is detected at the 1 μ M dose after 72 hours of treatment in the NUDT15-deficient cells (Figure 3.4). This supports

the previous finding that 1 μM , in this cell model, is a high enough dose to cause the arrest at G₂ phase while the previously published result in HR-deficient MEFs showed an arrest at a 100 nM dosage.⁸⁴ Interestingly, NUDT15 KO cells also show a significant difference in percentage of S phase cells at the 0.3 μM dose at both 48 and 72 hours. This dose, while effective in the colony forming assay and selectivity assays in causing cell death in the NUDT15 KO cells with minimal effect seen in the NUDT15-proficient cells, may not be high enough to cause the G₂ phase arrest but has caused cells to spend more time attempting to replicate damaged DNA during S phase. Note there is also an increase in parental cells in S phase after 72 hours as well, likely showing this same effect where 6-TG was not at a high enough dose to cause an arrest, but cells are attempting to replicate damaged DNA in S phase.

To determine 6-TG is in fact causing DNA damage at 0.3 μM or 1 μM doses, we first looked for changes in $\gamma\text{-H2AX}$ expression after 6-TG treatments. We saw an increase in $\gamma\text{-H2AX}$ in the NUDT15-deficient cells in as little as 48 hours after treatment of 0.3 μM and 1 μM doses of 6-TG with expression remaining much higher than NUDT15-proficient cells at the 72 hour time points (Figure 3.5). To further analyze damage to DNA, we also used metaphase spreads to observe chromosomal aberrations (Figure 3.6). Here, cells were treated with 0.3 μM or 1 μM doses of 6-TG for only 6 hours before being allowed to recover for 18 hours prior to a 4 hour colcemid block. There was a striking difference in aberrations signifying 6-TG is strongly contributing to chromosomal instability in the NUDT15-deficient cell line. Of note are the dramatic increases of complex exchanges. As mentioned, how these complex exchanges are formed is poorly understood but is likely the result of failed attempts at repairing broken chromosomes and secondary end-joining events. The

unnatural states of chromosomal DNA may make replication difficult for cells, thus causing the apparent increase of S phase cells at the lower doses of 6-TG, but still able to progress through eventual mitosis. Higher doses of 6-TG may cause so much damage that cells will simply remain at the G₂ phase until necrosis. While mitotic index was determined in previous work⁸⁴, the index should also be determined after 6-TG treatments in a NUDT15-deficient cell line.

Alkaline comet assay data also supports an increase in DNA damage after 6-TG treatments in NUDT15-deficient cells. While the data appears to show an increase in damage in the NUDT15-proficient cells at the 24 and 48 hour time points, it is worth noting that the percentage of tail DNA does not reach that of the largest percentage in the NUDT15-deficient cells at 1 μ M after 72 hours. Also, while considering the fold change of percentage of tail DNA, the NUDT15-deficient cells do show a larger shift of increased damage compared to the NUDT15-proficient cells at each dosage in the 48 and 72 hour time points. Worth noting, the alkaline comet assay will also detect cells undergoing DNA replication as “damage”. The slight increase in S phase cells shown in the cell cycle data may slightly skew the results of lower doses of 6-TG treatments to appear as more damaging. To determine the population of S phase cells, a modified comet assay that also detects actively synthesizing cells via BrdU incorporation would allow a means to differentiate between comets that are the result of DNA damage and the result of active DNA synthesis.

Overall, NUDT15-deficient cells show increased sensitivity to 6-thioguanine treatments with the cellular response ultimately remaining similar to the mechanism that has long been established regarding thiopurine treatments. The primary goal for

understanding the response to thiopurines in a NUDT15-deficient background revolves around expanding options for personalized medicine in patients presenting with a NUDT15-deficient cancer.

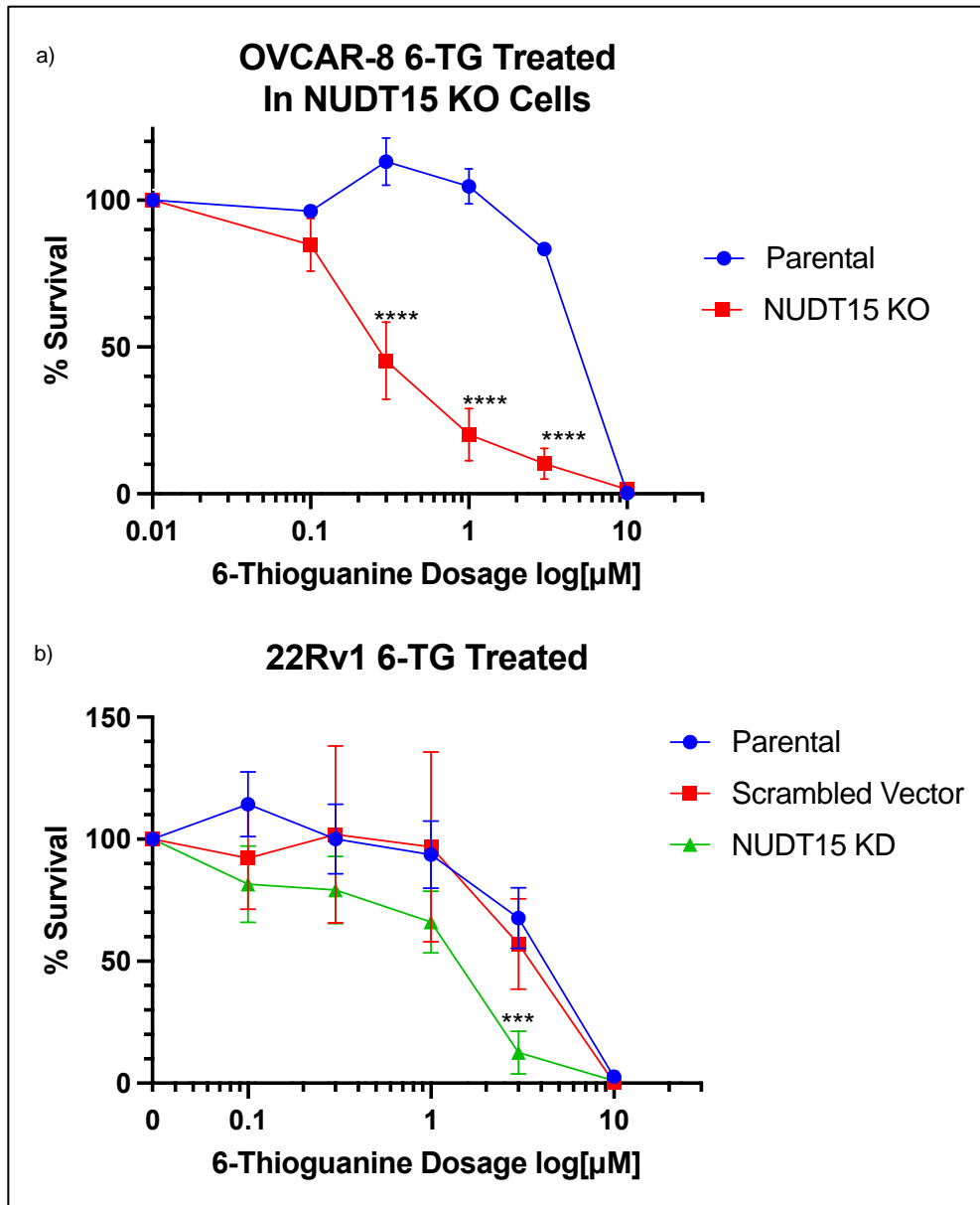


Figure 3.1 NUDT15 KO and KD cells show hypersensitivity to 6-thioguanine treatments. Colony forming assays of A) OVCAR-8 ovarian carcinoma and B) 22Rv1 prostate cancer cells with NUDT15 deficiency treated with 6-TG at the indicated doses. Survival is plotted compared to an untreated control. Each data point is a mean of 3 independent experiments. Statistical significance was determined by two-way ANOVA
 *** $p < 0.001$ **** $p < 0.0001$

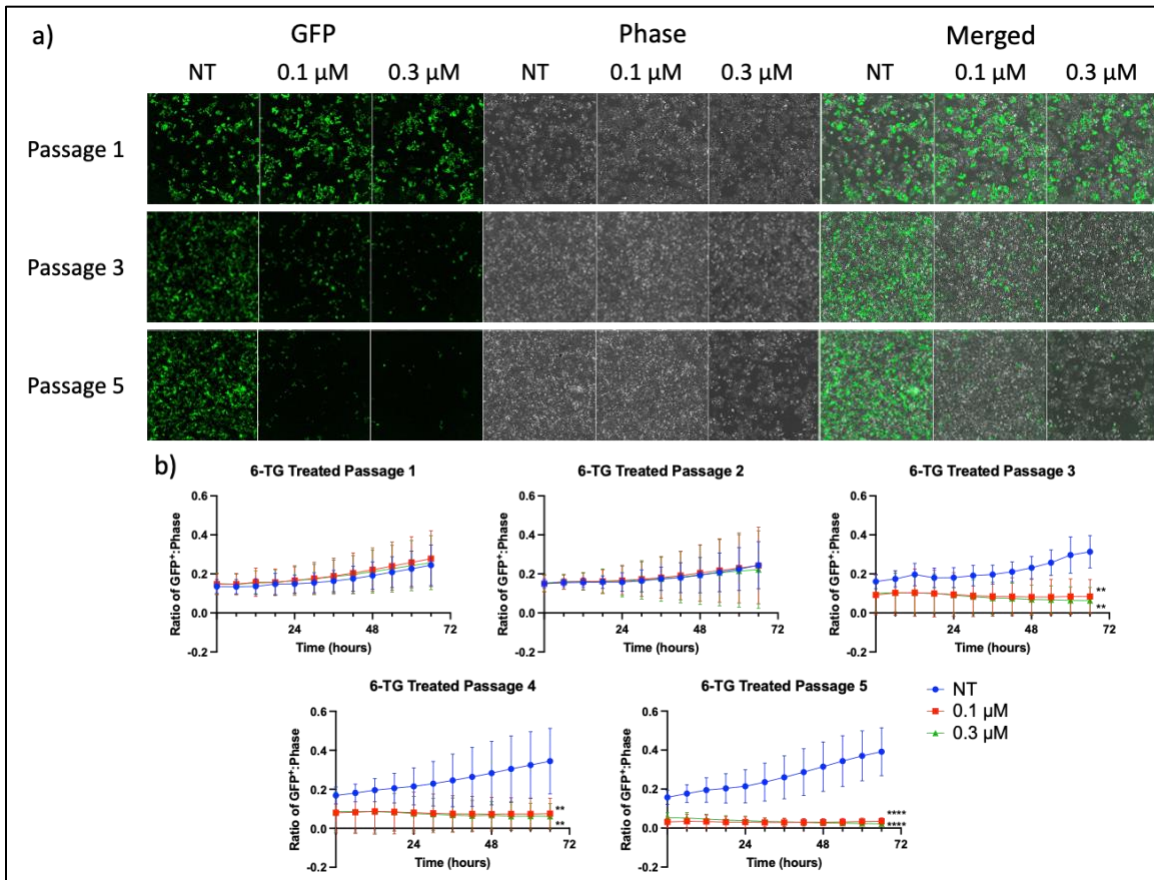


Figure 3.2 Selectivity assay shows a decrease in survival of GFP+ NUDT15 KO cells after continuous exposure to 6-TG. Live-cell imaging results show a loss in GFP+ NUDT15-deficient cells mixed with GFP- NUDT15-proficient cells. A) Representative images of Passage 1, Passage 3, and Passage 5 cells were taken after 66 hours of treatment. Images show GFP only (left), phase contrast (middle), and merged (right). B) Quantification of the ratio of GFP+ cells: Phase Contrast cells at each passage number over the course of 66 hours with 0.1 μ M or 0.3 μ M of continuous 6-TG exposure. Significance was determined by two-way ANOVA. ** $p < 0.01$ **** $p < 0.0001$

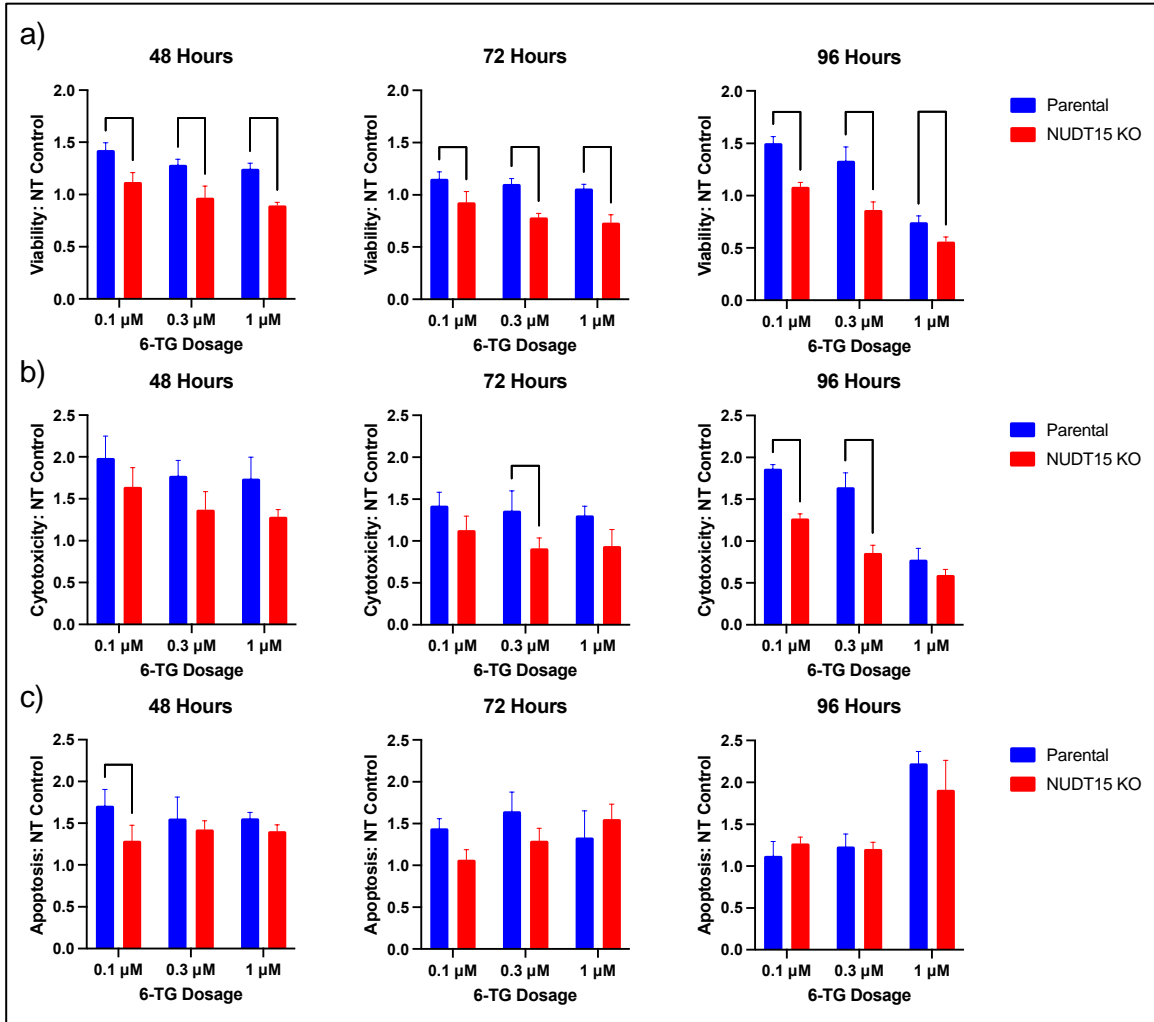


Figure 3.3 Triplex assay of NUDT15 KO cells treated with 6-TG. ApoTox-Glo Triplex assay of NUDT15-deficient cells were treated with 6-TG at the indicated doses for the indicated times. NUDT15 KO cells show decreased viability, cytotoxicity, and apoptosis compared to parental cells. A) Viability of parental cells (blue) and NUDT15 KO cells (red). B) Cytotoxicity of parental cells (blue) and NUDT15 KO cells (red). C) Apoptosis of parental cells (blue) and NUDT15 KO cells (red). Statistical significance was determined by two-way ANOVA * $p < 0.05$, ** $p < 0.01$, *** $p < 0.001$, **** $p < 0.0001$

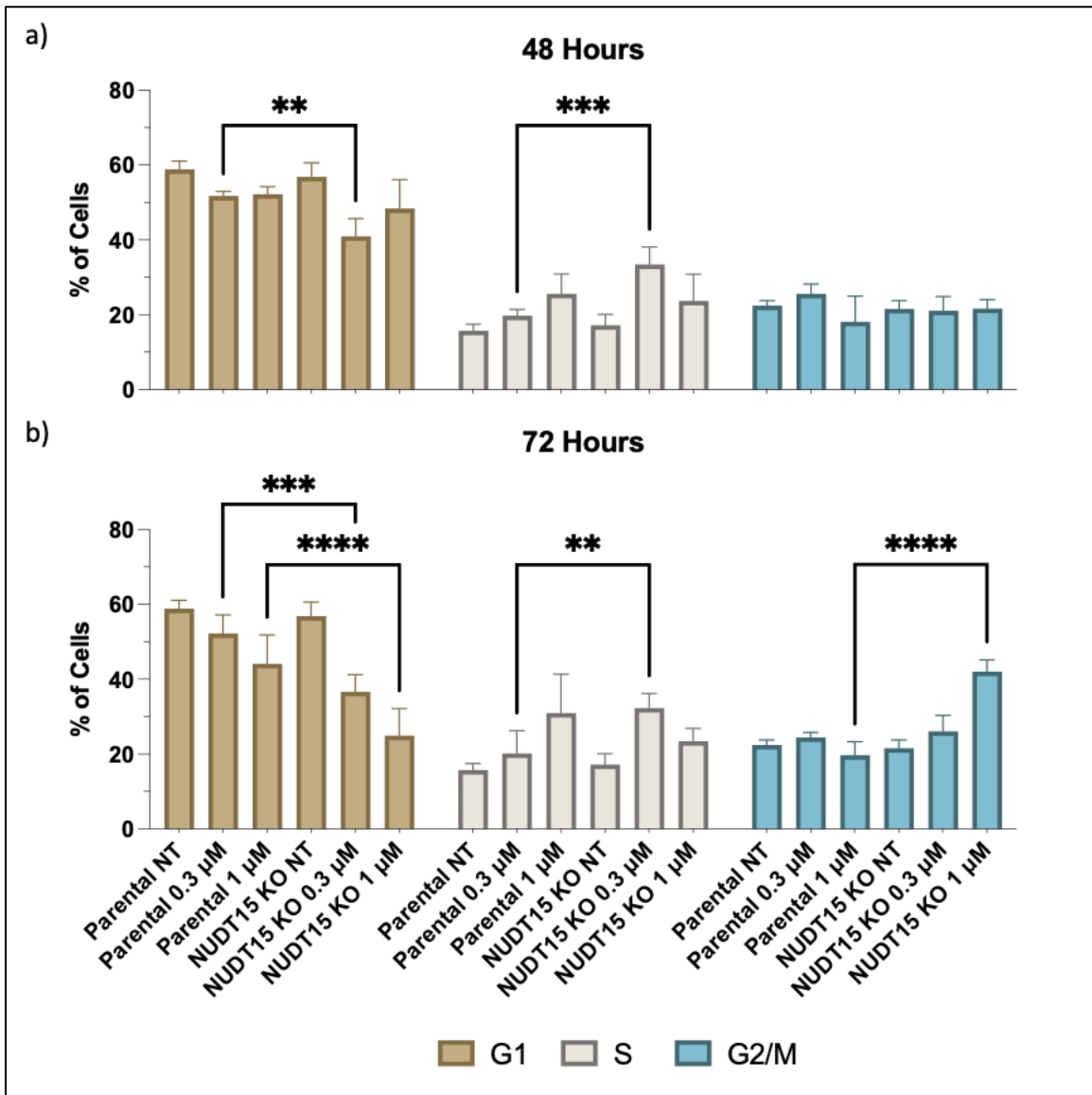


Figure 3.4 Cell-cycle profile of parental and NUDT15-deficient cells in response to 6-TG treatments. Flow cytometry results of NUDT15 KO cells treated with 6-TG at the indicated doses for the indicated time. NUDT15 KO cells show a slight S phase arrest at 48 hours and a G₂ arrest at 72 hours. Each panel shows the G₁, S phase, G₂/M phase populations of parental and NUDT15 KO cells after exposure to 6-TG for: A) 48 hours and B) 72 hours. Each bar represents three independent experiments. Statistical significance was determined by two-way ANOVA. ** p < 0.01, *** p < 0.001, **** p < 0.0001

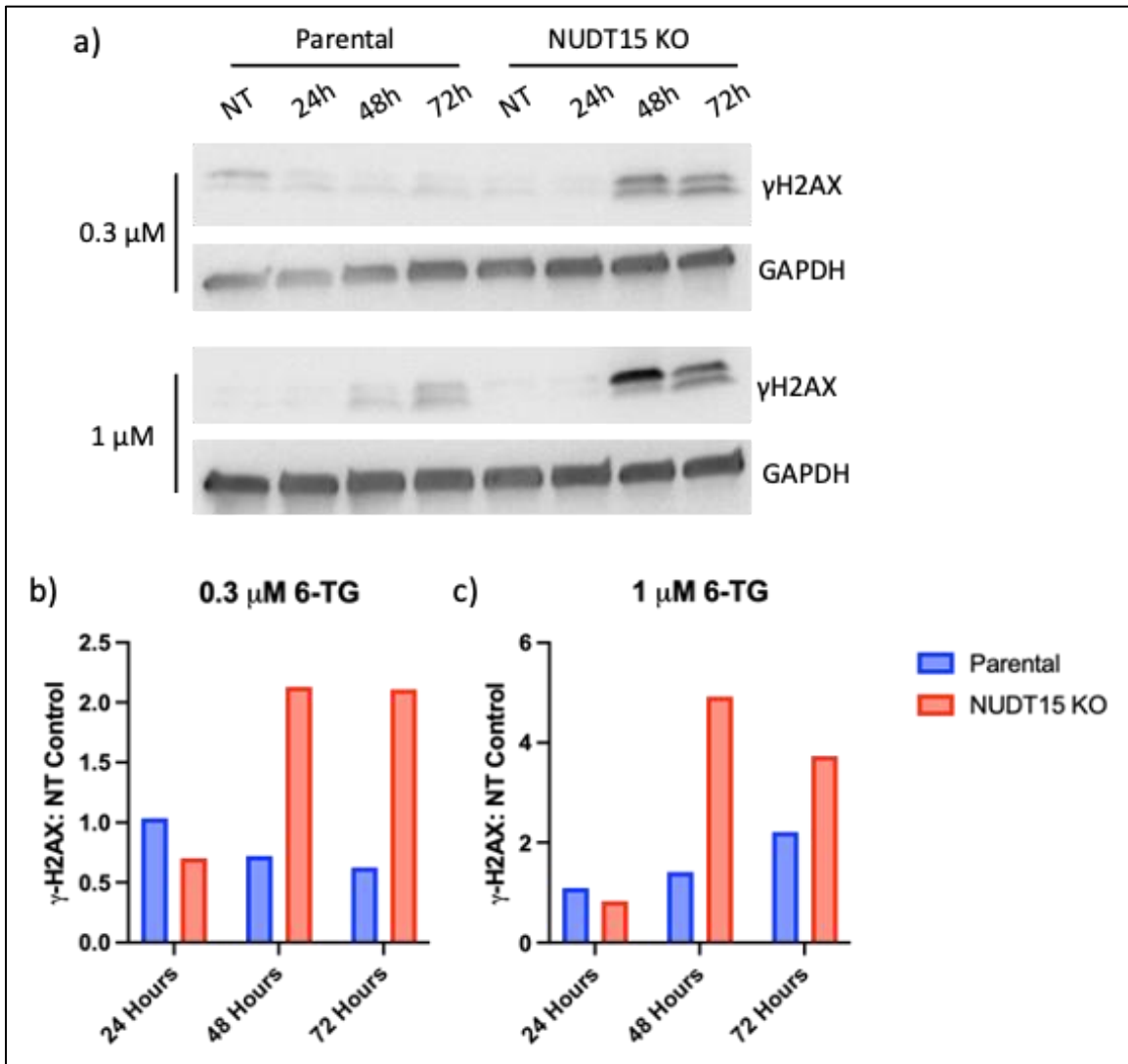


Figure 3.5 DNA Damage marker γ -H2AX induction after 6-TG treatments. Western blot shows an induction of γ -H2AX in NUDT15 KO cells after 6-TG treatments. A) The γ -H2AX signal after 6-TG treatments of 0.3 μ M and 1 μ M doses for 24, 48, and 72 hours in parental cells (lanes 1-4) and NUDT15 KO cells (lanes 5-8). B and C) Quantification of γ -H2AX bands normalized to GAPDH after 0.3 μ M (B) or 1 μ M (C) of 6-TG. Bars show total band volume of each lane compared to NT control

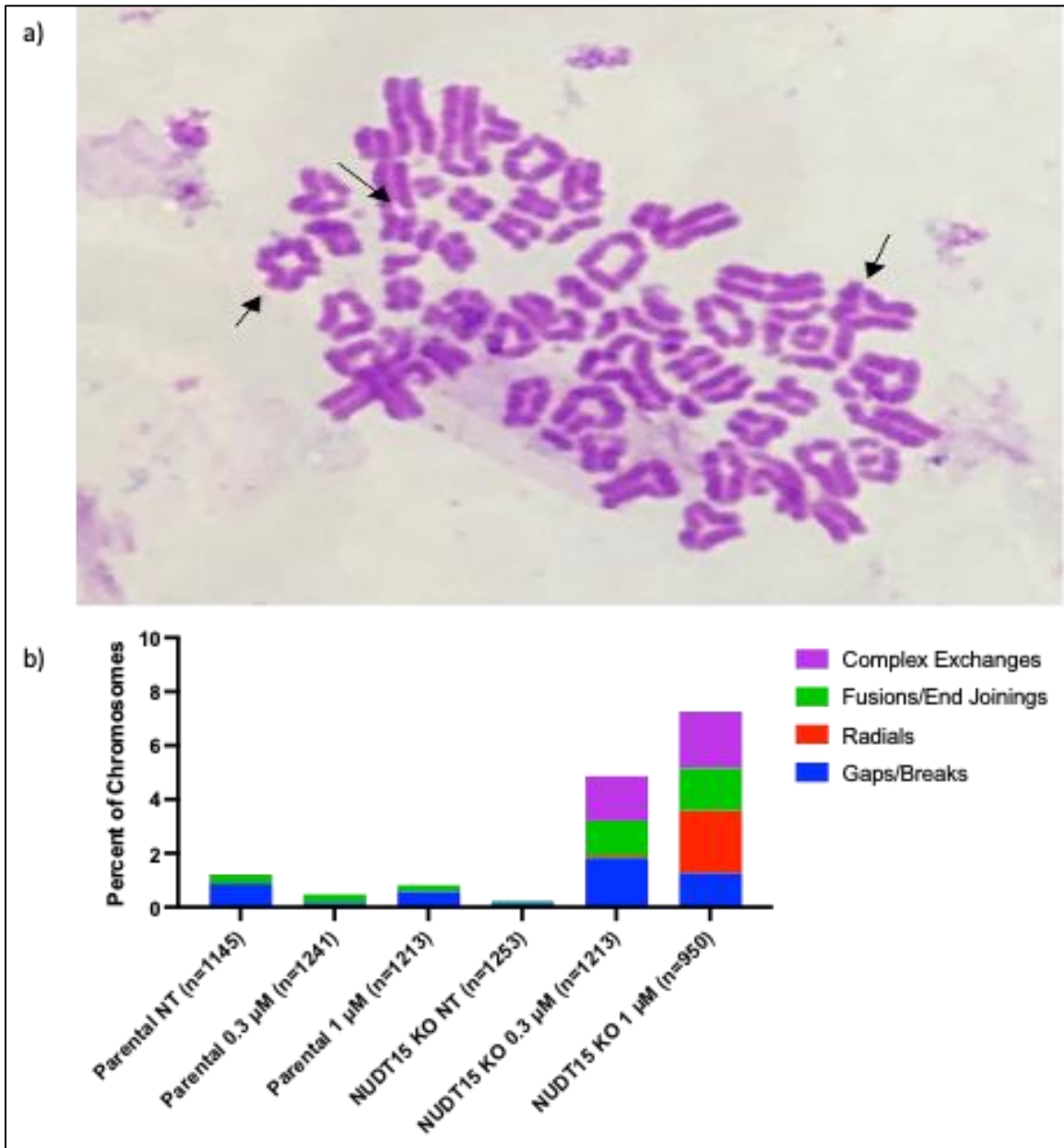


Figure 3.6 NUDT15 KO cells show increased chromosomal aberrations after 6-TG treatments. Metaphase spreads of NUDT15 KO cells treated with 6-TG. A) Representative image of metaphase spreads with scorable aberrations. Arrows indicate examples of aberrations. From left to right: Radial, Gap/Break, Complex Exchange. B) Quantification of aberrations in parental cells and NUDT15 KO cells after 6 hour treatments with 0.3 μ M or 1 μ M 6-TG.

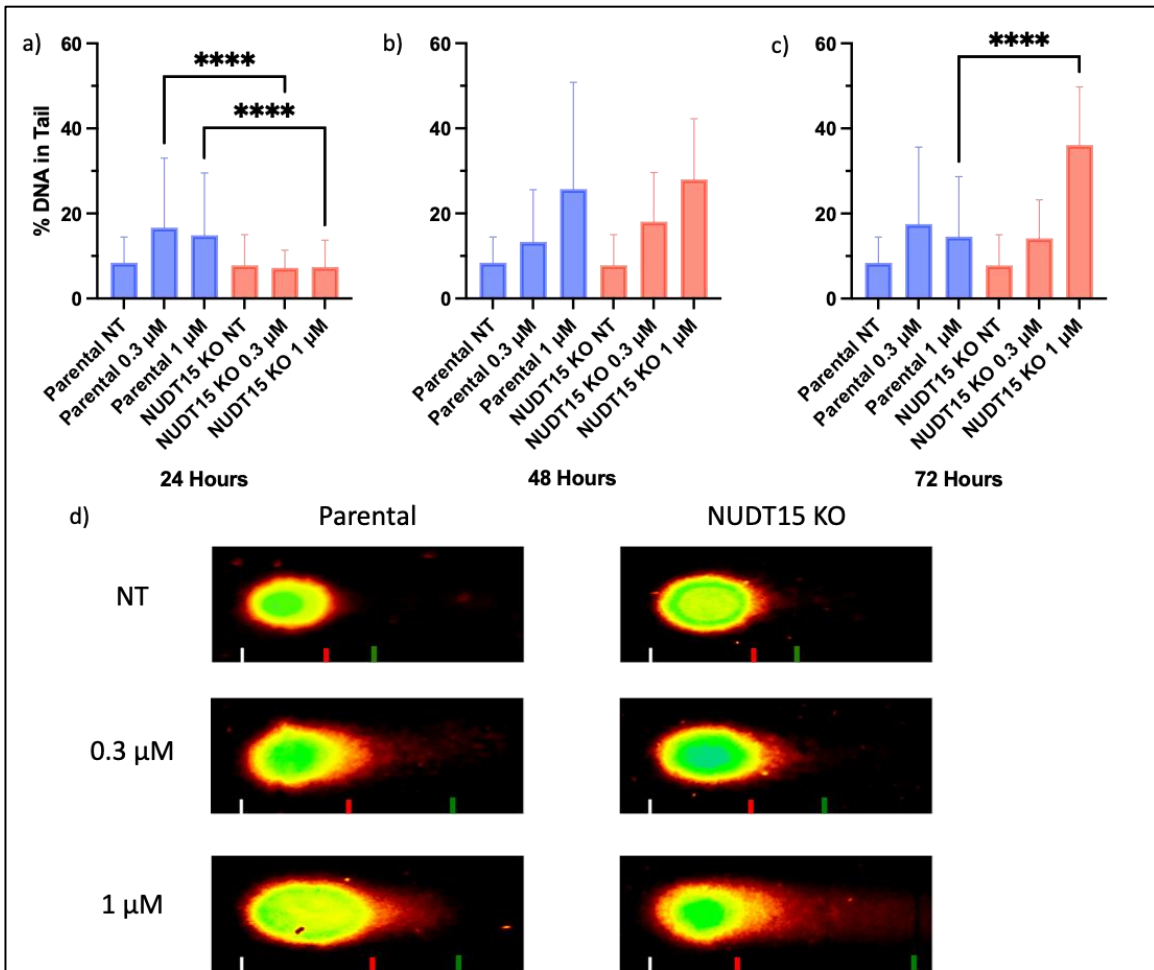


Figure 3.7 Comet assay measuring DNA damage in 6-TG treated NUDT15 KO and parental cells. Alkaline comet assay showing percentage of DNA in comet tails as an indicator for DNA damage in response to 6-TG treatments at the above doses for the above times. Percent DNA in tail for cells treated with 0.3 μM or 1 μM doses for A) 24 hours, B) 48 hours, and C) 72 hours. D) Representative images of comets after 72 hours of treatment at nontreated, 0.3 μM, and 1 μM doses. Statistical significance was determined by two-way ANOVA **** p < 0.0001

CHAPTER 4

NUDT15 AND ITS ROLE IN THE METABOLISM OF ACYCLOVIR

4.1 Introduction

The first publication of the guanine derivative acyclovir (ACV) appeared in 1977 with later evidence supporting an effective and selective treatment against herpes simplex virus (HSV) infected cells.^{47, 87} The mechanism of action for ACV involves phosphorylation by the HSV thymidine kinase in herpes infected cells prior to further activation by cellular kinases.⁴⁷⁻⁴⁹ After phosphorylation to the active form acyclovir triphosphate, ACV-TP is then incorporated into actively synthesizing DNA in place of the natural nucleotide deoxyguanosine triphosphate. Due to the missing 3'-hydroxyl group needed for the phosphodiester bond in the DNA backbone, elongation of DNA will halt, preventing any further replication.⁴⁷

As a guanine derivative, ACV remains in the nucleotide pool prior to activation and eventual incorporation into DNA. Recent evidence shows that the nucleotide pool sanitizing hydrolase NUDT15 may have activity towards ACV and that inactive NUDT15 polymorphisms increase the efficacy of ACV treatments.²² While the biological function of NUDT15 remains unknown, NUDT15 has been shown to metabolize the active forms of thiopurines.³³ However, the activity against ACV is a completely novel function that may allow an alternative use for ACV as a cancer treatment option. Though NUDT15 has shown activity against ACV, the effects of ACV treatments in a NUDT15-deficient cell line have yet to be explored.

As previously stated, NUDT15 copy number is a known passenger loss in cancers that have also lost copy number of the cell cycle regulating protein RB1. Datamining through The Cancer Genome Atlas and cBioPortal show a strong correlation between cancers that lose RB1 copy number with NUDT15 copy number also being lost, likely

because of both genes being located within 500 kb of each other on Chromosome 13. RB1 is commonly and effectively screened for in cancers prior to therapy,⁸³ therefore evidence of a loss in RB1 likely means NUDT15 is lost as well. This knowledge encourages further exploration of the roles NUDT15 has in cells and utilizing a NUDT15 deficiency to determine a course of cancer treatment.

Here, using a CRISPR-generated NUDT15 knockout ovarian carcinoma cell line, cancer cells are treated with acyclovir to determine the potential of repurposing ACV in a NUDT15-deficient cancer model. This chapter aims to provide justification for another treatment option in the clinic for patients presenting with cancers that show a loss in RB1 copy number and, likely, a loss in NUDT15 as well.

4.2 Results

4.2A NUDT15 KO OVCAR-8 cells show increased sensitivity to ACV

Recent evidence has shown that NUDT15 may have a role in the metabolism of anti-herpes drugs acyclovir (ACV) and ganciclovir.^{22, 53} While an increase in sensitivity to ganciclovir in CRISPR generated NUDT15 KO cells was not detected (Figure 2.6D), increased sensitivity to ACV in the NUDT15-deficient cells was observed (Figure 4.1). Using a resazurin viability assay, a significant ($p < 0.0001$) increase in sensitivity to ACV was observed in the NUDT15 KO cells (red squares) with an LC_{50} of $\sim 100 \mu\text{M}$, compared to the NUDT15-proficient cells (blue circles) with a 24% decrease in survival at $100 \mu\text{M}$. (Figure 4.1A). The efficacy of ACV treatments is thought to be reliant on the presence of the HSV thymidine kinase (HSV-TK) in herpes infected cells. After a transient addition of the HSV-TK, a significant ($p < 0.0001$) increase in sensitivity to ACV in the NUDT15 KO cells after an only 24 hour exposure at the indicated doses was observed with the LC_{50}

remaining at ~100 μM and the NUDT15-proficient cells showing only a 22% decrease in survival compared to the NT control cells (Figure 4.1B). Evidence of sensitivity to ACV is also seen in 22Rv1 prostate cancer cells after siRNA KD of NUDT15 in colony forming assays with 100 μM and 300 μM doses showing significantly ($p < 0.05$, $p < 0.0001$) decreased survival compared to the Parental and Scrambled Vector control cells (Figure 4.1C). This evidence supports that NUDT15-deficient cells show an increase in sensitivity to ACV in the presence or absence of HSV-TK.

To simulate chemotherapy treatment and provide additional evidence of increased sensitivity to ACV in NUDT15-deficient cells, long-term treatment selectivity assays were conducted using live-cell imaging. The NUDT15-deficient cells are GFP+ from the transfection of the sgRNA containing plasmid, providing a marker to track over the course of ACV treatments. Cells were treated with ACV over the course of 66 hours with images taken every 6 hours with time 0 being when the cells were first placed into the imager. Cells were treated with 30 μM and 100 μM of ACV to represent LC₁₀ and LC₅₀ doses in the NUDT15-deficient cells. Representative images show the expression of GFP+ cells remain at a similar presence as the GFP- negative cells after the first passage (Figure 4.2A, Top Row). Quantification of Passage 1 shows there was no significant difference between any of the treatment groups (Figure 4.2B Top Left). Quantification of Passage 2 again shows no significant difference in GFP+ cells between doses (Figure 4.2B, Top Middle). Representative images at Passage 3 begin to show a decrease in GFP+ cells at the 100 μM of ACV dose while the 30 μM dose continues to closely resemble the NT cells (Figure 4.2A, Middle Row). The quantification of GFP+ cells does show a significant ($p < 0.001$) difference in the 100 μM treated cells compared to the NT control cells while the 30 μM

treated cells show similar GFP+ ratios (Figure 4.2B, Top Right). Quantification of Passage 4 cells again show a significant ($p < 0.05$) difference in the GFP+ ratio in the 100 μM treatments compared to the NT controls with no significant difference at the 30 μM dose (Figure 4.2B, Bottom Left). The representative images for Passage 5 show a noticeable decrease in GFP+ cells at the 30 μM dose and a strikingly noticeable decrease in the 100 μM treated cells compared to the NT (Figure 4.2A, Bottom Row). The quantification of GFP+ cells in the 30 μM and 100 μM show significant ($p < 0.05$, $p < 0.0001$) differences compared to the NT control cells (Figure 4.2B, Bottom Right). Note that, even after five passages at a 100 μM dose, the GFP- NUDT15-proficient cells do not show a noticeable change in confluency, further supporting the NUDT15-deficient cells are far more sensitive to ACV treatments.

4.2B NUDT15-deficient cells show slightly decreased viability and increased induction of apoptosis after ACV treatments

To analyze the viability, cytotoxicity, and apoptosis in NUDT15 KO cells after ACV treatment, the ApoTox-Glo™ Triplex Assay was performed. NUDT15-proficient (blue bars) and NUDT15-deficient (red bars) cells were treated with 10 μM , 30 μM , or 100 μM doses of ACV for 24, 48, or 72 hours prior to the addition of ApoTox-Glo™ Triplex Assay reagents. While no significant difference in viability was observed after 24 hours (Figure 4.3A, left), a slight, though significant ($p < 0.05$), difference in viability was detected at the 100 μM dose after 48 hours in the NUDT15 KO cells compared to the NUDT15-proficient cells at the same dose, however the viability remained at a comparable level to NT NUDT15 KO control cells at the same time point (Figure 4.3A, middle). At 72 hours, a larger decrease in viability, compared to the NT control cells for each cell line,

was measured in both the parental and NUDT15 KO cells in the 30 μM doses with a more significant ($p < 0.05$) difference in viability being observed in the NUDT15 KO cells compared to the NUDT15-proficient cells (Figure 4.3A, right). There was a significant ($p < 0.001$) ~23% decrease in the viability of NUDT15-deficient cells at the 100 μM dose after 72 hours with little change in NUDT15-proficient cell viability at the same dose compared to the NT controls of both cell lines (Figure 4.3A, right).

Regarding cytotoxicity, there was no significant difference in measurable cytotoxicity in either cell lines at any dose after 24 or 48 hour exposures with all showing a slight increase in cytotoxicity compared the NT controls for both cell lines (Figure 4.3B, left and middle). However, after 72 hours there was a significant difference in cytotoxicity in the NUDT15-proficient and deficient cells at the 30 μM ($p < 0.05$) and 100 μM ($p < 0.01$) doses showing decreases of ~33% and ~37%, respectively, in toxicity in the NUDT15-deficient cells (Figure 4.3B, right). While the assay shows a significant difference with an apparent decrease in cytotoxicity in the NUDT15 KO cells, it is important to note there is not an increase of cytotoxicity in the parental cells as the cytotoxicity measurements remain at comparable amounts to the NT control cells at the same time point.

There was also no measurable difference in induction of apoptosis in the 24 or 48 hour treated cells regardless of NUDT15 status (Figure 4.3C, left and middle). However, at the 100 μM dose after 72 hours of exposure, a large, significant ($p < 0.001$) increase in apoptosis induction in the NUDT15 KO cells (Figure 4.3C, right). This almost 58% increase in apoptosis compared to the NT NUDT15 KO control cells likely explains the larger decrease in cytotoxicity seen at the same dosage and time point.

Taken together, NUDT15 KO cells show little change in viability, cytotoxicity, and apoptosis at 24 or 48 hours of treatment. However, at 72 hours, NUDT15 KO cells show a decrease in viability and cytotoxicity at 30 μ M and 100 μ M doses of ACV with a significant 58% increase in induced apoptosis at the 100 μ M dose. ACV is known to cause a termination of DNA synthesis after incorporation so cell cycle analysis should be performed as a means to determine if an arrest is contributing to a decrease in viability with little change in cytotoxicity.⁸⁵

4.2C NUDT15 KO cells show an S-phase arrest in response to ACV

Acyclovir's mechanism of action involves incorporation into DNA, leading to a termination of DNA synthesis during S phase of HSV infected cells.⁴⁷ Therefore, it was predicted NUDT15-deficient cells would show an arrest in S phase if NUDT15 is involved in the metabolism and prevention of ACV incorporation into DNA. Cells were treated with 30 μ M or 100 μ M doses of ACV for 24, 48, or 72 hours prior to incubation with EdU to detect cells actively synthesizing DNA in S phase. Cells with EdU incorporation were Click-iT chemistry labeled with Alexa Fluor 647. Following a method used by Ackerson *et. al.*,⁸⁸ the percentage of cells in S phase, determined by DAPI staining, would then be compared to the percentage of cells that show no signal of Alexa Fluor labeling of EdU to determine if cells are in S phase and actively synthesizing DNA or if synthesis has terminated.

After 24 hours, NUDT15-deficient cells in S phase increased by ~75% in 30 μ M treated and ~160% in 100 μ M treated cells compared to the NT NUDT15-deficient control cells (Figure 4.4A, tan bars 4-6). This increase in S phase cells is also a significant ($p < 0.001$, $p < 0.0001$) increase compared to the NUDT15-proficient cells at the same doses

(Figure 4.4A, tan bars 1-3). Evidence of DNA synthesis termination is present at 24 hours with ~90% and, significantly ($p < 0.01$), only ~80% of NUDT15 KO cells actively incorporating EdU or synthesizing DNA at 30 μM and 100 μM ACV doses, respectively (Figure 4.5A, red bars). There is a negligible effect on EdU incorporation in the NUDT15-proficient cells at the 24 hour time point with more than 95% of cells being EdU⁺, which is approximately background levels in NT control cells (Figure 4.5A, blue bars). There was also a slight but significant ($p < 0.05$) decrease in the G₂/M population of NUDT15 KO cells at the 100 μM dose compared to the proficient cell line at the same dosage (Figure 4.4A, teal bars). However, compared to the NT NUDT15 KO cells, there was only an ~6% decrease in the G₂/M population of the NUDT15-deficient cells at the 100 μM dose (Figure 4.4A, teal bars 4-6).

At the 48 hour time point, NUDT15 KO cells continue to show an increase of cells in S phase. There is an ~56% increase at the 30 μM dose and an ~59% increase at the 100 μM dose compared to the NT NUDT15 KO control cells (Figure 4.4B, tan bars 4-6). Both increases in S phase are significantly ($p < 0.001$, $p < 0.01$) different from the NUDT15-proficient cells at the same doses (Figure 4.4B, tans bars 1-3). While an increase in the percentage of S phase NUDT15 KO cells after ACV treatments was detected, the increase was not significant in EdU⁺ cells, however, a trend of decreasing EdU⁺ S phase cells was detected in the NUDT15-proficient cells at any dose (Figure 4.5B).

At the 72 hour mark, an increase of ~ 56% at the 30 μM and an increase of ~103% in the 100 μM doses in the NUDT15 KO cells compared to the NT control cells was observed (Figure 4.4C, tans lanes 4-6). Both values show a significant ($p < 0.0001$) difference in S phase cells compared to the NUDT15-proficient cells at the same doses

(Figure 4.4C, tans lanes 1-3). Regarding actively DNA synthesizing cells, a significant decrease in EDU⁺ NUDT15 KO cells in S phase in the 30 μ M treated cells was detected, however there is no significant increase in the 100 μ M cells at the same time point compared to NUDT15-proficient cells at the same dose (Figure 4.5C).

Overall, this data supports that NUDT15 KO cells will undergo an S phase arrest in response to ACV treatments and show a prominent termination in DNA synthesis after 24 hours and as late as 72 hours after treatments.

4.2D NUDT15 KO cells show increased DNA damage after ACV treatments

To assess DNA damage after ACV treatments in the NUDT15 KO cells, a western blot was used to observe changes in expression of γ -H2AX as well as the alkaline comet assay. γ -H2AX is a biomarker for DNA damage in cells so an increase in expression would support ACV treatments causing double-strand DNA breaks. The alkaline comet assay detects all DNA damage, including ssDNA during replication or stalls in replication. DNA damage is determined using the percentage of DNA in the tail as determined by the Trevigen Comet Analysis Software.

Regarding γ -H2AX, there was an increase in expression in the NUDT15 KO cells treated with 100 μ M ACV for 72 hours compared to the NUDT15-proficient cells at the same dose (Figure 4.6A). Quantification of γ -H2AX normalized to β -tubulin compared to the DMSO treated controls for both cell lines show an increase in γ -H2AX in the NUDT15 KO cells (red bars) compared to the NUDT15-proficient cells (blue bars) at the same dose.

Due to the kinetics of ACV being metabolized to the active form not being known for this study, cells were treated for a wider range of time periods to assess when ACV-induced DNA damage would begin to occur. NUDT15-proficient and deficient cells are at

a baseline range of 8-10% DNA in the tail for the NT control groups. After a 1 hour treatment, a significant ($p < 0.001$) difference in percentage of DNA in the tail is seen with ~22%, a 1.1-fold increase compared to the NT control cells, in the NUDT15-proficient cells (blue bars) at the 30 μM dose that is not seen in the NUDT15 KO cells (red bars) that are at ~14%, a 0.8-fold increase compared to NT control cells (Figure 4.7A). At the 100 μM dose, NUDT15-proficient cells show ~17% of DNA, a 0.7-fold increase, in the tail while the deficient show ~13%, also a 0.7-fold increase. At the 6 hour time point, there is a similar trend with a significant ($p < 0.01$) difference of ~16.4%, a 0.6-fold increase compared to NT but 0.25-fold decrease from the 1 hour treatment, in the tail of NUDT15-proficient cells at 30 μM of ACV compared to ~12%, also 0.6-fold increase, in the NUDT15 KO cells at the same dose (Figure 4.7B). However, the percentage in the NUDT15-proficient cells at 100 μM only increases to 12%, a 0.2-fold change, while the NUDT15-deficient cells remain at ~13%, a 0.7-fold increase, in the tail. At the 12 hour exposure, there was still a slightly significant ($p < 0.05$) difference in NUDT15-proficient cells at the 30 μM dose with ~17.4% of DNA in the tail, a 0.7-fold increase, compared to ~12.6%, also a 0.7-fold increase, DNA in the tail in the NUDT15 KO cells (Figure 4.7C). At the 100 μM dosage, NUDT15-proficient cells remain slightly above baseline percentage at ~14%, a 0.4-fold increase, while the NUDT15-deficient cells remain at ~13%, a 0.7-fold increase, like the one and six hour time points. Overall, the 1, 6, and 12 hour time points seem to consistently show a slight increase in percentage of tail DNA at the lower dose of ACV in the NUDT15-proficient cells compared to the NUDT15 KO cells, however, both cell lines show a similar fold change of DNA in the tail. This supports there is not a significant increase of DNA damage at these time points regardless of NUDT15 status.

After 24 hours, there was still a slight but significant ($p < 0.001$) difference of ~13.4%, a 0.6-fold increase, DNA in the tail in the NUDT15-proficient cells compared to ~8.9%, a 0.2-fold increase, in the NUDT15 KO cells at the same dose (Figure 4.7D). While the proficient cells show slightly more damage at the lower dose, the 100 μM dose in the NUDT15 KO cells shows an increase, though insignificant, in the percentage of DNA in the tail to ~11.7%, a 0.5-fold increase, compared to the ~10%, a 0.2-fold increase, in the NT NUDT15 KO control cells (Figure 4.7D, red bars). At the 48 hour mark after 100 μM ACV treatments, there is a significant ($p < 0.0001$) difference between ~16.8%, a 1.2-fold increase, DNA in the tail in the tail of NUDT15 KO cells compared to ~7.3%, a 0.1-fold decrease, in the NUDT15-proficient cells at the same dose (Figure 4.7E). Worth noting at the 48 hour time point, there is minimal change in the percentage of DNA in the tail of the NUDT15-proficient cells regardless of dose while the NUDT15-deficient cells are showing a dose response with increasing percentages as dosage increases. At the 72 hour time point, there is again a significant ($p < 0.0001$) increase to ~20.2%, a 1.6-fold increase, tail DNA in the NUDT15 KO cells at the 100 μM dose compared to ~9.4%, a 0.1-fold increase, tail DNA in the NUDT15-proficient cell lines (Figure 4.7F). Again, there is minimal change in tail DNA in the NUDT15-proficient cell line while the NUDT15 KO line shows an increase in damage as the dosage of ACV increases. Representative images of NUDT15-proficient and deficient cells treated with ACV for 72 hours show an increase in DNA in the tail in the NUDT15 KO cells (right) that is not seen in the parental cells (left) at the 30 μM or 100 μM doses (Figure 4.7E).

Altogether, an increase in $\gamma\text{-H2AX}$ expression and the increase of percentage of tail DNA in the alkaline comet assay supports a significant increase of DNA damage caused

by ACV treatments in NUDT15-deficient cells. The comet assay also shows that ACV first begins to effect NUDT15-deficient cell lines after 24 hour exposures at the doses used with the largest effect being observed after 72 hours of exposure.

4.3 Discussion

NUDT15 is a member of a large family of NUDIX hydrolases with biological functions that remain largely unknown. These family members appear to commonly have activity against nucleotide analogs that contain a diphosphate group that they then hydrolyze prior to the incorporation of the analog into DNA. One such analog that was recently found to be acted on by NUDT15 is the anti-viral drug ACV, with NUDT15 polymorphisms showing increased efficacy of ACV in HSV infected cells.²² The mechanism of action for ACV allows increased specificity to target only HSV-infected cells through the virally encoded HSV thymidine kinase enzyme. This allows ACV to only cause a termination in DNA synthesis and eventual induction of apoptosis in infected cells, leaving healthy cells largely unaffected.⁸⁷ Understanding how ACV becomes more effective in a NUDT15-deficient cancer cell line would allow an additional method of treating cancer where cancerous cells would become more sensitive while the healthy cells would remain unaffected, even at high doses of the drug. With the evidence from the TCGA and cBioPortal databases showing the strong correlation between RB1 loss and NUDT15 as a passenger loss, ACV could be used as a first line treatment to begin targeting NUDT15-deficient cells without much of a risk to healthy cells.

While Nishii *et. al* show the increase in effects of ACV treatments in HSV and cytomegalovirus infected cells, little is shown on the mechanism for how NUDT15-deficient cells respond to more efficacious ACV treatments. Using a resazurin assay,

CRISPR generated NUDT15 KO cells show increased sensitivity to ACV with or without the HSV-TK protein (Figure 4.1). Worth noting is that NUDT15 KO cells expressing HSV-TK do appear to be more sensitive to ACV at a shorter exposure time of 24 hours while cells that are not expressing HSV-TK show equal sensitivity after a 72 hour exposure. This data supports that HSV-TK does increase the efficacy of ACV but may not be needed in a NUDT15-deficient cell line. To further support this finding, cells were treated with ACV without HSV-TK being present. The doses of 30 μ M and 100 μ M were also consistently used because of similar doses being commonly used and easily attainable by intravenous injections in the clinic.⁸⁹

Selectivity assays were used to simulate a course of chemotherapy using ACV with continuous exposure over the course of several cell passages (Figure 4.2). The results support that ACV treatments will selectively decrease the prevalence of the GFP+ NUDT15 KO cells, however, a more striking difference would likely become apparent with more passages with continuous treatments at a higher dose. Images of cells are also encouraging in the sense that the GFP- NUDT15-proficient cells do not appear to have their growth hindered over the course of treatments, even after 5 passages of continuous 100 μ M of ACV treatments. The evidence provided by the resazurin and selectivity assays support that NUDT15-deficient cells are at a selective disadvantage after ACV treatments compared to NUDT15-proficient cells but the mechanism for this needed to be further analyzed.

The ApoTox-Glo™ assay was used to determine changes in viability, cytotoxicity, and apoptosis induction to determine at what time and dose are the NUDT15-deficient cells beginning to show signs of increased efficacy of ACV treatments (Figure 4.3). Viability of

NUDT15-deficient cells did not seem to have a drastic effect after 24 hours of treatment with the indicated doses. However, there was a decrease in viability in the deficient cell lines at the 100 μ M dose after 48 hours and at the 30 μ M and 100 μ M doses after 72 hours of exposure. The detection of viable NUDT15-deficient cells remains comparable to the NT control cells up to the 48 hour exposure mark where viability then begins to drop below the baseline NT control cell value. Note the NUDT15-proficient cells remain mostly at or above baseline values compared to the NT control cells, supporting ACV is decreasing viability in the NUDT15-deficient cells. Cytotoxicity values appear slightly above baseline levels in both cell lines regardless of NUDT15 status after 24 and 48 hour exposure. At the 72 hour time point, what appears to be a slight, though a significant difference in cytotoxicity values is seen at the 30 μ M and 100 μ M doses with values sinking below baseline in the NUDT15-deficient cells. This apparent decrease in cytotoxicity could be the result of apoptosis after ACV treatments or a cell cycle arrest. Note there is not an increase in cytotoxicity in the NUDT15-proficient cells as the values remain similar to baseline values. NUDT15-deficient cells show a significant difference in the induction of apoptosis at the 100 μ M dose after 72 hours with no change in apoptosis in the NUDT15-proficient cells. The induction in the deficient cells likely explains why there was such a large decrease in cytotoxicity values at the same dose and time signifying cells undergo controlled cell death versus necrosis.

The mechanism of action for ACV involves a termination of DNA synthesis after the active metabolite becomes incorporated. Using flow cytometry, a significant percentage of cells were arrested in S phase were detected in NUDT15-deficient cells at 24, 48, and 72 hour timepoints at both 30 μ M and 100 μ M doses (Figure 4.4). There were

also minimal changes in S phase cells in the NUDT15-proficient cells further supporting that NUDT15 is involved in the prevention of ACV causing the S phase arrest. More importantly, using Click-iT chemistry to detect EdU incorporation into DNA being actively synthesized prior to fixing cells, the percentage of cells in S phase that are not actively incorporating DNA were evaluated (Figure 4.5). A significant decrease in EdU+ S phase cells were observed at the 24 hour time point in the NUDT15-deficient cells. At no point was there a significant change in the EdU+ S phase NUDT15-proficient cells, further supporting that this effect was exclusive to the NUDT15-deficient line. While the 24 hour time point has the largest significant difference of EdU+ S phase cells compared to NUDT15-proficient cells, the 48 hour point shows a decrease of EdU+ S phase cells in both doses compared to the NT NUDT15-deficient cells, though the data is not statistically different from the NUDT15-proficient cells at the same doses. Overall, the cell cycle data supports that NUDT15-deficient cells are undergoing an S phase arrest after treatments with ACV which would be the expected phenotype based on what is already known regarding the mechanism of action of ACV.

While evidence supports ACV is causing an arrest in S phase in NUDT15-deficient cells, we next wanted to see if ACV treatments were causing increased DNA damage as well. A western blot did show an increase in γ -H2AX signaling after 72 hours at a 100 μ M dosage of ACV, supporting an increase in DNA damage at that time and dose (Figure 4.6). While 72 hours at 100 μ M does show the greatest increase in apoptosis induction, other doses and time points need to be considered as well to be able to determine when most of the DNA damage signaling is occurring.

The alkaline comet assay was also used to determine DNA damage after ACV treatments (Figure 4.7). Because of uncertainty with the timing of the metabolism for ACV to become activated and incorporated in DNA, earlier time points of 1, 6, and 12 hour exposures were used in addition to 24, 48, and 72 hour exposures. While the parental cells do show a higher percentage of DNA in the tail at the 1, 6, and 12 hour exposures, the fold change in damage is approximately equal to the fold change seen in the NUDT15-deficient cell lines at the same times and doses. While the percentage of tail DNA may show a significant difference between NUDT15-proficient and deficient cells at the 30 μM doses for the three earlier time points, the fold change compared to the NT controls of each cell lines were nearly identical. This supports that there was no difference DNA damage at the earlier time points after ACV treatments, regardless of NUDT15 status. After 24 hours, a larger fold increase in percentage of tail DNA is observed in the NUDT15-deficient cells at the 100 μM dose. A noticeable trend of an increase in dose leading to an increase in tail DNA percentage is then seen at the 48 and 72 hour treatments. The NUDT15-proficient cells do show a slightly higher fold change in DNA tail percentage at the 30 μM dose after 24 hours compared to the NUDT15-deficient cells. However, later time points show minimal change in percentage of tail DNA at either 30 μM or 100 μM doses in the NUDT15-proficient cell line. The NUDT15-deficient cells show the largest increase in tail DNA percentage at the 100 μM dose after 48 and 72 hours supporting a potential increase in DNA damage. One caveat, as with the alkaline comet assays, S phase cells will also be detected as “damage”, which also supports the need for a modified BrdU comet assay to determine which cells are truly damaged and which are undergoing DNA replication. With the significant increase in S phase NUDT15-deficient cells, it is worth exploring

differences in tail DNA percentage of cells actively synthesizing DNA and cells at other stages of the cell cycle.

Overall, the findings support that NUDT15-deficient cells are more sensitive to the anti-viral drug acyclovir. NUDT15-deficient cells show decrease survivability in long-term exposure to acyclovir in a colony forming assay and the selectivity assay performed. NUDT15-deficient cells also show significant cell cycle arrest in S phase which supports the known mechanism of ACV causing DNA synthesis termination after incorporation. This finding is supported by NUDT15-deficient cells lacking incorporation of EdU in cells detected in S phase by flow cytometry while the NUDT15-proficient cells remain largely unaffected. NUDT15-deficient cells also show increased damage signaling via γ -H2AX expression and an increase in tail DNA percentage. These findings support the use of ACV as a treatment option in NUDT15-deficient cancer cells, both as an effective means to cause damage in NUDT15-deficient cells as well as creating a large therapeutic window that will show a minimal effect on healthy, NUDT15-proficient cells.

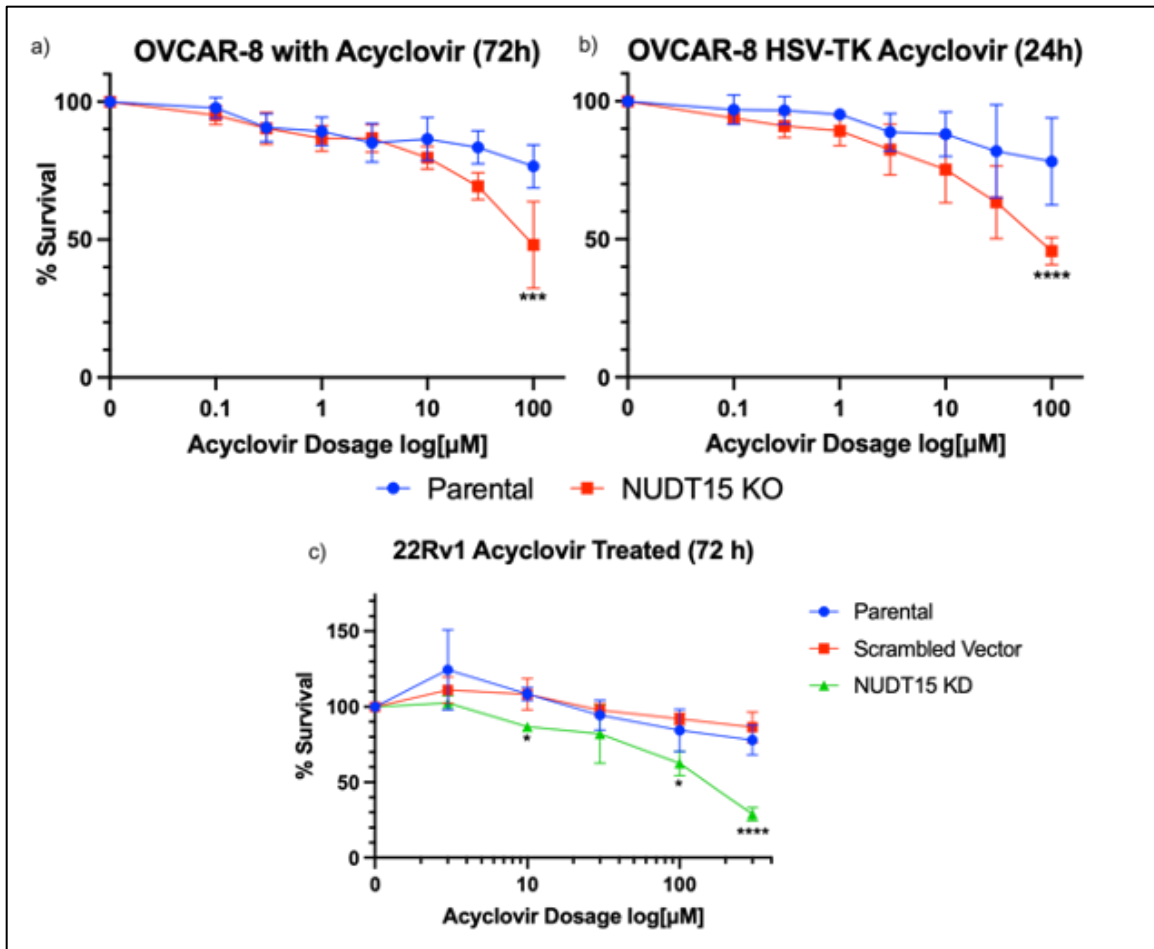


Figure 4.1 NUDT15-deficient cells show increased sensitivity to acyclovir treatments. A resazurin assay shows increased sensitivity to acyclovir in NUDT15 KO cells with or without the addition of the Herpes Simplex Virus Thymidine Kinase (HSV-TK) at the indicated doses for the indicated time. 22Rv1 prostate cancer cells with NUDT15 siRNA show increased sensitivity to ACV in a colony forming assay. A) After 72 hours of exposure to ACV at the indicated doses, percent survival is plotted compared to nontreated control cells. B) After transfection with HSV-TK, cells were treated with ACV for 24 hours at the indicated doses and allowed to recover for 48 hours prior to addition of resazurin. C) 22Rv1 prostate cancer cells treated with ACV in a colony forming assay. Statistical significance was determined using two-way ANOVA. * $p < 0.05$ **** $p < 0.0001$

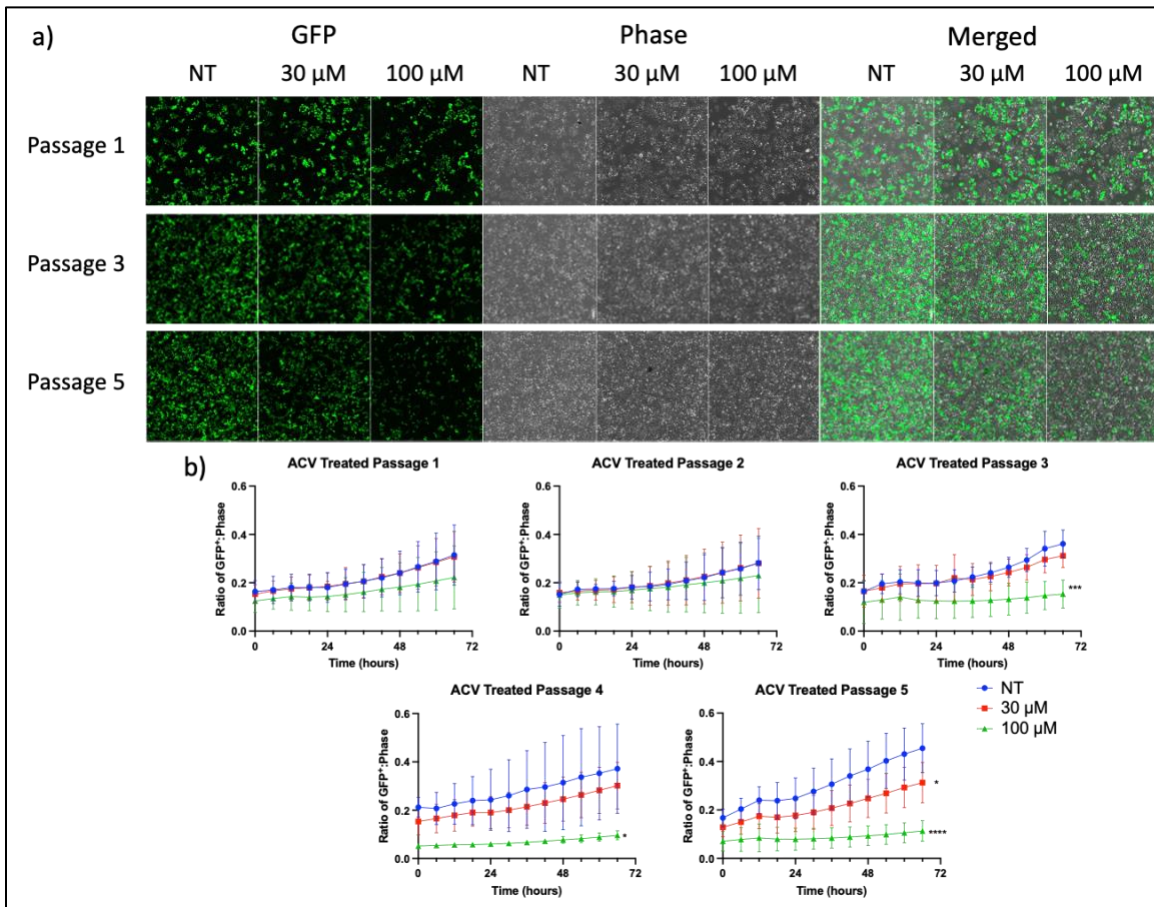


Figure 4.2 Selectivity assay shows a decrease in survival of GFP⁺ NUDT15 KO cells after continuous exposure to ACV. Live-cell imaging results show a loss in GFP⁺ NUDT15-deficient cells mixed with GFP⁻ NUDT15-proficient cells. A) Representative images of Passage 1, Passage 3, and Passage 5 cells after 66 hours of treatment. Images show GFP only (left), phase contrast (middle), and merged (right). B) Quantification of the ratio of GFP⁺ cells: Phase Contrast cells at each passage number over the course of 66 hours with 30 μ M or 100 μ M of continuous ACV exposure. Significance was determined by two-way ANOVA. * $p < 0.05$ *** $p < 0.001$ **** $p < 0.0001$

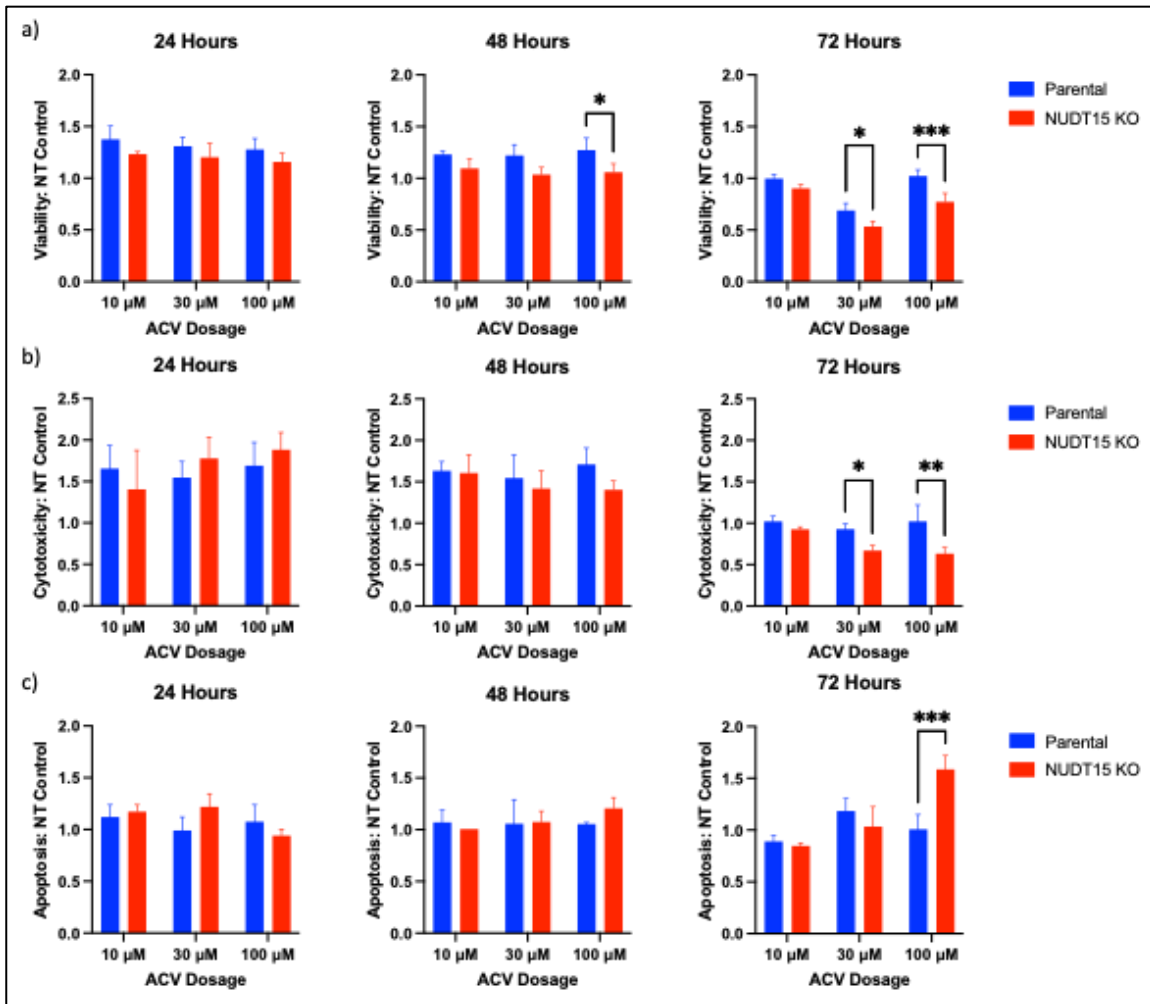


Figure 4.3 Triplex assay of NUDT15 KO cells treated with ACV. ApoTox-Glo Triplex assay of NUDT15-deficient cells were treated with ACV at the indicated doses for the indicated times. NUDT15 KO cells show decreased viability and cytotoxicity but increased apoptosis compared to parental cells. A) Viability of parental cells (blue) and NUDT15 KO cells (red). B) Cytotoxicity of parental cells (blue) and NUDT15 KO cells (red). C) Apoptosis of parental cells (blue) and NUDT15 KO cells (red). Statistical significance determined with two-way ANOVA. * $p < 0.05$, ** $p < 0.01$, *** $p < 0.001$

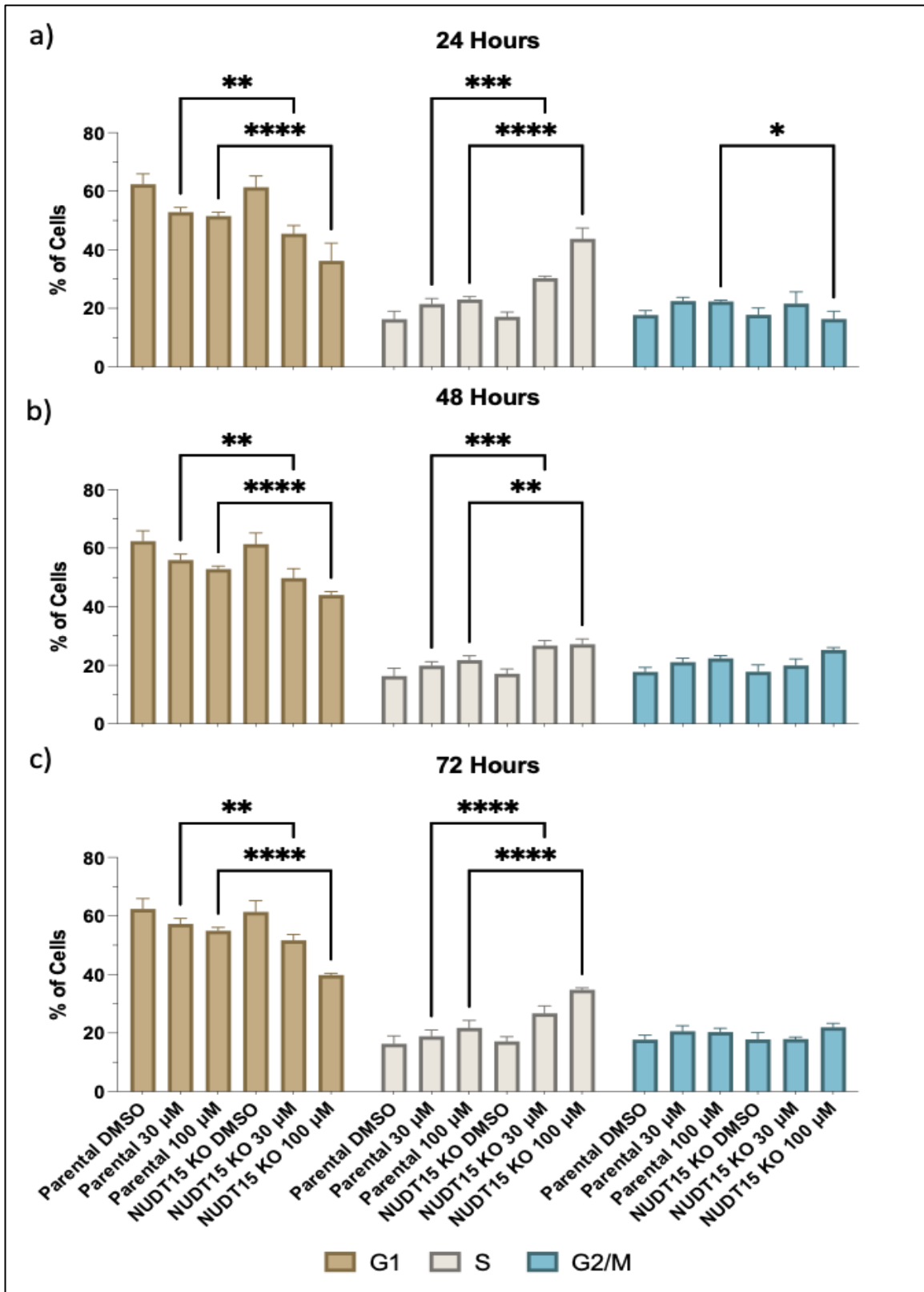


Figure 4.4 Cell-cycle profile of parental and NUDT15-deficient cells in response to ACV treatments (Previous Page). Flow cytometry results of NUDT15 KO cells treated with ACV at the indicated doses for the indicated time. NUDT15 KO cells show significant S phase arrests at 30 μ M and 100 μ M doses at 24, 48, and 72 hour timepoints. Each panel shows the G₁, S phase, G₂/M phase populations of parental and NUDT15 KO cells after exposure to 6-TG for: A) 24 hours, B) 48 hours, and C) 72 hours. Each bar represents three independent experiments. Statistical significance was determined by two-way ANOVA. * $p < 0.05$ ** $p < 0.01$, *** $p < 0.001$, **** $p < 0.0001$

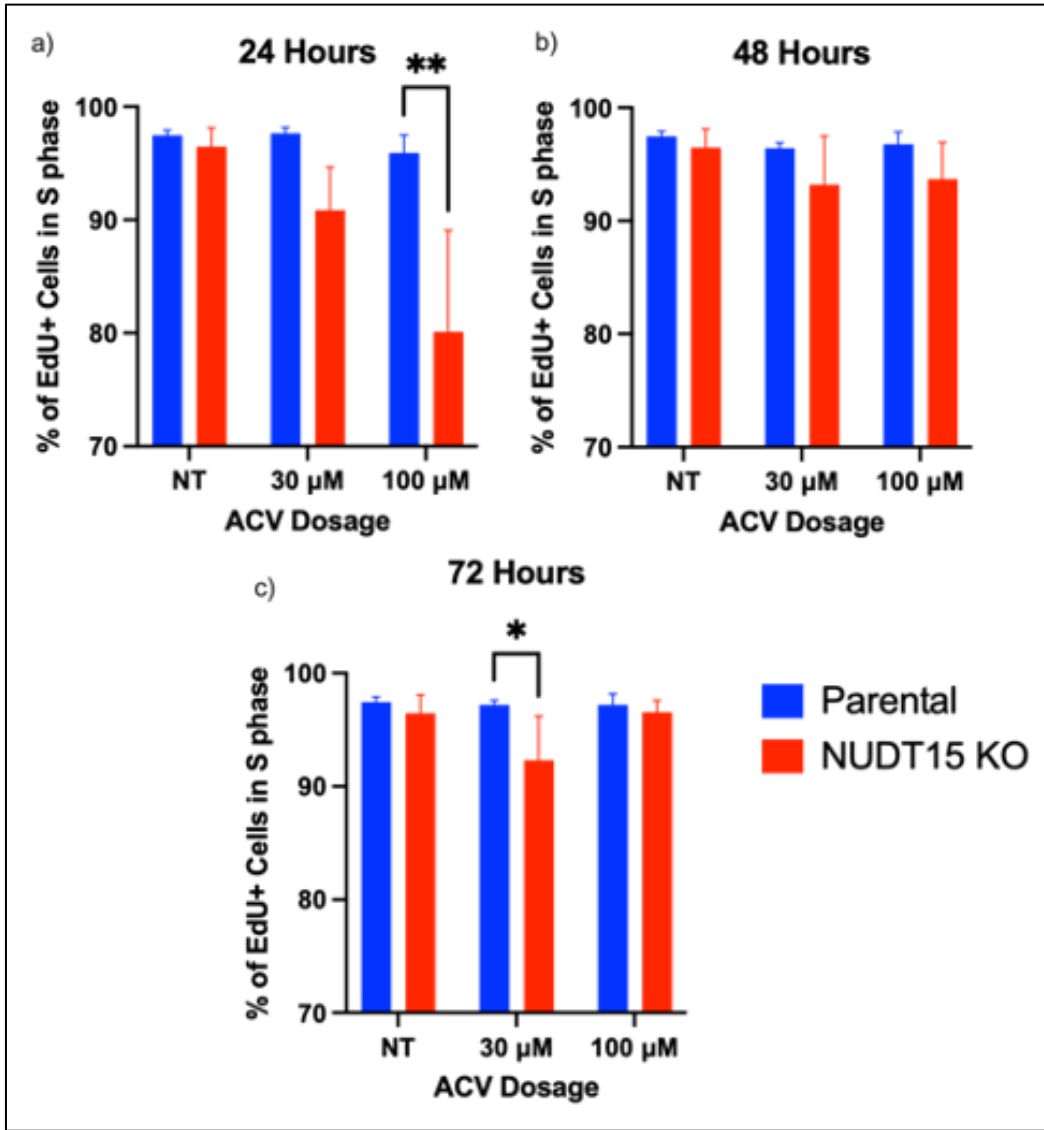


Figure 4.5 ACV treated NUDT15 KO cells are not actively synthesizing DNA in S phase. Cells actively synthesizing DNA were analyzed using Click-iT chemistry to detect incorporation of the thymidine analog EdU. The bars show the percentage of NUDT15-proficient (blue), and deficient (red) cells counted in S phase by DAPI that were actively incorporating EdU after exposures of NT, 30 μM, and 100 μM ACV at A) 24 hours B) 48 hours and C) 72 hours. Statistical significance was determined by two-way ANOVA. * p < 0.05 ** p < 0.01

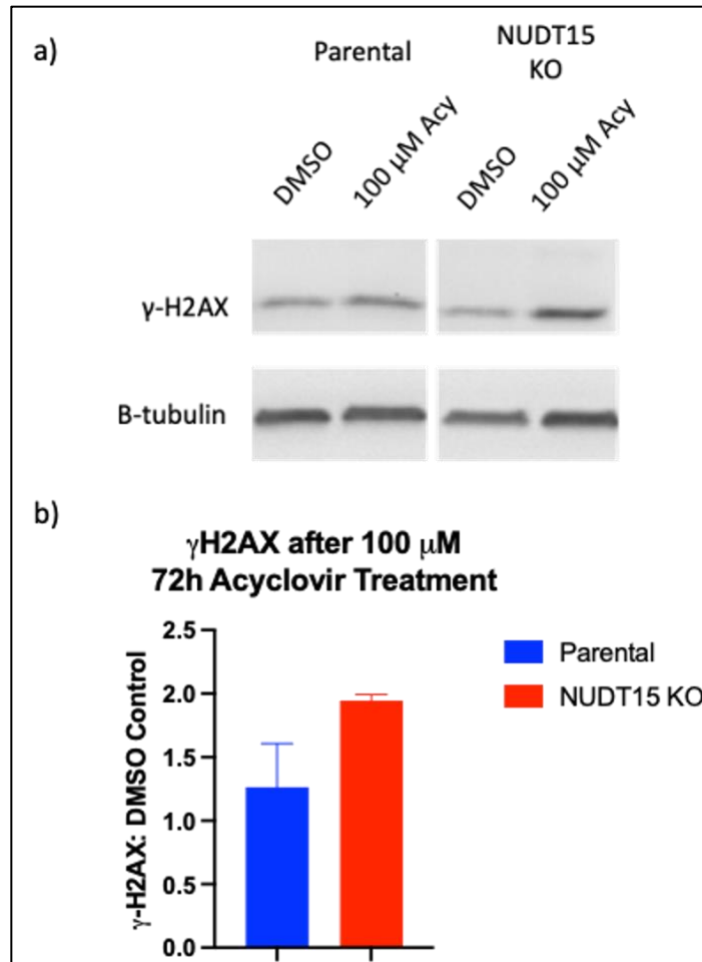


Figure 4.6 DNA Damage marker γ -H2AX is induced after ACV treatments. A) Induction of γ -H2AX after treatment with 6-TG for 72 hours at a 100 μ M dose in parental (lanes 1 &2), NUDT18 KO and NUDT15 KO (Lanes 3 & 4) cells. β - tubulin serves as a loading control. B) Quantification of γ -H2AX in the indicated cell lines compared to DMSO only control cells with expression normalized to β - tubulin.

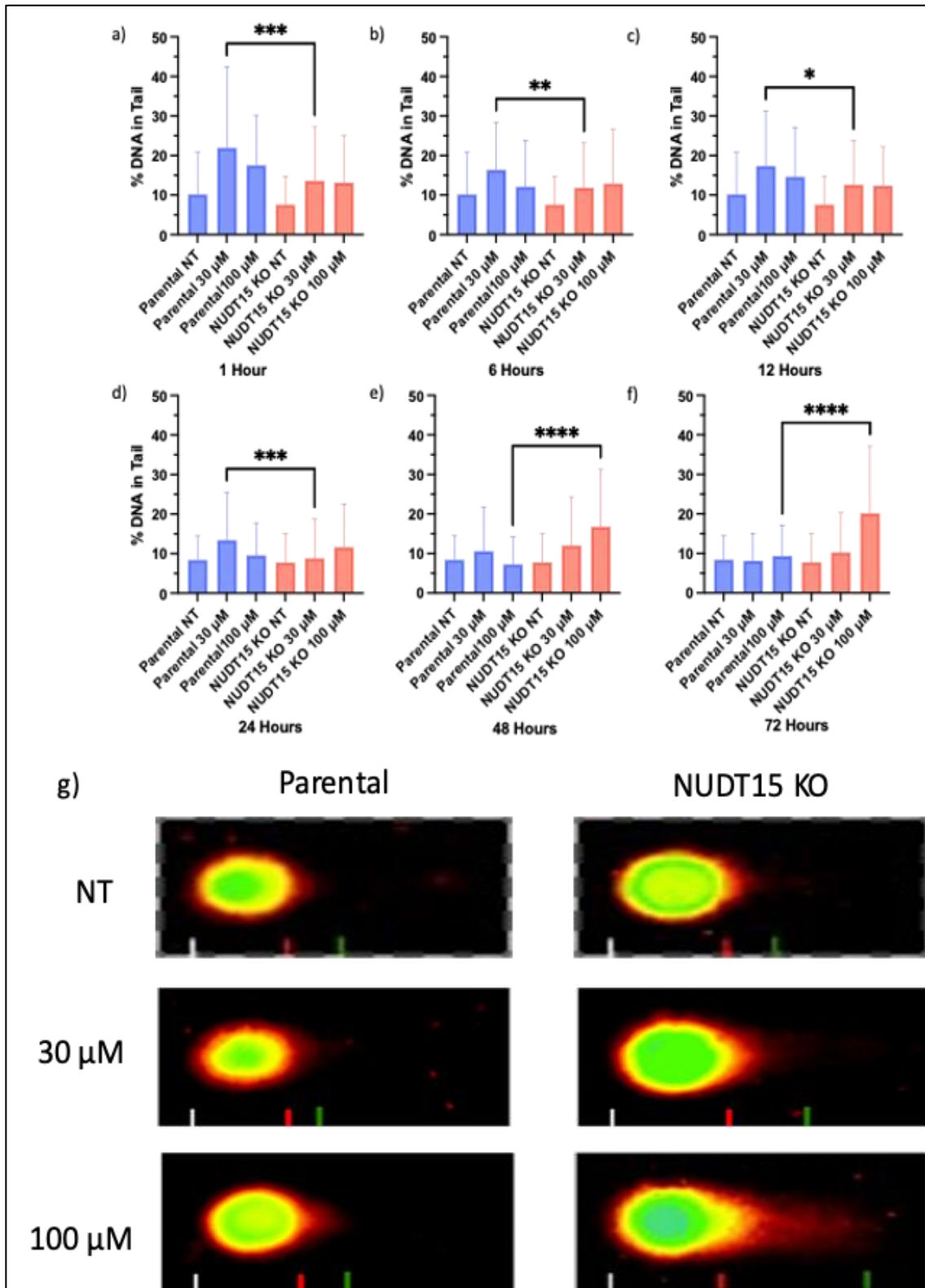


Figure 4.7 Comet assay measuring DNA damage in ACV treated NUDT15 KO and parental cells (Previous Page). Alkaline comet assay showing percentage of DNA in comet tails as an indicator for DNA damage in response to ACV treatments at the above doses for the above times. Percent DNA in tail for cells treated with 30 μM or 100 μM doses for A) 1 hour, B) 6 hours, C) 12 hours, D) 24 hours, E) 48 hours, F) 72 hours. G) Representative images of comets after 72 hours of treatment at nontreated, 30 μM , and 100 μM doses. Statistical significance was determined by two-way ANOVA **** $p < 0.0001$

CHAPTER 5
GENERAL CONCLUSIONS

The long-term purpose of the project was to advance personalized medicine with drug repurposing. The goal of this project was to identify biomarkers of gene deficiencies that could be therapeutically exploitable with old, cheap drugs for which there is much clinical experience. Identifying compounds that exploit a deficiency in a gene of interest can create a new therapeutic window, to cause selective lethality in cancer cells while minimizing the cytotoxic effects on healthy tissues. The NUDIX hydrolases serve as valuable enzymes to study since so little is known about the family. The biological functions of the majority of the 22 members remain undefined. Increasing the understanding of additional roles will allow other researchers to increase the efficacy of nucleotide analog based treatments. This project also raises the importance of screening prior to starting cancer treatments. Screening is not only important to assess increased risks that may have caused the cancer, but also to detect additional mutations that can then be utilized in the cancer treatment.

NUDT15 and NUDT18 are excellent examples that are involved with the goals of the project. While our understanding of the nonbiological functions of NUDT15 against the active forms of thiopurines and acyclovir are becoming increasingly understood^{22, 33}, very little is known about the functions of NUDT18 altogether. This study utilized patient derived organoid data as well as published *in vitro* data as guidance to begin exploring metabolites that might be substrates of NUDT18. The experimental approach utilized NUDT18 knock out cells, confirmed by RT-PCR, and noticeably, a change in proliferation was observed in the NUDT18 KO cells, which was not further explored in this study. Analysis of the cellular sensitivity of the NUDT18 KO cells to a range of metabolites did not reveal any revealing data that would suggest those metabolites are metabolized by the

NUDT18 enzyme. Analysis of changes in mutational signature or metabolomic analysis may provide more insight as to why the NUDT18-deficient cells had decreased proliferation compared to the parental cells and the NUDT15-deficient cell lines.

The second NUDT family member, NUDT15, was pursued because of the link to a loss of RB1 in cancer cells. Searches through The Cancer Genome Atlas and cBioPortal databases show that in cancers with a copy number loss of RB1, that cancer nearly always shows a loss of NUDT15 copy number as well. While the loss of RB1 may contribute to oncogenesis, a loss in NUDT15 seems to be a passenger loss that does not contribute or detract from the development of cancer. However, we aimed to show cancer cells that have a deficiency of NUDT15 can be targeted by 6-TG or ACV with little effect being seen in normal, healthy cells with functioning NUDT15.

It was previously established that NUDT15-deficient cells show increased sensitivity to 6-TG and that NUDT15 is involved in the hydrolysis of the active 6-thio-(d)GTP metabolites³³ but the cellular effects had not been explored beyond cell death. Here we show that NUDT15-deficient cells are not only hypersensitive to 6-TG, but with careful dose selection over time, exposure to 6-TG selectively kills NUDT15-deficient cells whereas NUDT15 proficient cells continue proliferating. We show that NUDT15-deficient cells can be treated with a low enough dose of 6-TG that the proliferation of parental cells is not affected while the NUDT15-deficient cells are strongly selected against, which would be the case for a patient's non-tumor cells. This study did not investigate any mutagenicity associated with prolonged 6-TG exposure in the NUDT15-proficient cells, but the low dose of 6-TG being so efficacious in killing NUDT15-deficient cells without hindering NUDT15-proficient cell growth allows hope for minimal mutagenicity.

Our findings also support that the NUDT15-deficient cells show decreased viability after 6-TG treatments using the ApoTox-Glo™ triplex assay. The findings of the triplex assay also support previous findings that the cytotoxic effects and induction of apoptosis from 6-TG require time to become observable beyond the 96 hours that we used for this experiment.^{38, 39, 84, 86} The findings support evidence of a cell cycle arrest, which was observed using flow cytometry. It was previously published that cells treated with lower doses of 6-TG can pass through the cell cycle and mitosis with damaged DNA, while higher doses of 6-TG will cause a G₂ arrest, likely due to too high amount of DNA damage to allow mitosis to proceed.⁸⁴ The NUDT15-deficient cells showed an arrest in G₂ phase after 72 hours of exposure to 1 μM of 6-TG as expected. Interestingly, NUDT15-deficient cells also showed a slight arrest in S phase at the 0.3 μM dose after 48 and 72 hours. This arrest in S phase may be a result of cells attempting to replicate DNA that has already undergone attempts at faithful repair, thus prolonging the amount of time in S phase. Chromosomal aberration data supports that there is a striking increase in radials and complex chromosome exchanges that are not present in the NUDT15-proficient cells at the same dose. While the formation of radials and complex exchanges remain a poorly understood process, they are assumed to be the result of failed attempts at repairing double-strand breaks and secondary end-joining. It can be inferred that these unnatural DNA structures would be difficult for cells replicate, possibly explaining this build-up in S phase. We also observed increases in DNA damage signaling by γ-H2AX expression and overall DNA damage using the alkaline comet assay, providing additional evidence that 6-TG causes increased DNA damage in NUDT15-deficient cells.

For future directions, the downstream metabolism of 6-thio-dGMP that are produced resulting from NUDT15 hydrolyzing 6-thio-dGTP remains unknown. A proposed pathway would be phosphorylation, potentially by the guanylate kinase GUK1, allows 6-thio-dGDP to then rejoin the known thiopurine metabolism pathway before being deactivated NUDT15 again or become incorporated into DNA. This pathway could result in a potentially futile cycle where NUDT15 is constantly hydrolyzing 6-thio-dGTP to 6-thio-dGMP until other, unidentified enzymes further break down the monophosphate form. The other pathway could be that 6-thio-dGTP is metabolized to 6-thio-dGMP by NUDT15 and 6-thio-dGMP is quickly broken down by other unidentified enzymes, potentially TPMT. This model is graphically represented in Figure 5.1.

While evidence of NUDT15 acting on the 6-TG active metabolites has been known since 2015,³³ evidence of increased efficacy of acyclovir in NUDT15-deficient cells was unknown prior to this work. Indeed, our observations of NUDT15 deficiency causing sensitivity to ACV was independently published very recently,²² which nicely concurs with our observations. As with 6-TG, little has been analyzed regarding the mechanism that is involved in increasing ACV effectiveness in NUDT15-deficient cells. Using resazurin and sensitivity assays, we observe supportive evidence that the NUDT15-deficient cells are more sensitive to ACV treatments. Notably, sensitivity is seen without the HSV-TK enzyme. Note that the mechanism of action and the basis for its selectivity as an antiviral agent relies on the fact that ACV is not efficiently phosphorylated into its active nucleotide precursor, whereas in HSV-infected cells that express the HSV-TK enzyme, ACV is phosphorylated and once incorporated into DNA, then blocks replication of the virally infected human cells. Among all the nucleoside analogs clinically used as antiviral

therapeutics, ACV is among the safest with regards to therapeutic index and lack of serious side effects. It was therefore surprising and interesting to see that in the prostate and ovarian cancer cell lines used in this study, the loss of NUDT15 revealed a cellular sensitivity to ACV. The selectivity assay was performed in the absence of HSV-TK as well, adding additional evidence that a NUDT15-deficiency is sufficient to increase the efficacy of ACV treatments. We speculate that there must be inefficient activation of ACV in the absence of HSV-TK by human kinases, but only the absence of NUDT15 reveals this sensitivity. The evidence of an increase in sensitivity to ACV in the NUDT15-deficient cells supported further exploration into the mechanism.

Using the ApoTox-Glo™ assay, we saw a decrease in NUDT15-deficient cell viability after 48 hours at the 100 μ M dose and at the 30 μ M and 100 μ M doses after 72 hours. While we did not see an increase in cytotoxicity, there was an induction of apoptosis at the 100 μ M dose after 72 hours. These results, like 6-TG, supported a potential cell cycle arrest. Based on the known mechanism for ACV, we expected to see NUDT15-deficient cells arrest in S phase because of a termination in DNA synthesis. Using flow cytometry to analyze the cycle profile, significant arrests in S phase at the 30 μ M and 100 μ M doses at 24, 48, and 72 hour exposures in the NUDT15-deficient cells were observed. There was no significant change in the cell cycle profile of the NUDT15-proficient cells. Using a thymidine analog, EdU, and Click-iT chemistry to visualize EdU incorporated into DNA during replication, we were able to detect the percentage of S phase cells that were actively synthesizing DNA. After 24 hours at the 30 μ M and 100 μ M doses, significant decreases in EdU+ S phase cells were detected in the NUDT15-deficient cells. This data supports that in NUDT15-deficient cells, ACV seems to follow its accepted mechanism of action as

an antiviral, namely incorporation into DNA and subsequent halting of DNA synthesis in S phase.

There was also an observed increase in DNA damage in the NUDT15-deficient cells after treatments with ACV. There was an increase in γ -H2AX signaling, as detected by western blot, after 72 hours with 100 μ M of ACV. Other time points at lower doses should also be tested to confirm if there are changes of expression, especially at the 24 hour time point where there was significant evidence of a halt in DNA synthesis. The alkaline comet assay data also supports an increase in DNA damage in response to ACV treatments in the NUDT15-deficient cells. While shorter time points appear to show an increase in percentage of tail DNA in the NUDT15-proficient cells, the fold change is quite similar to and even smaller than the fold change in the NUDT15-deficient cells. The more significant and noticeable increase in tail DNA percentage is seen at the 48 and 72 hour time points where the NUDT15-deficient cells show increased damage in the tail as dose of ACV increases. As previously stated, cells undergoing replication appear as “damaged” in an alkaline assay. A modified comet assay using BrdU incorporation to detect cells actively in S phase would allow a method to distinguish between damaged cells and replicating cells.

For future directions, the initial activation of acyclovir in the absence of HSV-TK needs to be explored. The selectivity of ACV is attributed to the increased activation in herpes infected cells due to being phosphorylated by the virally transcribed herpes thymidine kinase. However, in a NUDT15-deficient cell line, ACV appears to become phosphorylated by other means, supporting a novel mechanism for activation in cells that are not infected with HSV. Normally, ACV may become phosphorylated at a much lower

efficiency with cellular kinases than with HSV-TK, however NUDT15 prevents the eventual incorporation into DNA. This supports NUDT15 being a large contributor to the selectivity of ACV treatments in HSV-infected cells while a NUDT15-deficiency provides selectivity against cancerous cells compared to healthy tissue. The model of these findings is represented in Figure 5.2.

As mentioned above, the identification of ACV as a substrate for NUDT15 is novel and was very recently independently shown by another group. Although no novel substrates were discovered to be more effective in NUDT18 KO cell lines, the data does allow potential other directions to direct future research, especially metabolomic studies. We also were able to analyze the mechanism in NUDT15-deficient cells after treatments to 6-TG and ACV. While more research is needed to identify the proper dosage and time for 6-TG and ACV treatments for solid tumors with defects in NUDT15, the overall evidence supports use of either drug for personalized treatment of individual cancers harboring such Achilles heel defects.

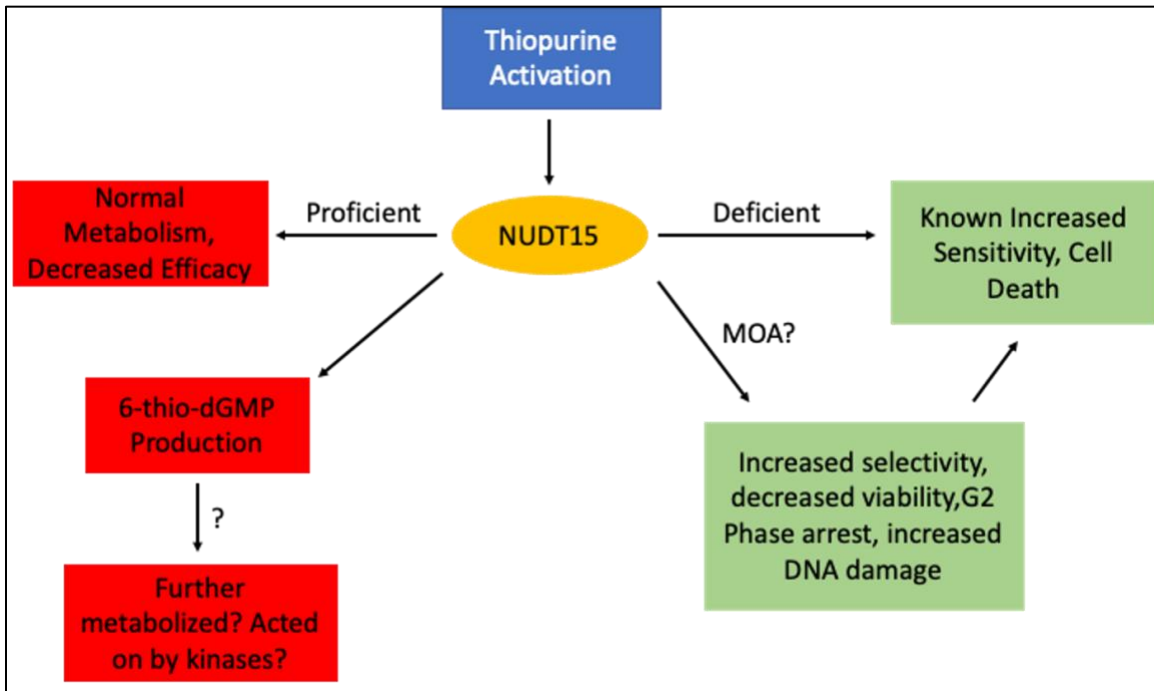


Figure 5.1 Proposed model for 6-TG treatments in NUDT15-deficient cells. A schematic showing the known and unknown results in NUDT15-proficient or deficient cells treated with thiopurines. NUDT15 proficient cells undergo normal thiopurine metabolism with NUDT15 decreasing the efficacy of thiopurine treatments with known production of 6-thio-dGMP, however the downstream metabolism of 6-thio-dGMP remains unknown. NUDT15-deficient cells are known to show increased sensitivity and cell death after thiopurine treatments, however the mechanism of action for this increased sensitivity needed to be determined. The findings of this project provided more understanding for the mechanism of the sensitivity increase.

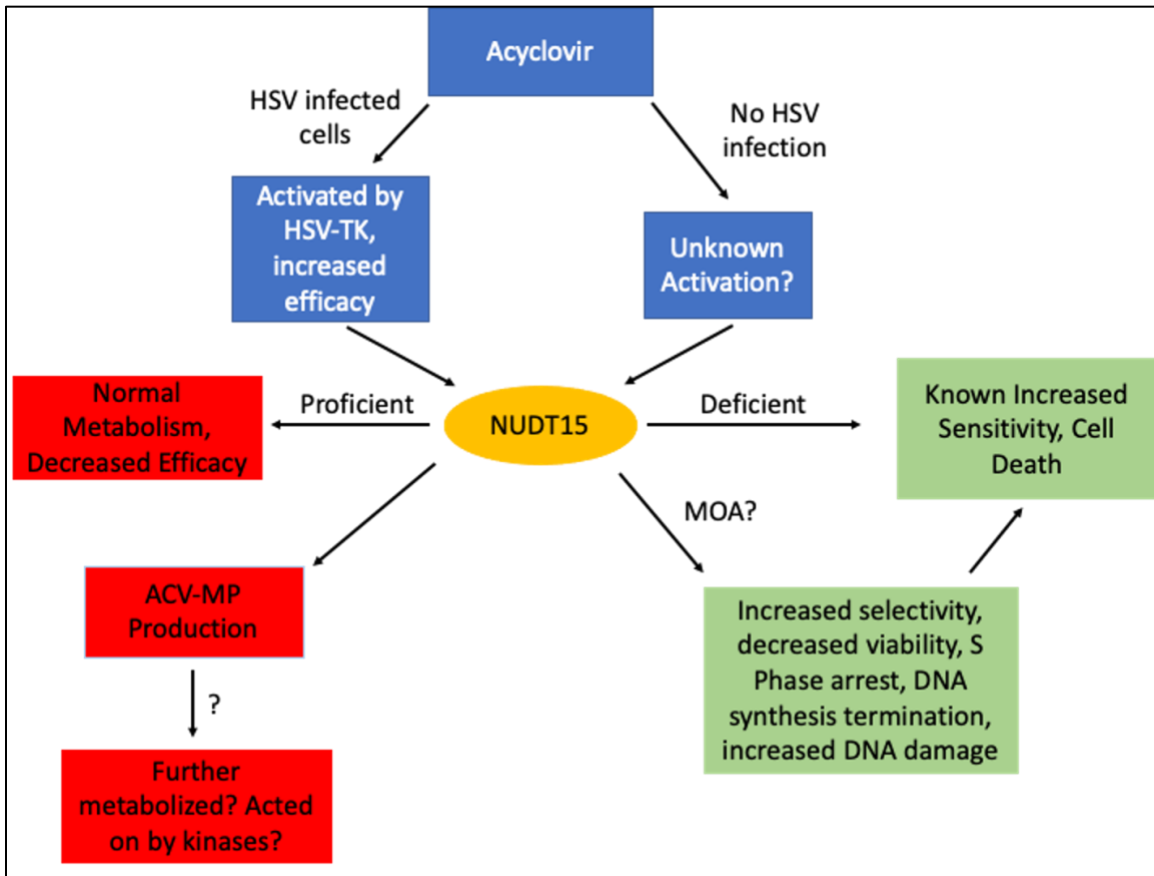


Figure 5.2 Proposed model for ACV treatments in NUDT15-deficient cells. A schematic showing the known and unknown results in NUDT15-proficient or deficient treated with acyclovir. While the mechanism for how acyclovir is activated in cells that do not have HSV-TK remains unknown, there is a change in sensitivity based on the status of NUDT15. NUDT15-proficient cells show normal metabolism and have decreased sensitivity to ACV; however, the generation of ACV-MP and its downstream metabolism do need to be further explored. ACV treatments are known to have increased efficacy causing more sensitivity in NUDT15-deficient cells, however the mechanism of action for this increased sensitivity needed to be determined. The findings of this project provide more understanding for the mechanism of the increase in sensitivity in NUDT15-deficient cells.

CHAPTER 6

MATERIALS AND METHODS

Cell Culture

OVCAR-8 cells were purchased from the American Type Culture Collection (ATCC) and were maintained in RPMI-1640 and 25 mM HEPES media supplemented with 10% fetal bovine serum and 1% penicillin/streptomycin. HEK 293FT cells were generously acquired by Dr. Michael Shtutman and were maintained in DMEM High Glucose media supplemented with 10% fetal bovine serum. 22Rv1 cells were generously provided by Dr. Mengqian Chen and were maintained in RPMI-1640 media supplemented with 10% fetal bovine serum, 1% penicillin/streptomycin, 2mM L-glutamine, 10 mM HEPES, 1 mM sodium pyruvate, 4500 mg/L glucose, and 1500 mg/L sodium bicarbonate. All cells were grown at 37°C in 5% CO₂. Cells were checked for mycoplasma contamination. 6-Thioguanine was purchased from Sigma-Aldrich, A4882-1G. Acyclovir was purchased from VWR, 10189-162.

Generation of CRISPR Knockouts

The Cas9 expressing lentiviral vector pCLIP-Cas9-Nuclease-EFS-RFP-v87 was generously provided by Dr. Phillip Buckhaults. Lentiviral production was carried out as described using pCMV- Δ 8.91 and pVSV-G packaging constructs generously provided by Dr. Michael Shtutman.⁹⁰ Lentivirus containing pCLIP-Cas9 were generated in HEK 293FT cells using PEI as a transfection reagent. Virus-containing media was collected and filtered in a .45 μ m filter. OVCAR-8 cells were then treated 2x for 24 hours each time with virus containing media with 8 μ g/mL of polybrene. Cells were then placed under selection with 15 μ g/mL of blasticidin (VWR, 10191-144) for 72 hours. Confirmation of FLAG-tagged Cas9 expressing cells was confirmed by western blot.

E. coli containing pCLIP-dual gRNA plasmids for NUDT15 (ID: TEDH-1053952) and NUDT18 (ID: TEDH-1053968, TEDH-1053969, TEDH-1053971) dual-gRNA vectors were acquired from Transomic Technologies via the University of South Carolina Lentiviral Core. The plasmids were isolated using the ZymoPURE II Plasmid Maxiprep Kit (Zymo Research, D4203) according to manufacturer's instructions. Plasmids were then packaged into lentivirus following the protocol described above. Media containing lentivirus was then added to OVCAR-8 cells 2x for 24 hours each with 8 µg/mL of polybrene. Cells were then placed under selection with 2 µg/mL of puromycin for 96 hours. Cells were then checked for knockout of the gene of interest via western blotting and RT-qPCR.

Whole Cell Protein Extraction

Plates containing cells were washed with PBS prior to trypsinization, collected, and spun down at 1100 \times g for 5 minutes. The supernatant was removed and cell pellets containing 1.5-2 \times 10⁶ cells were then washed with PBS prior to being centrifuged again. The pellet was then disrupted in 200 µL of RIPA lysis buffer (VWR, 97063-270) with protease and phosphatase inhibitor cocktail (Thermo Fisher, A32959) and placed on a rocking table at 4°C for 30 minutes. The samples were then sonicated 3 times (10 seconds on/5 seconds off) at 40% amplitude and rested on ice for 5-10 minutes. Protein concentrations were then determined with the BCA assay (Thermo Fisher, 23225).

Western Blot Analysis

Each sample had 25-35 µg of protein that were run by SDS-PAGE and transferred to a PVDF membrane overnight. All membranes were blocked with 5% milk blocking buffer (Bio-Rad) in PBST (1x PBS with 0.05% Tween-20) or TBST (1x TBS with 0.05%

Tween-20) prior to primary antibody addition. Membranes to analyze phospho- γ H2AX (Abcam, ab11174, 1:5000) were blocked for 1 hour prior to overnight incubation with primary antibody. Membranes to analyze NUDT15 (ABclonal, A8368, 1:2000) were blocked for 1 hour prior to overnight incubation with primary antibody. Membranes to analyze GAPDH (Cell Signaling, 5174S, 1:2000) as a loading control were blocked for 1 hour prior to overnight incubation with primary antibody. Membranes to analyze β -Tubulin (Novus Biologicals, NB600-936, 1:2000) as a loading control were blocked for 1 hour prior to overnight incubation with primary antibody. All overnight primary incubations were done at 4°C on a plate rocker. After overnight incubation, membranes were washed with PBST or TBST three times for ten minutes. Anti-rabbit-HRP secondary antibodies (Sigma Aldrich, NA9340V, 1:2000) were then added in 5% milk and allowed to incubate at RT for 1-2 hours on a plate rocker. The membranes were then washed with PBST or TBST three times for ten minutes. Membranes then had ECL blotting substrate (Pierce, 32106) added and were imaged using the ChemiDoc Touch Imaging System (Bio-Rad). Quantification of bands used Bio-Rad Image Lab software normalized to GAPDH or β -Tubulin expression.

RT-qPCR

Cells were trypsinized, washed with PBS, and pelleted prior to RNA isolation. RNA was isolated using the Zymo Direct-zol RNA Miniprep kit (Zymo, R2053) following manufacturer recommendation using TRI Reagent (Zymo). RNA concentration and purity was then determined using a Nanodrop. To synthesize cDNA from RNA samples, a final concentration of 1 μ g/ μ L of high purity RNA was added to iScript Reverse Transcription Supermix (Bio-Rad, 1708841) following manufacturer recommendation. After cDNA

synthesis, 3 µg of cDNA was added to iTaq Universal SYBR Green Supermix (Bio-Rad, 1725121) and 1 mM each of forward and reverse primers to a final concentration of 20 µL per reaction. Each reaction was performed in triplicate in a 96-well qPCR plate. The plate was placed in a Bio-Rad Icyler Thermocycler and iQ5 Optical System for qPCR analysis.

Metaphase Spreads

Cells were plated at a density of 30,000 cells per well and allowed to incubate at 37°C overnight. Cells were then treated in a final volume of 2 mL of media for 6 hours. After 6 hours, cells were washed with PBS and fresh 2 mL of media were added. Cells were allowed to incubate for 18 hours at 37°C. After incubation, media containing 20 ng/mL of colcemid was added and cells were allowed to incubate for 4 hours. After incubation, cells were trypsinized and placed into a hypotonic solution (2 mg/mL KCl in double distilled water) for 10 minutes at RT. Cells were pelleted and resuspended in an ice-cold fixative solution containing a 3:1 mixture of methanol to glacial acetic acid twice. To prepare the chromosome spreads, cells were resuspended in fixative solution and dropped by pipet onto slides, air dried, and stained in 10% Giemsa (Sigma). The slides were then washed with water and allowed to air dry overnight. Slides were observed on a Nikon Eclipse E600 Microscope using the 100x objective. Chromosomal aberrations were scored with a minimum of 950 chromosomes.

Colony Forming Assay

Cells were plated at a density of 1000 cells per well in a 6 well plate and allowed to incubate for 24 hours. For cells treated with chemotherapy drugs, the media was removed and 3 mL of fresh media containing the chemotherapy was added. For ionizing radiation treated cells, cells were treated in the RadSource RS2000 on ice. Media was then

removed, and the cells were washed once with PBS and 3 mL of fresh media was added. After treatments, cells were then placed in the incubator for 9-11 days. After recovery, the media was removed, and cells were fixed in 100% methanol for 10 minutes. The methanol was removed, and plates were allowed to air dry. The colonies were then stained with filtered 10% Giemsa stain and imaged with the ChemiDoc Touch Imaging System (Bio-Rad). The area of colonies in each well were quantified using the Colony Area Plugin for ImageJ.^{91, 92}

Resazurin Assay

Cells were plated at a density of 1000 cells per well in a 96-well plate and allowed to incubate for 24 hours. After 24 hours, the media was removed and 200 μ L of media containing treatments was added in triplicate. Cells were allowed to incubate for 72 hours. After incubation, the media was removed and media containing resazurin sodium salt (VWR, 89138-252) at concentration of 70 μ M to a volume of 100 μ L. Cells were allowed to incubate at 37°C and 5% CO₂ for 3-6 hours. Absorbance was then measured at 570 and 600 nm on a SpectraMax iD5 plate reader. The values for absorbance at 600 nm were then subtracted from the values measured at 570 nm.

Selectivity Assays

Cells were seeded in 6-well plates at a density of 80,000 cells per well with a 50-50 mixture between wild type and knockout cells. Cells were seeded in a well containing complete media without drugs and two wells with the LD₅₀ and LD₁₀ doses of drug. The cells were then placed into a BioTek BioSpa 8 live-cell imager for 72 hours with images at 4x magnification taken every 6 hours until the end of the treatment. The cells were stored at 37°C with 5% CO₂ over the course of the treatments. Images included phase contrast

and GFP fluorescent filter images. After the 72 hour treatments, cells were then split 1:5 and added to a new plate containing fresh media following the same treatment conditions for a total of 5 passages. The images were then compiled with the total number of cells and the disappearance of GFP+ cells over time being quantified.

Flow Cytometry

Cells were collected and washed with 2 mL of ice cold 1x PBS with 1% FBS and cells were pelleted at 1100 \times g for 5 minutes. The supernatant was removed, and cells were then gently resuspended in 2 mL of ice cold 1x PBS. Two milliliters of ice cold 100% ethanol were added dropwise, then 3 mL of ice cold 100% ethanol was added to a final volume of ~70%. The cells were then stored at -20°C for at least one night.

To determine the cell cycle profile, cells were pelleted, the supernatant was removed, and cells were washed with 2 mL of 1x PBS + 1% FBS. The cells were centrifuged, the supernatant was removed, and cells were then gently resuspended in 1 mL of 1x PBS with 3 μ M of DAPI and allowed to incubate for 15 minutes at room temperature in the dark. The samples were run on a BD LSR II Flow Cytometer in the Microscopy and Flow Cytometry Facility at the University of South Carolina, College of Pharmacy. At least 10,000 cells were analyzed per experiment.

To detect S-phase cells, 50 μ M of EdU was added 30 minutes prior to collection. Cells were then fixed as described above. EdU was detected using Click-iT chemistry, according to manufacturer's instructions using Alexa Fluor 647 (Thermo Fisher, C10635). Cells were suspended in 500 μ L of the Click-iT reaction cocktail and incubated for 30 minutes in the dark at room temperature. Five milliliters of PBS + 1% FBS was added, and

samples were spun at 1100 \times g for 5 minutes. The samples were then resuspended with DAPI and ran as described above with more than 20,000 cells analyzed per experiment.

Alkaline Comet Assay

Cells were plated in a 24 well plate at a density of 1000 cells per well and allowed to incubate for 24 hours. Cells were then treated over the course of 72 hours. After treatment, cells were then trypsinized, washed with PBS, and stored on ice as much as possible. Cells were then collected in 30 μ L of PBS at a density of 1×10^5 cells/mL and mixed with 300 μ L of molten 1% low melting agarose in PBS at 37°C. Using pre-coated slides that were warmed to 37°C (Trevigen, 4252-040-01), 50 μ L of the cell and agarose mixture were added and spread evenly with the side of the pipet tip. Slides were then stored at 4°C in the dark for 20 minutes. Slides were then immersed in the dark in pre-chilled lysis buffer (Trevigen, 4250-010-01) for at least 1 hour to no longer than overnight. The lysis buffer was then removed and replaced with freshly made, pre-chilled unwinding solution (200 mM NaOH, 1 mM EDTA, pH > 13) for 1 hour at 4°C in the dark. Slides were then moved into the Trevigen CometAssay ES unit with freshly made, pre-chilled alkaline running solution (200 mM NaOH, 1 mM EDTA, pH > 13) and run at 21 V for 20 minutes according to manufacturer's recommendations. The slides were then immersed in RT ddH₂O twice for 5 minutes each and RT 70% EtOH for 5 minutes. The slides were then allowed to completely dry overnight at 37°C before imaging.

For imaging, slides were stained with 1x SYBR Gold in 1x TE buffer for 30 minutes and de-stained with ddH₂O. The cells were allowed to dry for 20 minutes at 37°C in the dark. The cells were imaged using the Carl Zeiss LSM Confocal Microscope camera using Zen Pro image processing system at a 10x magnification. The images were then scored

using Trevigen Comet Analysis Software. At least 50 comets were scored per treatment group. Statistical significance was determined using two-way ANOVA with GraphPad Prism.

ApoTox-Glo Triplex Assay

Cells were seeded at a density of 1000 cells per well in a clear-bottomed, black-walled 96-well plate and allowed to incubate overnight at 37°C. Cells were then treated with 100 µL of media containing treatments for the appropriate exposure period. After treatments, the ApoTox-Glo Assay (Promega, G6320) was performed with slight alterations. Cells were treated with 330 µM of the viability and cytotoxicity substrate for 1 hour at 37°C prior to reading fluorescence on a SpectraMax iD5 plate reader following manufacturer's recommendation. For assessment of apoptosis, Caspase-Glo 3/7 substrate was prepared in Caspase 3/7 buffer following manufacturer's recommendation prior to 50 µL of the mixture being added to cells. Cells were allowed to incubate at RT in the dark for 1 hour before luminescence was measured using a SpectraMax iD5 plate reader.

REFERENCES

- [1] Hanahan, D., and Weinberg, R. A. (2011) Hallmarks of cancer: the next generation, *Cell* 144, 646-674.
- [2] Rudd, S. G., Valerie, N. C. K., and Helleday, T. (2016) Pathways controlling dNTP pools to maintain genome stability, *DNA Repair (Amst)* 44, 193-204.
- [3] Farber, S., and Diamond, L. K. (1948) Temporary remissions in acute leukemia in children produced by folic acid antagonist, 4-aminopteroyl-glutamic acid, *N Engl J Med* 238, 787-793.
- [4] Burchenal, J. H., Murphy, M. L., Ellison, R. R., Sykes, M. P., Tan, T. C., Leone, L. A., Karnofsky, D. A., Craver, L. F., Dargeon, H. W., and Rhoads, C. P. (1953) Clinical evaluation of a new antimetabolite, 6-mercaptopurine, in the treatment of leukemia and allied diseases, *Blood* 8, 965-999.
- [5] Hakala, M. T., Zakrzewski, S. F., and Nichol, C. A. (1961) Relation of folic acid reductase to amethopterin resistance in cultured mammalian cells, *J Biol Chem* 236, 952-958.
- [6] Nelson, J. A., Carpenter, J. W., Rose, L. M., and Adamson, D. J. (1975) Mechanisms of action of 6-thioguanine, 6-mercaptopurine, and 8-azaguanine, *Cancer Res* 35, 2872-2878.
- [7] Coskun, M., Steenholdt, C., de Boer, N. K., and Nielsen, O. H. (2016) Pharmacology and Optimization of Thiopurines and Methotrexate in Inflammatory Bowel Disease, *Clin Pharmacokinet* 55, 257-274.
- [8] Schmiegelow, K., Nielsen, S. N., Frandsen, T. L., and Nersting, J. (2014) Mercaptopurine/Methotrexate maintenance therapy of childhood acute lymphoblastic leukemia: clinical facts and fiction, *J Pediatr Hematol Oncol* 36, 503-517.
- [9] Lane, A. N., and Fan, T. W. (2015) Regulation of mammalian nucleotide metabolism and biosynthesis, *Nucleic Acids Res* 43, 2466-2485.
- [10] Tong, X., Zhao, F., and Thompson, C. B. (2009) The molecular determinants of de novo nucleotide biosynthesis in cancer cells, *Curr Opin Genet Dev* 19, 32-37.
- [11] Vander Heiden, M. G., and DeBerardinis, R. J. (2017) Understanding the Intersections between Metabolism and Cancer Biology, *Cell* 168, 657-669.
- [12] Cohen, S. S., Flaks, J. G., Barner, H. D., Loeb, M. R., and Lichtenstein, J. (1958) The Mode of Action of 5-Fluorouracil and Its Derivatives, *Proc Natl Acad Sci U S A* 44, 1004-1012.
- [13] Curtin, N. J., Harris, A. L., and Aherne, G. W. (1991) Mechanism of cell death following thymidylate synthase inhibition: 2'-deoxyuridine-5'-triphosphate accumulation, DNA damage, and growth inhibition following exposure to CB3717 and dipyridamole, *Cancer Res* 51, 2346-2352.
- [14] Doong, S. L., and Dolnick, B. J. (1988) 5-Fluorouracil substitution alters pre-mRNA splicing in vitro, *J Biol Chem* 263, 4467-4473.

- [15] Parker, J. B., and Stivers, J. T. (2011) Dynamics of uracil and 5-fluorouracil in DNA, *Biochemistry* 50, 612-617.
- [16] Yoo, B. K., Gredler, R., Vozhilla, N., Su, Z. Z., Chen, D., Forcier, T., Shah, K., Saxena, U., Hansen, U., Fisher, P. B., and Sarkar, D. (2009) Identification of genes conferring resistance to 5-fluorouracil, *Proc Natl Acad Sci U S A* 106, 12938-12943.
- [17] Kasai, H., and Nishimura, S. (1984) Hydroxylation of deoxy guanosine at the C-8 position by polyphenols and aminophenols in the presence of hydrogen peroxide and ferric ion, *Gan* 75, 565-566.
- [18] Kasai, H., Tanooka, H., and Nishimura, S. (1984) Formation of 8-hydroxyguanine residues in DNA by X-irradiation, *Gan* 75, 1037-1039.
- [19] Bessman, M. J., Frick, D. N., and O'Handley, S. F. (1996) The MutT proteins or "Nudix" hydrolases, a family of versatile, widely distributed, "housecleaning" enzymes, *J Biol Chem* 271, 25059-25062.
- [20] McLennan, A. G. (1999) The MutT motif family of nucleotide phosphohydrolases in man and human pathogens (review), *Int J Mol Med* 4, 79-89.
- [21] Maki, H., and Sekiguchi, M. (1992) MutT protein specifically hydrolyses a potent mutagenic substrate for DNA synthesis, *Nature* 355, 273-275.
- [22] Nishii, R., Mizuno, T., Rehling, D., Smith, C., Clark, B. L., Zhao, X., Brown, S. A., Smart, B., Moriyama, T., Yamada, Y., Ichinohe, T., Onizuka, M., Atsuta, Y., Yang, L., Yang, W., Thomas, P. G., Stenmark, P., Kato, M., and Yang, J. J. (2021) NUDT15 polymorphism influences the metabolism and therapeutic effects of acyclovir and ganciclovir, *Nat Commun* 12, 4181.
- [23] Watanabe, A., Hobara, N., and Nagashima, H. (1978) Demonstration of enzymatic activity converting azathioprine to 6-mercaptopurine, *Acta Med Okayama* 32, 173-179.
- [24] Stuckert, A. J., Schafer, E. S., Bernhardt, M. B., Baxter, P., and Brackett, J. (2020) Use of allopurinol to reduce hepatotoxicity from 6-mercaptopurine (6-MP) in patients with acute lymphoblastic leukemia (ALL), *Leuk Lymphoma* 61, 1246-1249.
- [25] Gisbert, J. P., and Gomollon, F. (2008) Thiopurine-induced myelotoxicity in patients with inflammatory bowel disease: a review, *Am J Gastroenterol* 103, 1783-1800.
- [26] Haglund, S., Vikingsson, S., Soderman, J., Hindorf, U., Granno, C., Danelius, M., Coulthard, S., Peterson, C., and Almer, S. (2011) The role of inosine-5'-monophosphate dehydrogenase in thiopurine metabolism in patients with inflammatory bowel disease, *Ther Drug Monit* 33, 200-208.
- [27] Derijks, L. J., Gilissen, L. P., Engels, L. G., Bos, L. P., Bus, P. J., Lohman, J. J., van Deventer, S. J., Hommes, D. W., and Hooymans, P. M. (2006) Pharmacokinetics of 6-thioguanine in patients with inflammatory bowel disease, *Ther Drug Monit* 28, 45-50.
- [28] Ansari, A., Hassan, C., Duley, J., Marinaki, A., Shobowale-Bakre, E. M., Seed, P., Meenan, J., Yim, A., and Sanderson, J. (2002) Thiopurine methyltransferase activity and the use of azathioprine in inflammatory bowel disease, *Aliment Pharmacol Ther* 16, 1743-1750.
- [29] Ansari, A., Aslam, Z., De Sica, A., Smith, M., Gilshenan, K., Fairbanks, L., Marinaki, A., Sanderson, J., and Duley, J. (2008) Influence of xanthine oxidase on thiopurine metabolism in Crohn's disease, *Aliment Pharmacol Ther* 28, 749-757.
- [30] Dubinsky, M. C. (2004) Azathioprine, 6-mercaptopurine in inflammatory bowel disease: pharmacology, efficacy, and safety, *Clin Gastroenterol Hepatol* 2, 731-743.

- [31] Amin, J., Huang, B., Yoon, J., and Shih, D. Q. (2015) Update 2014: advances to optimize 6-mercaptopurine and azathioprine to reduce toxicity and improve efficacy in the management of IBD, *Inflamm Bowel Dis* 21, 445-452.
- [32] Dubinsky, M. C., Lamothe, S., Yang, H. Y., Targan, S. R., Sinnett, D., Theoret, Y., and Seidman, E. G. (2000) Pharmacogenomics and metabolite measurement for 6-mercaptopurine therapy in inflammatory bowel disease, *Gastroenterology* 118, 705-713.
- [33] Valerie, N. C., Hagenkort, A., Page, B. D., Masuyer, G., Rehling, D., Carter, M., Bevc, L., Herr, P., Homan, E., Sheppard, N. G., Stenmark, P., Jemth, A. S., and Helleday, T. (2016) NUDT15 Hydrolyzes 6-Thio-DeoxyGTP to Mediate the Anticancer Efficacy of 6-Thioguanine, *Cancer Res* 76, 5501-5511.
- [34] Warren, D. J., Andersen, A., and Slørdal, L. (1995) Quantitation of 6-Thioguanine Residues in Peripheral Blood Leukocyte DNA Obtained from Patients Receiving 6-Mercaptopurine-based Maintenance Therapy¹, *Cancer Research* 55, 1670-1674.
- [35] Ling, Y. H., Nelson, J. A., Cheng, Y. C., Anderson, R. S., and Beattie, K. L. (1991) 2'-Deoxy-6-thioguanosine 5'-triphosphate as a substrate for purified human DNA polymerases and calf thymus terminal deoxynucleotidyltransferase in vitro, *Mol Pharmacol* 40, 508-514.
- [36] Aquilina, G., Giammarioli, A. M., Zijno, A., Di Muccio, A., Dogliotti, E., and Bignami, M. (1990) Tolerance to O6-methylguanine and 6-thioguanine cytotoxic effects: a cross-resistant phenotype in N-methylnitrosourea-resistant Chinese hamster ovary cells, *Cancer Res* 50, 4248-4253.
- [37] Swann, P. F., Waters, T. R., Moulton, D. C., Xu, Y. Z., Zheng, Q., Edwards, M., and Mace, R. (1996) Role of postreplicative DNA mismatch repair in the cytotoxic action of thioguanine, *Science* 273, 1109-1111.
- [38] Yan, T., Berry, S. E., Desai, A. B., and Kinsella, T. J. (2003) DNA mismatch repair (MMR) mediates 6-thioguanine genotoxicity by introducing single-strand breaks to signal a G2-M arrest in MMR-proficient RKO cells, *Clin Cancer Res* 9, 2327-2334.
- [39] Rajesh, P., Litvinchuk, A. V., Pittman, D. L., and Wyatt, M. D. (2011) The homologous recombination protein RAD51D mediates the processing of 6-thioguanine lesions downstream of mismatch repair, *Mol Cancer Res* 9, 206-214.
- [40] Yang, J. J., Landier, W., Yang, W., Liu, C., Hageman, L., Cheng, C., Pei, D., Chen, Y., Crews, K. R., Kornegay, N., Wong, F. L., Evans, W. E., Pui, C. H., Bhatia, S., and Relling, M. V. (2015) Inherited NUDT15 variant is a genetic determinant of mercaptopurine intolerance in children with acute lymphoblastic leukemia, *J Clin Oncol* 33, 1235-1242.
- [41] Krynetski, E., and Evans, W. E. (2003) Drug methylation in cancer therapy: lessons from the TPMT polymorphism, *Oncogene* 22, 7403-7413.
- [42] Sparrow, M. P., Hande, S. A., Friedman, S., Lim, W. C., Reddy, S. I., Cao, D., and Hanauer, S. B. (2005) Allopurinol safely and effectively optimizes thioguanine metabolites in inflammatory bowel disease patients not responding to azathioprine and mercaptopurine, *Aliment Pharmacol Ther* 22, 441-446.
- [43] Ansari, A., Patel, N., Sanderson, J., O'Donohue, J., Duley, J. A., and Florin, T. H. (2010) Low-dose azathioprine or mercaptopurine in combination with allopurinol can bypass many adverse drug reactions in patients with inflammatory bowel disease, *Aliment Pharmacol Ther* 31, 640-647.

- [44] Appell, M. L., Wagner, A., and Hindorf, U. (2013) A skewed thiopurine metabolism is a common clinical phenomenon that can be successfully managed with a combination of low-dose azathioprine and allopurinol, *J Crohns Colitis* 7, 510-513.
- [45] Shih, D. Q., Nguyen, M., Zheng, L., Ibanez, P., Mei, L., Kwan, L. Y., Bradford, K., Ting, C., Targan, S. R., and Vasiliauskas, E. A. (2012) Split-dose administration of thiopurine drugs: a novel and effective strategy for managing preferential 6-MMP metabolism, *Aliment Pharmacol Ther* 36, 449-458.
- [46] Balfour, H. H., Jr. (1999) Antiviral drugs, *N Engl J Med* 340, 1255-1268.
- [47] Elion, G. B., Furman, P. A., Fyfe, J. A., de Miranda, P., Beauchamp, L., and Schaeffer, H. J. (1977) Selectivity of action of an antiherpetic agent, 9-(2-hydroxyethoxymethyl) guanine, *Proc Natl Acad Sci U S A* 74, 5716-5720.
- [48] Fyfe, J. A., Keller, P. M., Furman, P. A., Miller, R. L., and Elion, G. B. (1978) Thymidine kinase from herpes simplex virus phosphorylates the new antiviral compound, 9-(2-hydroxyethoxymethyl)guanine, *J Biol Chem* 253, 8721-8727.
- [49] Klysik, K., Pietraszek, A., Karewicz, A., and Nowakowska, M. (2020) Acyclovir in the Treatment of Herpes Viruses - A Review, *Curr Med Chem* 27, 4118-4137.
- [50] Alibek, K., Bekmurzayeva, A., Mussabekova, A., and Sultankulov, B. (2012) Using antimicrobial adjuvant therapy in cancer treatment: a review, *Infect Agent Cancer* 7, 33.
- [51] Soderlund, J., Erhardt, S., and Kast, R. E. (2010) Acyclovir inhibition of IDO to decrease Tregs as a glioblastoma treatment adjunct, *J Neuroinflammation* 7, 44.
- [52] Shaimerdenova, M., Karapina, O., Mektepbayeva, D., Alibek, K., and Akilbekova, D. (2017) The effects of antiviral treatment on breast cancer cell line, *Infect Agent Cancer* 12, 18.
- [53] Zhang, S. M., Rehling, D., Jemth, A. S., Throup, A., Landazuri, N., Almlöf, I., Gottmann, M., Valerie, N. C. K., Borhade, S. R., Wakchaure, P., Page, B. D. G., Desroses, M., Homan, E. J., Scobie, M., Rudd, S. G., Berglund, U. W., Soderberg-Naucler, C., Stenmark, P., and Helleday, T. (2021) NUDT15-mediated hydrolysis limits the efficacy of anti-HCMV drug ganciclovir, *Cell Chem Biol* 28, 1693-1702 e1696.
- [54] Akiyama, M., Maki, H., Sekiguchi, M., and Horiuchi, T. (1989) A specific role of MutT protein: to prevent dG.dA mispairing in DNA replication, *Proc Natl Acad Sci U S A* 86, 3949-3952.
- [55] Furuichi, M., Yoshida, M. C., Oda, H., Tajiri, T., Nakabeppu, Y., Tsuzuki, T., and Sekiguchi, M. (1994) Genomic structure and chromosome location of the human mutT homologue gene MTH1 encoding 8-oxo-dGTPase for prevention of A:T to C:G transversion, *Genomics* 24, 485-490.
- [56] Sekiguchi, M. (1996) MutT-related error avoidance mechanism for DNA synthesis, *Genes Cells* 1, 139-145.
- [57] Sakumi, K., Furuichi, M., Tsuzuki, T., Kakuma, T., Kawabata, S., Maki, H., and Sekiguchi, M. (1993) Cloning and expression of cDNA for a human enzyme that hydrolyzes 8-oxo-dGTP, a mutagenic substrate for DNA synthesis, *J Biol Chem* 268, 23524-23530.
- [58] Mo, J. Y., Maki, H., and Sekiguchi, M. (1992) Hydrolytic elimination of a mutagenic nucleotide, 8-oxodGTP, by human 18-kilodalton protein: sanitization of nucleotide pool, *Proc Natl Acad Sci U S A* 89, 11021-11025.
- [59] Kakuma, T., Nishida, J., Tsuzuki, T., and Sekiguchi, M. (1995) Mouse MTH1 protein with 8-oxo-7,8-dihydro-2'-deoxyguanosine 5'-triphosphatase activity that prevents

transversion mutation. cDNA cloning and tissue distribution, *J Biol Chem* 270, 25942-25948.

[60] Cai, J. P., Kakuma, T., Tsuzuki, T., and Sekiguchi, M. (1995) cDNA and genomic sequences for rat 8-oxo-dGTPase that prevents occurrence of spontaneous mutations due to oxidation of guanine nucleotides, *Carcinogenesis* 16, 2343-2350.

[61] Nakabeppu, Y., Ohta, E., and Abolhassani, N. (2017) MTH1 as a nucleotide pool sanitizing enzyme: Friend or foe?, *Free Radic Biol Med* 107, 151-158.

[62] Carreras-Puigvert, J., Zitnik, M., Jemth, A. S., Carter, M., Unterlass, J. E., Hallstrom, B., Loseva, O., Karem, Z., Calderon-Montano, J. M., Lindskog, C., Edqvist, P. H., Matuszewski, D. J., Ait Blal, H., Berntsson, R. P. A., Haggblad, M., Martens, U., Studham, M., Lundgren, B., Wahlby, C., Sonnhammer, E. L. L., Lundberg, E., Stenmark, P., Zupan, B., and Helleday, T. (2017) A comprehensive structural, biochemical and biological profiling of the human NUDIX hydrolase family, *Nat Commun* 8, 1541.

[63] Carter, M., Jemth, A. S., Hagenkort, A., Page, B. D., Gustafsson, R., Griese, J. J., Gad, H., Valerie, N. C., Desroses, M., Bostrom, J., Warpman Berglund, U., Helleday, T., and Stenmark, P. (2015) Crystal structure, biochemical and cellular activities demonstrate separate functions of MTH1 and MTH2, *Nat Commun* 6, 7871.

[64] Takagi, Y., Setoyama, D., Ito, R., Kamiya, H., Yamagata, Y., and Sekiguchi, M. (2012) Human MTH3 (NUDT18) protein hydrolyzes oxidized forms of guanosine and deoxyguanosine diphosphates: comparison with MTH1 and MTH2, *J Biol Chem* 287, 21541-21549.

[65] Gad, H., Koolmeister, T., Jemth, A. S., Eshtad, S., Jacques, S. A., Strom, C. E., Svensson, L. M., Schultz, N., Lundback, T., Einarsdottir, B. O., Saleh, A., Gokturk, C., Baranczewski, P., Svensson, R., Berntsson, R. P., Gustafsson, R., Stromberg, K., Sanjiv, K., Jacques-Cordonnier, M. C., Desroses, M., Gustavsson, A. L., Olofsson, R., Johansson, F., Homan, E. J., Loseva, O., Brautigam, L., Johansson, L., Hogle, A., Hagenkort, A., Pham, T., Altun, M., Gaugaz, F. Z., Vikingsson, S., Evers, B., Henriksson, M., Vallin, K. S., Wallner, O. A., Hammarstrom, L. G., Wiita, E., Almlöf, I., Kalderén, C., Axelsson, H., Djureinovic, T., Puigvert, J. C., Haggblad, M., Jeppsson, F., Martens, U., Lundin, C., Lundgren, B., Granelli, I., Jensen, A. J., Artursson, P., Nilsson, J. A., Stenmark, P., Scobie, M., Berglund, U. W., and Helleday, T. (2014) MTH1 inhibition eradicates cancer by preventing sanitation of the dNTP pool, *Nature* 508, 215-221.

[66] Luo, M., He, H., Kelley, M. R., and Georgiadis, M. M. (2010) Redox regulation of DNA repair: implications for human health and cancer therapeutic development, *Antioxid Redox Signal* 12, 1247-1269.

[67] Kettle, J. G., Alwan, H., Bista, M., Breed, J., Davies, N. L., Eckersley, K., Fillery, S., Foote, K. M., Goodwin, L., Jones, D. R., Kack, H., Lau, A., Nissink, J. W., Read, J., Scott, J. S., Taylor, B., Walker, G., Wissler, L., and Wylot, M. (2016) Potent and Selective Inhibitors of MTH1 Probe Its Role in Cancer Cell Survival, *J Med Chem* 59, 2346-2361.

[68] Petrocchi, A., Leo, E., Reyna, N. J., Hamilton, M. M., Shi, X., Parker, C. A., Mseeh, F., Bardenhagen, J. P., Leonard, P., Cross, J. B., Huang, S., Jiang, Y., Cardozo, M., Draetta, G., Marszalek, J. R., Toniatti, C., Jones, P., and Lewis, R. T. (2016) Identification of potent and selective MTH1 inhibitors, *Bioorg Med Chem Lett* 26, 1503-1507.

[69] Zhang, S. M., Desroses, M., Hagenkort, A., Valerie, N. C. K., Rehling, D., Carter, M., Wallner, O., Koolmeister, T., Throup, A., Jemth, A. S., Almlöf, I., Loseva, O., Lundback, T., Axelsson, H., Regmi, S., Sarno, A., Kramer, A., Pudielko, L., Brautigam, L., Rasti, A.,

- Gottmann, M., Wiita, E., Kutzner, J., Schaller, T., Kalderen, C., Cazares-Korner, A., Page, B. D. G., Krimpenfort, R., Eshtad, S., Altun, M., Rudd, S. G., Knapp, S., Scobie, M., Homan, E. J., Berglund, U. W., Stenmark, P., and Helleday, T. (2020) Development of a chemical probe against NUDT15, *Nat Chem Biol* 16, 1120-1128.
- [70] Rehling, D., Zhang, S. M., Jemth, A. S., Koolmeister, T., Throup, A., Wallner, O., Scaletti, E., Moriyama, T., Nishii, R., Davies, J., Desroses, M., Rudd, S. G., Scobie, M., Homan, E., Berglund, U. W., Yang, J. J., Helleday, T., and Stenmark, P. (2021) Crystal structures of NUDT15 variants enabled by a potent inhibitor reveal the structural basis for thiopurine sensitivity, *J Biol Chem* 296, 100568.
- [71] Tanaka, Y., Kato, M., Hasegawa, D., Urayama, K. Y., Nakadate, H., Kondoh, K., Nakamura, K., Koh, K., Komiyama, T., and Manabe, A. (2015) Susceptibility to 6-MP toxicity conferred by a NUDT15 variant in Japanese children with acute lymphoblastic leukaemia, *Br J Haematol* 171, 109-115.
- [72] Kakuta, Y., Naito, T., Onodera, M., Kuroha, M., Kimura, T., Shiga, H., Endo, K., Negoro, K., Kinouchi, Y., and Shimosegawa, T. (2016) NUDT15 R139C causes thiopurine-induced early severe hair loss and leukopenia in Japanese patients with IBD, *Pharmacogenomics J* 16, 280-285.
- [73] Yang, S. K., Hong, M., Baek, J., Choi, H., Zhao, W., Jung, Y., Haritunians, T., Ye, B. D., Kim, K. J., Park, S. H., Park, S. K., Yang, D. H., Dubinsky, M., Lee, I., McGovern, D. P., Liu, J., and Song, K. (2014) A common missense variant in NUDT15 confers susceptibility to thiopurine-induced leukopenia, *Nat Genet* 46, 1017-1020.
- [74] Moyer, A. M. (2021) NUDT15: A bench to bedside success story, *Clin Biochem* 92, 1-8.
- [75] Yang, J. J., Whirl-Carrillo, M., Scott, S. A., Turner, A. J., Schwab, M., Tanaka, Y., Suarez-Kurtz, G., Schaeffeler, E., Klein, T. E., Miller, N. A., and Gaedigk, A. (2019) Pharmacogene Variation Consortium Gene Introduction: NUDT15, *Clin Pharmacol Ther* 105, 1091-1094.
- [76] Gao, J., Aksoy, B. A., Dogrusoz, U., Dresdner, G., Gross, B., Sumer, S. O., Sun, Y., Jacobsen, A., Sinha, R., Larsson, E., Cerami, E., Sander, C., and Schultz, N. (2013) Integrative analysis of complex cancer genomics and clinical profiles using the cBioPortal, *Sci Signal* 6, pii.
- [77] Cerami, E., Gao, J., Dogrusoz, U., Gross, B. E., Sumer, S. O., Aksoy, B. A., Jacobsen, A., Byrne, C. J., Heuer, M. L., Larsson, E., Antipin, Y., Reva, B., Goldberg, A. P., Sander, C., and Schultz, N. (2012) The cBio cancer genomics portal: an open platform for exploring multidimensional cancer genomics data, *Cancer Discov* 2, 401-404.
- [78] Hashiguchi, K., Hayashi, M., Sekiguchi, M., and Umezu, K. (2018) The roles of human MTH1, MTH2 and MTH3 proteins in maintaining genome stability under oxidative stress, *Mutat Res* 808, 10-19.
- [79] Datta, K., Suman, S., Kallakury, B. V., and Fornace, A. J., Jr. (2012) Exposure to heavy ion radiation induces persistent oxidative stress in mouse intestine, *PLoS One* 7, e42224.
- [80] Yanokura, M., Takase, K., Yamamoto, K., and Teraoka, H. (2000) Cell death and cell-cycle arrest induced by incorporation of [3H]thymidine into human haemopoietic cell lines, *Int J Radiat Biol* 76, 295-303.
- [81] Hitchings, G. H., Elion, G. B., Falco, E. A., Russell, P. B., and Vanderwerff, H. (1950) Studies on analogs of purines and pyrimidines, *Ann N Y Acad Sci* 52, 1318-1335.

- [82] Bradford, K., and Shih, D. Q. (2011) Optimizing 6-mercaptopurine and azathioprine therapy in the management of inflammatory bowel disease, *World J Gastroenterol* 17, 4166-4173.
- [83] Rushlow, D., Piovesan, B., Zhang, K., Prigoda-Lee, N. L., Marchong, M. N., Clark, R. D., and Gallie, B. L. (2009) Detection of mosaic RB1 mutations in families with retinoblastoma, *Hum Mutat* 30, 842-851.
- [84] Wyatt, M. D., Reilly, N. M., Patel, S., Rajesh, P., Schools, G. P., Smiraldo, P. G., and Pittman, D. L. (2018) Thiopurine-induced mitotic catastrophe in Rad51d-deficient mammalian cells, *Environ Mol Mutagen* 59, 38-48.
- [85] Niles, A. L., Moravec, R. A., and Riss, T. L. (2008) Update on in vitro cytotoxicity assays for drug development, *Expert Opin Drug Discov* 3, 655-669.
- [86] Karran, P. (2006) Thiopurines, DNA damage, DNA repair and therapy-related cancer, *Br Med Bull* 79-80, 153-170.
- [87] Elion, G. B. (1982) Mechanism of action and selectivity of acyclovir, *Am J Med* 73, 7-13.
- [88] Ackerson, S. M., Gable, C. I., and Stewart, J. A. (2020) Human CTC1 promotes TopBP1 stability and CHK1 phosphorylation in response to telomere dysfunction and global replication stress, *Cell Cycle* 19, 3491-3507.
- [89] Laskin, O. L. (1983) Clinical pharmacokinetics of acyclovir, *Clin Pharmacokinet* 8, 187-201.
- [90] Oliver, D., Ji, H., Liu, P., Gasparian, A., Gardiner, E., Lee, S., Zenteno, A., Perinskaya, L. O., Chen, M., Buckhaults, P., Broude, E., Wyatt, M. D., Valafar, H., Pena, E., and Shtutman, M. (2017) Identification of novel cancer therapeutic targets using a designed and pooled shRNA library screen, *Sci Rep* 7, 43023.
- [91] Schneider, C. A., Rasband, W. S., and Eliceiri, K. W. (2012) NIH Image to ImageJ: 25 years of image analysis, *Nat Methods* 9, 671-675.
- [92] Guzman, C., Bagga, M., Kaur, A., Westermarck, J., and Abankwa, D. (2014) ColonyArea: an ImageJ plugin to automatically quantify colony formation in clonogenic assays, *PLoS One* 9, e92444.